Near-field radiative heat transfer and Casimir forces in two-and many-body systems

R. Messina

Habilitation à diriger des recherches

Near-field radiative heat transfer and Casimir forces in two- and many-body systems

---

Riccardo MESSINA

Soutenue le 25 juin 2021 devant le jury composé de :

Yannick DE WILDE ..... Rapporteur

Shanhui FAN ..... Examinateur

Karl JOULAIN ..... Rapporteur

Paulo MAIA NETO ..... Rapporteur

Bruno PALPANT ..... Examinateur

Lilia WOODS ..... Examinatrice

Contents

Introduction

The purpose of this manuscript is to give an overview of my research activity in view of the obtention of my *Habilitation à diriger des recherches*. After a brief review of the results obtained during my PhD and my two postdocs, the second and main part of the manuscript will concern the results I obtained since the beginning of my permanent position at CNRS in 2013.

Since my very first contact with research, photons have been at the heart of my activity. As a matter of fact, since 2006 I have focused my attention of the fluctuations of the electromagnetic field, of quantum and thermal origin, and on the physical effects they can entail. More specifically, I have addressed several aspects of two phenomena directly connected to these fluctuations: Casimir forces and near-field radiative heat transfer.

Casimir forces exist between any couple of electrically neutral bodies, also in the ground state of the electromagnetic field. Even if in this scenario the average electric and magnetic fields vanish, the fact that Heisenberg uncertainty relations prevent the variance of these fields to vanish led Hendrik Casimir in 1948 to theoretically prove the existence of an attractive force between two perfectly conducting parallel plates [1]. In the same year, he also unveiled, in collaboration with Dirk Polder, the existence of an analogous effect between a neutral atom and a perfectly conducting plate [2]. These intriguing results were generalized to the case of arbitrary dielectric properties by Lifshitz and collaborators [3]. Several theoretical developments followed these pioneering results, starting to delve deeper into the role played by optical properties, temperature and geometry of the system, as highlighted by several review papers on this topic [4–7].

Almost 50 years had to be waited for the first unambiguous experimental demonstration of the Casimir force in a macroscopic system [8], followed by many others experiments [9–33], performed in a variety of geometrical configurations, involving spheres, cylinders, along with the initially considered plane - plane configuration. On a parallel side, several experiments explored the behavior of the Casimir-Polder force in systems involving atoms [34–41]. All these investigations confirmed the predictions and gave a further boost to the theoretical studies, leading to

a variety of theoretical frameworks to deal with Casimir forces in very general scenarios [42–46].

A further important step in the history of Casimir forces came in 2004, with the first theoretical study of the effect of the absence of thermal equilibrium on the behavior of the force, both in macroscopic systems and in configurations involving atoms [47–50]. It was shown that the dependence of the force on the distance can be qualitatively modified, and that a repulsive force can also arise. Shortly after these works, these findings were experimentally confirmed by an experiment involving Bose-Einstein condensates [51].

At this stage, it was already clear that a precise knowledge of the Casimir force could be relevant in several applicative domains [52]. More specifically, the ongoing miniaturization of technological devices, and thus the transition towards distances between the operating parts (in the micron and sub-micron range) where the Casimir force can be the dominant effect, paved the way toward a more and more precise assessment in configurations such as the ones of Micro- and Nano-Electromechanical Systems (MEMS and NEMS) [53, 54]. As a matter of fact, it was shown that not only is a precise knowledge of the force mandatory to prevent adhesion of the (possibly) moving parts (usually referred to as *stiction*), but the force can be ideally actively exploited for the correct functioning of these devices [12, 13].

Around the same years when Casimir forces were initially theoretically discovered, the development of the rigorous framework of fluctuational electrodynamics by Rytov [55], enriched by the important results of Polder and van Hove [56] some years later, set the foundations of a new paradigm in the domain of radiative heat transfer. The fact that two bodies at different temperature, even separated by a vacuum gap, exchanged heat mediated by photons had been known already for a long time. Nevertheless, the comprehension of this phenomenon was based on the traditional approach of ray optics, expected to fail when the distance separating the bodies or their size become smaller than the thermal wavelength $\lambda_{\text{th}} = \hbar c/k_B T$, of the order of $10\,\mu$m at ambient temperature. Under this approximation, Stefan-Boltzmann's law sets an upper limit to the radiative heat transfer between two bodies, attained only in the ideal scenario of two black bodies (absorbing all the radiation impinging on them). On the contrary, for distances smaller than λ_{th}, in the so-called *near field*, tunneling of photons can take place and the energy exchange can be dominated by evanescent waves, ignored within a ray-optics approach. The first observation, along with the impressive amount of further theoretical developments, described e.g. by several review papers on this topic [57–61], allowed to highlight the fact that near-field radiative heat flux can go beyond the black-body limit even by several orders of magnitude, especially when the interacting bodies support surface resonant modes such as phonon-polaritons in the case of polar materials.

As in the case of Casimir forces, a long time separates the first theoretical predictions from

the first clear experimental observations. Nevertheless, also in this case, these led to a renewed interest and to an impressively high amount of experimental confirmations in a variety of geometrical configurations [62–92]. Also in this case, this significantly nourished the theoretical interest, paving the way to some general theoretical approaches to near-field radiative heat transfer in arbitrary configurations [93–98]. Interestingly, at this stage it became clear that Casimir forces and radiative heat transfer shared a common origin and could be studied also within a common formalism [99–102].

The control of temperature and energy fluxes at the nanoscale is indeed a very relevant topic in the context of micro- and nano-technology. In this sense, several works were devoted to the control of near-field radiative heat transfer. In this recent branch of thermal management [103], a relevant role is played by those works in which a way to control energy flux by means of an externally adjustable parameters, such as a magnetic field [104] or the chemical potential [105, 106].

In the same spirit of active manipulation of near-field radiative heat transfer, the recent development of *thermotronics* has to be mentioned (see [107] and refs. therein), whose purpose is the development of thermal analogs of basic components of electrical circuits (diode, transistors, ...). This has recently led to the first experimental realization of a near-field radiative thermal diode [88].

A further relevant applicative domain in which near-field radiative heat transfer could play a key role is energy conversion. More specifically, around 20 years ago it was suggested that near field could have a significant impact on thermophotovoltaic cells [108–110]. In these systems, the thermal energy coming from a source (and not directly from the Sun as in ordinary photovoltaic cells) is converted into an electric current. As suggested by Refs. [108–110], the efficiency of such energy-conversion devices could benefit from the known dramatic amplification of radiative flux due to the transition to the near-field regime. Since the initial proposal, several theoretical studies have been presented (see Ref. [111] and references therein). Among the recent developments [76, 112], an experimental realization of a near-field thermophotovoltaic device in the nanometer range of distances has to be mentioned [87].

Albeit the impressive amount of theoretical and experimental developments in these fields, several aspects have been somehow surprisingly almost ignored until very recently. A common one between Casimir forces and radiative heat transfer is the role played by many-body effects. As a matter of fact, it is known since the early theoretical results that both effects are non-additive, in the sense that in the presence of more than two bodies, the effect on a given one cannot be predicted as the sum of the individual two-body contributions which would exist in the absence of the other bodies. This implies that a correct prediction of the force and energy

transfer in configurations implying more than two bodies, of increasing relevance especially for technological applications, requires an exact many-body approach, and that the precision of results obtained within an additive approximations cannot be assessed in advance. This topic has been indeed one of the main ones of my activity during the last decade. It has led to the development of general theoretical frameworks describing the Casimir force and radiative heat transfer in arbitrary systems made of two bodies (in the presence of an environment), three bodies and later N planar slabs. These results are the topic of Chapter 3. These general approaches have been at the origin of a variety of theoretical predictions of many-body effects, of which an overview is given in Chapter 4.

A further part of the results obtained concerns the theoretical analysis of Casimir forces and heat transfer in systems involving gratings, i.e. periodically nanostructured surfaces. This topic fits the general topic of the active manipulation of these physical effects by means of geometrical and material parameters. The results obtained in this context, as well as the techniques used to obtain them are described in Chapter 5.

Finally, an aspect which has not received the deserved attention is in my opinion the coupling between conductive and radiative heat transfer. As a matter of fact, in almost all theoretical works on radiative heat transfer, the main assumption is that the temperature within each interacting body is constant, as the result of the contact with an external thermostat. While in some cases this is fully justified by the comparison between conductive and radiative contributions, some of the results I obtained during the last years have unveiled scenarios in which this assumption can even dramatically fail. This has in my opinion on one hand a remarkable theoretical interest, but plays also a key role in a precise quantitative prediction of the value of the radiative flux. The results, obtained in the specific case of Fourier regime and within the more general approach based on the Boltzmann transport equation, are the topic of Chapter 6.

Part I

General overview and background

CHAPTER 1

Curriculum vitae

Personal information

Place and date of birth	Palermo (Italy), 7 May 1983
Citizenships	Italian, French
Professional address	Laboratoire Charles Fabry UMR CNRS 8501 2 avenue Augustin Fresnel, 91127 Palaiseau (France)

Current position

Since 01/2018	CNRS CRCN researcher (Section 03) at Laboratoire Charles Fabry UMR 8501 (CNRS, Institut d'Optique Graduate School), Palaiseau (France).

Past positions

10/2013 - 12/2017	CNRS CR2 researcher (Section 03) at Laboratoire Charles Coulomb UMR 5221 (CNRS, Université de Montpellier), Montpellier (France).
01/2012 - 06/2013	Postdoctoral researcher at Laboratoire Charles Fabry (CNRS, Institut d'Optique Graduate School), Palaiseau (France).

01/2010 - 12/2011	Postdoctoral researcher at SYRTE (Observatoire de Paris), Paris (France).

University education

01/2007 - 12/2009	Phd in Physics Laboratoire Kastler Brossel (École Normale Supérieure de Paris, CNRS, Université Pierre et Marie Curie Paris 6) Università degli Studi di Palermo Vote: *Très honorable*
10/2004 - 09/2006	Master degree in Physics Università degli Studi di Palermo Vote: 110/110 *cum laude*
10/2001 - 10/2004	Bachelor degree in Physics Università degli Studi di Palermo Vote: 110/110 *cum laude*

PhD thesis

Title	*Casimir - Polder force between atom and surface: geometrical and dynamical effects*
Supervisors	A. Lambrecht and R. Passante
Date of defense	1 April 2010
Committee	Marie-Christine Angonin Giovanni Carugno Astrid Lambrecht Carugno Roberto Passante Francesco Saverio Persico Giuseppe Ruoso
Mark	*Très honorable*

Master thesis

Title	*Fluttuazioni delle forze di Casimir e di Casimir - Polder (Fluctuations of Casimir and Casimir - Polder forces)*
Supervisor	R. Passante
Date of defense	20 September 2006
Mark	110/110 *cum laude*

Teaching experience

2020 - 2021	14 hours - Tutorials on *Electromagnetism* (third year of bachelor's degree, Institut d'Optique Graduate School)
2020 - 2021	19 hours - Tutorials and practical work on *Numerical Physics* (third year of bachelor's degree, École Normale Supérieure de Paris-Saclay)
2019 - 2020	14 hours - Tutorials on *Electromagnetism* (third year of bachelor's degree, Institut d'Optique Graduate School)
2019 - 2020	19 hours - Tutorials and practical work on *Numerical Physics* (third year of bachelor's degree, École Normale Supérieure de Paris-Saclay)
2018 - 2019	14 hours - Tutorials on *Electromagnetism* (third year of bachelor's degree, Institut d'Optique Graduate School)
2018 - 2019	19 hours - Tutorials and practical work on *Numerical Physics* (third year of bachelor's degree, École Normale Supérieure de Paris-Saclay)
2012 - 2013	9 hours - Tutorials on *Electromagnetism* (third year of bachelor's degree, Institut d'Optique Graduate School)
2012 - 2013	36 hours - Tutorials and practical work on *Random Variables* (third year of bachelor's degree, Institut d'Optique Graduate School)

2011 - 2012	52 hours - Oral tests on *Electromagnetism* (second year of bachelor's degree, University Paris 7 Denis Diderot)
2011 - 2012	44 hours - Oral tests on *Mechanics* (first year of bachelor's degree, University Paris 7 Denis Diderot)
2010 - 2011	50 hours - Tutorial of 5 students of the DU (*Universitary Diploma*) *Celestial Mechanics and Astronomy* organized by the Observatoire de Paris.

Supervision of PhD students and postdocs

2018 - present	Co-direction of the work of of Marta REINA PhD student at Laboratoire Charles Fabry (Palaiseau)
2015 - 2017	Co-direction of the work of of Pierre DOYEUX PhD student at Laboratoire Charles Coulomb (Montpellier) Defense on 20 November 2017
2013 -2015	Supervision of the work of of Bruno LEGGIO Postdoc at Laboratoire Charles Coulomb (Montpellier)
2014 - 2016	Supervision of the work of of Antonio NOTO PhD student at Laboratoire Charles Coulomb (Montpellier) Defense on 21 March 2016
2010 - 2012	Supervision of the work of Sophie PELISSON PhD student at SYRTE (Paris) Defense on 25 October 2012

Scientific visits

04 - 05/2019	"Visiting Research Scholar" at Princeton University, Department of Electrical Engineering (USA)
08 - 10/2018	Invited researcher at Princeton University, Department of Electrical Engineering (USA)

04 - 05/2017	"Visiting Research Scholar" at Princeton University, Department of Electrical Engineering (USA)
04/2015	Invited researcher at Los Alamos National Laboratory (USA), visit to the group of Diego Dalvit
2010 - 2012	Visits to the group of M. Antezza, Laboratoire Charles Coulomb, Université de Montpellier 2 (France)
11/2010	Visit to the group of M. Fromhold, School of Physics and Astronomy, University of Nottingham (UK)
11/2008	Visit to the Kavli Institute of Theoretical Physics, Santa Barbara (USA)

Grants and awards

2021 - 2024	PI of ANR (French national funding agency) *NearHeat* (two laboratories involved, total funding 319 k€, 3 years starting from March 2021)
2018	Fulbright Visiting Scholar Fellowship, French - American Fulbright commission (6 k€).
2018 - 2020	PICS (*Projet International de Coopération Scientifique*) project ("Many-body effects in near-field radiative heat-transfer and coupling with conduction"), CNRS (21 k€, 3 years).
2017	Funding for a 2-month visiting-sholar position to Princeton University, Laboratoire Charles Coulomb, Montpellier (5 k€).
2015 - 2018	PEDR (*Prime d'encadrement doctoral et de recherche*), CNRS (4 years).
2007	*Gugino* prize for the best master thesis in Mathematics and Physics, Università degli Studi di Palermo.

Conference organization

2022 — Chair of the conference *Eurotherm Seminar 114 - Nanoscale and Microscale Heat Transfer VII*, Palermo (Italy).

2018 — Chair of the conference *Eurotherm Seminar 111 - Nanoscale and Microscale Heat Transfer VI*, 2 - 7 December, Levi (Finland).

2015 — Organization of the special session *Advances in Diffraction Gratings Theories* at the conference PIERS 2015, 5 - 9 July, Prague (Czech Republic).

Invited talks

Montpellier (France) — **Université de Montpellier**

13 January 2020 — R. Messina, *Near-field radiative heat transfer: surface-assisted amplification and coupling with mechanical motion*

Rome (Italy) — **PIERS 2019, special session *Fluctuational electrodynamics and heat transfer***

17 - 20 June 2019 — R. Messina, S.-A. Biehs, T. Ziehm, A. Kittel, and P. Ben-Abdallah, *Heat transfer between two metals through subnanometric vacuum gaps*

Cancun (Mexico) — **XXVIII IMRC 2018, special session *Heat Transfer at the Nanoscale***

18 - 23 August 2018 — R. Messina, *Surface-mode assisted amplification of radiative heat transfer between nanoparticles*

Oldenburg (Germany) — **Institut für Physik, Carl von Ossietzky Universität**

29 June 2017 — R. Messina, *Radiative heat transfer in the presence of temperature gradients: new asymptotic laws and coupling with conduction*

Paris (France)	**Institut Langevin**
20 September 2016	R. Messina, *Transfert radiatif de chaleur en présence de gradients de température : nouvelles lois asymptotiques et couplage avec conduction*
Prague (Czech Republic)	**PIERS 2015, special session *Casimir Effect and Heat Transfer***
5 - 9 July 2015	R. Messina, P. A. Maia Neto, B. Guizal, and M. Antezza, *Casimir interaction between a sphere and a grating*
Los Alamos (USA)	**Quantum Lunch Seminar at Los Alamos National Laboratory**
16 April 2015	R. Messina, *Momentum and energy transfer out of thermal equilibrium: three-body and nanostructuring effects*
Guangzhou (China)	**PIERS 2014, special session *Casimir Effect and Heat Transfer***
24 - 28 August 2014	R. Messina, A. Noto, B. Guizal, and M. Antezza, *Non-equilibrium Casimir-Lifshitz force between dielectric gratings*
Les Houches (France)	**Casimir Physics**
30 March - 4 April 2014	R. Messina and M. Antezza, *Three-body radiative heat transfer and Casimir-Lifshitz force out of thermal equilibrium for arbitrary bodies*
Sharjah (United Arab Emirates)	**META'13**
19 - 22 March 2013	R. Messina and P. Ben-Abdallah, *Near-field optical properties of graphene-based heterosystems: application to thermophotovoltaic energy conversion*
Montpellier (France)	**13èmes Journées de la Matière Condensée, special session *Transfert de chaleur et forces optiques aux échelles nanométriques***
27 - 31 August 2012	R. Messina, M. Antezza, and P. Ben-Abdallah, *Energy and momentum transfer in three-body systems*

San Feliu de Guixols (Spain)	**Phonons and Fluctuations 3**
21 - 24 May 2012	R. Messina, M. Antezza, and P. Ben-Abdallah, *Near-field heat transfer in three-body systems*
Paris (France)	**META'12, special session *Quantum metamaterials***
19 - 22 April 2012	R. Messina, M. Antezza, and P. Ben-Abdallah, *Near-field heat transfer in three-body systems*
Montpellier (France)	**Laboratoire Charles Coulomb, Université de Montpellier 2**
11 April 2011	R. Messina and M. Antezza, *Force de Casimir et transfert de chaleur hors équilibre thermique*
Nottingham (UK)	**University of Nottingham**
17 November 2010	R. Messina, *Scattering approach to dispersive atom - surface interactions*
Bertinoro (Italy)	**Open Problems in Quantum Mechanics**
3 - 7 December 2007	R. Messina and R. Passante, *Casimir - Polder interaction between a neutral atom and conducting surfaces: fluctuations and different geometries*

Contributed talks

Lille (France)	**Thermal NanoSciences and NanoEngineering**
23 - 24 November 2017	R. Messina, A. Noto, B. Guizal, and M. Antezza, *Radiative heat transfer between metallic gratings using Fourier modal method with adaptive spatial resolution*
Santorini (Greece)	**Eurotherm 108 - Nanoscale and Microscale Heat Transfer V**
26 - 30 September 2016	R. Messina, W. Jin, and A. W. Rodriguez, *Strongly coupled near-field radiative and conductive heat transfer*

Bordeaux (France)	**15èmes Journées de la Matière Condensée, special session *Nanoconduction and Nanoradiation***
22 - 26 August 2016	R. Messina, W. Jin, and A. W. Rodriguez, *Strongly coupled near-field radiative and conductive heat transfer between planar objects*
Palermo (Italy)	**FisMat 2015, special session *Quantum Fluctuations and Casimir Forces***
28 September - 2 October 2015	R. Messina, P. A. Maia Neto, B. Guizal, and M. Antezza, *Casimir interaction between a sphere and a grating*
Poitiers (France)	**Eurotherm 91, Microscale Heat Transfer III**
29 - 31 August 2011	R. Messina and M. Antezza, *Scattering - matrix approach to heat transfer and Casimir - Lifshitz force between arbitrary bodies*
Paris (France)	**Gravitation and Fundamental Physics in Space**
22 - 24 June 2010	R. Messina, D. A. R. Dalvit, P. A. Maia Neto, A. Lambrecht, and S. Reynaud, *Scattering approach to dispersive atom - surface interactions*
Turku (Finland)	**Central European Workshop on Quantum Optics**
23 - 27 May 2009	R. Messina, D. A. R. Dalvit, P. A. Maia Neto, A. Lambrecht, and S. Reynaud, *Scattering approach to dispersive atom - surface interactions*
Palermo (Italy)	**Central European Workshop on Quantum Optics**
1 - 5 June 2007	R. Messina and R. Passante, *Casimir – Polder force density between an atom and a conducting plate*

Poster contributions

La Thuile (Italy)	**Gravitation and Fundamental Physics in Space**
20 - 27 March 2011	R. Messina, S. Pelisson, M.-C. Angonin, and P. Wolf, *Atomic states in optical traps near a planar surface*

Les Houches (France)	**Casimir, van der Waals, and nanoscale interactions**
11 - 16 April 2010	R. Messina, D. A. R. Dalvit, P. A. Maia Neto, A. Lambrecht, and S. Reynaud, *Dispersive interactions between atoms and non planar surfaces*
Santa Fe (USA)	**New Frontiers in Casimir Force Control**
27 - 29 September 2009	R. Messina, D. A. R. Dalvit, P. A. Maia Neto, A. Lambrecht, and S. Reynaud, *Dispersive interactions between atoms and non planar surfaces*
Norman (USA)	**Quantum Field Theory under the Influence of External Conditions 2009**
21 - 25 September 2009	R. Messina, D. A. R. Dalvit, P. A. Maia Neto, A. Lambrecht, and S. Reynaud, *Dispersive interactions between atoms and non planar surfaces*

Referee activity for scientific funding agencies

ANR (Agence Nationale de la Recherche, French Research Foundation)
DFG (Deutsche Forschungsgemeinschaft, German Research Foundation)

Referee activity for peer-reviewed international journals

Nature Photonics, Nature Communications, Physical Review Letters, A, B, D, E and Applied, ACS Photonics, Optics Express, Optica, Nanoscale Horizons, Mathematics, Journal of the Optical Society of America B, Scientific Reports, Journal of Quantitative Spectroscopy and Radiative Transfer, ASME Journal of Heat Transfer, International Journal of Heat and Mass Transfer, Europhysics Letters, The European Physical Journal D, Nanoscale and Microscale Thermophysical Engineering, Materials, Physica Scripta, Proceedings of the Royal Society A, Physics Letters A, Journal of Physics D: Applied Physics, The Journal of Chemical Physics, Physical Chemistry Chemical Physics, International Journal of Nanotechnology

Publications on peer - reviewed international journals

[1] M. Wang, L. Tang, C. Y. Ng, R. Messina, B. Guizal, J. A. Crosse, M. Antezza, C. T. Chan, and H. B. Chan, *Strong geometry dependence of the Casimir force between interpenetrated rectangular gratings*, Nat. Commun. **12**, 600 (2021).

[2] M. Reina, R. Messina, and P. Ben-Abdallah, *Conduction-Radiation Coupling between Two Closely Separated Solids*, Phys. Rev. Lett. **125**, 224302 (2020).

[3] P. S. Venkataram, R. Messina, J. C. Cuevas, P. Ben-Abdallah, and A. W. Rodriguez, *Mechanical relations between conductive and radiative heat transfer*, Phys. Rev. B **102**, 085404 (2020).

[4] I. Latella, R. Messina, S.-A. Biehs, J. M. Rubi, and P. Ben-Abdallah, *Saturation of radiative heat transfer due to many-body thermalization*, Sci. Rep. **10**, 8938 (2020).

[5] R. Messina and P. Ben-Abdallah, *Many-body near-field radiative heat pumping*, Phys. Rev. B **101**, 165435 (2020).

[6] C. Kathmann, M. Reina, R. Messina, P. Ben-Abdallah, and S.-A. Biehs, *Scalable radiative thermal logic gates based on nanoparticle networks*, Sci. Rep. **10**, 3596 (2020).

[7] M. Reina, R. Messina, S.-A. Biehs, and P. Ben-Abdallah, *Thermomechanical bistability of phase-transition oscillators driven by near-field heat exchange*, Phys. Rev. B **101**, 041409(R) (2020).

[8] M. Antezza, H. B. Chan, B. Guizal, V. Marachevsky, R. Messina, and M. Wang, *Giant Casimir Torque between Rotated Gratings and the $\theta = 0$ Anomaly*, Phys. Rev. Lett. **124**, 013903 (2020).

[9] A. Ott, R. Messina, P. Ben-Abdallah, and S.-A. Biehs, *Radiative thermal diode driven by nonreciprocal surface waves*, Appl. Phys. Lett. **114**, 163105 (2019).

[10] A. Ott, R. Messina, P. Ben-Abdallah, and S.-A. Biehs, *Magnetothermoplasmonics: from theory to applications*, J. Photon. Energy **9**, 032711 (2019).

[11] C. Kathmann, R. Messina, P. Ben-Abdallah, and S.-A. Biehs, *Limitations of kinetic theory to describe near-field heat exchanges in many-body systems*, Phys. Rev. B **98**, 115434 (2018).

[12] I. Latella, R. Messina, J. M. Rubi, and P. Ben-Abdallah, *Radiative Heat Shuttling*, Phys. Rev. Lett. **121**, 023903 (2018).

[13] C. Khandekar, R. Messina, and A. W. Rodriguez, *Near-field refrigeration and tunable heat exchange through four-wave mixing*, AIP Advances **8**, 055029 (2018).

[14] R. Messina, S.-A. Biehs, and P. Ben-Abdallah, *Surface-mode-assisted amplification of radiative heat transfer between nanoparticles*, Phys. Rev. B **97**, 165437 (2018).

[15] I. Latella, S.-A. Biehs, R. Messina, A. W. Rodriguez, and P. Ben-Abdallah, *Ballistic near-field heat transport in dense many-body systems*, Phys. Rev. B **97**, 035423 (2018).

[16] R. Messina, P. Ben-Abdallah, B. Guizal, and M. Antezza, *Graphene-based amplification and tuning of near-field radiative heat transfer between dissimilar polar materials*, Phys. Rev. B **96**, 045402 (2017).

[17] W. Jin, R. Messina, and A. W. Rodriguez, *Overcoming limits to near-field radiative heat transfer in uniform planar media through multilayer optimization*, Opt. Express **25**, 14746 (2017).

[18] I. Latella, P. Ben-Abdallah, S.-A. Biehs, M. Antezza, and R. Messina, *Radiative heat transfer and nonequilibrium Casimir-Lifshitz force in many-body systems with planar geometry*, Phys. Rev. B **95**, 205404 (2017).

[19] W. Jin, R. Messina, and A. W. Rodriguez, *General formulation of coupled radiative and conductive heat transfer between compact bodies*, Phys. Rev. B **95**, 161409(R) (2017).

[20] R. Messina, A. Noto, B. Guizal, and M. Antezza, *Radiative heat transfer between metallic gratings using Fourier modal method with adaptive spatial resolution*, Phys. Rev. B **95**, 125404 (2017).

[21] W. Jin, R. Messina, and A. W. Rodriguez, *Near-Field Radiative Heat Transfer under Temperature Gradients and Conductive Transfer*, Z. Naturforsch. A **72**, 141 (2017).

[22] P. Doyeux, R. Messina, B. Leggio, and M. Antezza, *Excitation injector in an atomic chain: Long-range transport and efficiency amplification*, Phys. Rev. A **95**, 012138 (2017).

[23] R. Messina, W. Jin, and A. W. Rodriguez, *Exact formulas for radiative heat transfer between planar bodies under arbitrary temperature profiles: Modified asymptotics and sign-flip transitions*, Phys. Rev. B **94**, 205438 (2016).

[24] R. Messina, W. Jin, and A. W. Rodriguez, *Strongly coupled near-field radiative and conductive heat transfer between planar bodies*, Phys. Rev. B **94**, 121410(R) (2016).

[25] R. Messina, P. Ben-Abdallah, B. Guizal, M. Antezza, and S.-A. Biehs, *Hyperbolic waveguide for long-distance transport of near-field heat flux*, Phys. Rev. B **94**, 104301 (2016).

[26] N. Bartolo, R. Messina, D. A. R. Dalvit, and F. Intravaia, *Nonequilibrium Casimir-Polder plasmonic interactions*, Phys. Rev. A **93**, 042111 (2016).

[27] P. Doyeux, B. Leggio, R. Messina, and M. Antezza, *Quantum thermal machine acting on a many-body quantum system: Role of correlations in thermodynamic tasks*, Phys. Rev. E **93**, 022134 (2016).

[28] R. Messina, P. A. Maia Neto, B. Guizal, and M. Antezza, *Casimir interaction between a sphere and a grating*, Phys. Rev. A **92**, 062504 (2015).

[29] B. Leggio, P. Doyeux, R. Messina, and M. Antezza, *Distributed thermal tasks on many-body systems through a single quantum machine*, Europhys. Lett. **112**, 40004 (2015).

[30] B. Leggio, R. Messina, and M. Antezza, *Thermally activated nonlocal amplification in quantum energy transport*, Europhys. Lett. **110**, 40002 (2015).

[31] A. Noto, R. Messina, B. Guizal, and M. Antezza, *Casimir-Lifshitz force out of thermal equilibrium between dielectric gratings*, Phys. Rev. A **90**, 022120 (2014).

[32] R. Messina and M. Antezza, *Three-body radiative heat transfer and Casimir-Lifshitz force out of thermal equilibrium for arbitrary bodies*, Phys. Rev. A **89**, 052104 (2014).

[33] P. Ben-Abdallah, R. Messina, S.-A. Biehs, M. Tschikin, K. Joulain, and C. Henkel, *Heat Superdiffusion in Plasmonic Nanostructure Networks*, Phys. Rev. Lett. **111**, 174301 (2013).

[34] R. Messina, M. Tschikin, S.-A. Biehs, and P. Ben-Abdallah, *Fluctuational-electrodynamic theory and dynamics of heat transfer in multiple dipolar systems*, Phys. Rev. B **88**, 104307 (2013).

[35] M. Tschikin, S.-A. Biehs, R. Messina, and P. Ben-Abdallah, *On the limits of the effective description of hyperbolic materials in presence of surface waves*, J. Opt. **5**, 105101 (2013).

[36] S. Pelisson, R. Messina, M.-C. Angonin, et P. Wolf, *Lifetimes of atoms trapped in an optical lattice in proximity of a surface*, Phys. Rev. A **88**, 013411 (2013).

[37] S.-A. Biehs, M. Tschikin, R. Messina, and P. Ben-Abdallah, *Super-Planckian Near-Field Thermal Emission with Phonon-Polaritonic Hyperbolic Metamaterials*, Appl. Phys. Lett. **102**, 131106 (2013).

[38] R. Messina and P. Ben-Abdallah, *Graphene-based photovoltaic cells for near-field thermal energy conversion*, Sci. Rep. **3**, 1383 (2013).

[39] R. Messina, J.-P. Hugonin, J.-J. Greffet, F. Marquier, Y. De Wilde, A. Belarouci, L. Frechette, Y. Cordier, and P. Ben-Abdallah, *Tuning the electromagnetic local density of states in graphene-covered systems via strong coupling with graphene plasmons*, Phys. Rev. B **87**, 085421 (2013).

[40] B. Bellomo, R. Messina, D. Felbacq, and M. Antezza, *Quantum systems in a stationary environment out of thermal equilibrium*, Phys. Rev. A **87**, 012101 (2013).

[41] R. Messina, M. Antezza, and P. Ben-Abdallah, *Three-body amplification of photon heat tunneling*, Phys. Rev. Lett. **109**, 244302 (2012).

[42] B. Bellomo, R. Messina, and M. Antezza, *Dynamics of an elementary quantum system in environments out of thermal equilibrium*, Europhys. Lett. **100**, 20006 (2012).

[43] S. Pelisson, R. Messina, M.-C. Angonin, and P. Wolf, *Dynamical aspects of atom interferometry in an optical lattice in proximity to a surface*, Phys. Rev. A **86**, 013614 (2012).

[44] R. Messina and M. Antezza, *Scattering - matrix approach to Casimir - Lifshitz force and heat transfer out of thermal equilibrium between arbitrary bodies*, Phys. Rev. A **84**, 042102 (2011).

[45] R. Messina and M. Antezza, *Casimir - Lifshitz force out of thermal equilibrium and heat transfer between arbitrary bodies*, Europhys. Lett. **95**, 61002 (2011).

[46] R. Messina, S. Pelisson, M.-C. Angonin, and P. Wolf, *Atomic states in optical traps near a planar surface*, Phys. Rev. A **83**, 052111 (2011).

[47] R. Messina, R. Vasile, and R. Passante, *Dynamical Casimir - Polder force on a partially dressed atom near a conducting wall*, Phys. Rev. A **82**, 062501 (2010).

[48] G. Moreno, R. Messina, D. A. R. Dalvit, A. Lambrecht, P. A. Maia Neto, and S. Reynaud, *Disorder in Quantum Vacuum: Casimir - Induced Localization of Matter Waves*, Phys. Rev. Lett. **105**, 210401 (2010).

[49] S. Reynaud, A. Canaguier-Durand, R. Messina, A. Lambrecht, and P. A. Maia Neto, *The scattering approach to the Casimir force*, Int. J. Mod. Phys. **25**, 2201 (2010).

[50] R. Messina, D. A. R. Dalvit, P. A. Maia Neto, A. Lambrecht, and S. Reynaud, *Dispersive interactions between atoms and nonplanar surfaces*, Phys. Rev. A **80**, 022119 (2009).

[51] R. Vasile, R. Messina, and R. Passante, *Time - dependent Maxwell field operators and field energy density for an atom near a conducting wall*, Phys. Rev. A **79**, 062106 (2009).

[52] R. Messina, R. Passante, L. Rizzuto, S. Spagnolo, and R. Vasile, *Casimir - Polder forces, boundary conditions and fluctuations*, J. Phys. A: Math. Theor. **41**, 164031 (2008).

[53] R. Messina and R. Passante, *Fluctuations of the Casimir - Polder force between an atom and a conducting wall*, Phys. Rev. A **76**, 032107 (2007).

[54] R. Messina, M. A. Jivulescu, A. Messina, and A. Napoli, *Riccati equation - based generalization of Dawson's integral function*, Math. Meth. Appl. Sci. **30**, 2055 (2007).

[55] R. Messina and R. Passante, *Casimir - Polder force density between an atom and a conducting wall*, Phys. Rev. A **75**, 042113 (2007).

[56] R. Messina, A. Napoli, and A. Messina, *Unitary Transfer of Entanglement in Multipartite Two - Level Systems*, Acta Phys. Hung. B **23**, 75 (2005).

Conference proceedings

[1] R. Messina, R. Passante, L. Rizzuto, S. Spagnolo, and R. Vasile, *Dynamical Casimir-Polder potentials in non-adiabatic conditions*, Phys. Scripta **T160**, 014032 (2014).

[2] S.-A. Biehs, M. Tschikin, R. Messina, and P. Ben-Abdallah, *Super-Planckian near-field heat transfer*, 7th International Congress on Advanced Electromagnetic Materials in Microwaves and Optics (METAMATERIALS), 560 (2013).

[3] R. Messina, S. Pelisson, M.-C. Angonin, and P. Wolf, *Modification of atomic states in a vertical optical trap near a surface*, in *Proceedings of the 46th Rencontres de Moriond and GPhyS Colloquium on Gravitational Waves and Experimental Gravity* (The Gioi Publishers, Hanoi, 2011), p. 447

[4] S. Pelisson, R. Messina, M.-C. Angonin, and P. Wolf, *Observability of short-range gravitation with the experiment FORCA-G*, in *Proceedings of the 46th Rencontres de Moriond and GPhyS Colloquium on Gravitational Waves and Experimental Gravity* (The Gioi Publishers, Hanoi, 2011), p. 347

[5] B. Pelle, G. Tackmann, Q. Beaufils, X. Wang, A. Hilico, F. Pereira Dos Santos, S. Pelisson, R. Messina, M.-C. Angonin, and P. Wolf, *Forca-G: A trapped atom interferometer for the measurement of short range forces*, in *Proceedings of the 46th Rencontres de Moriond and GPhyS Colloquium on Gravitational Waves and Experimental Gravity* (The Gioi Publishers, Hanoi, 2011), p. 237

[6] M. N. A. Halif, R. Messina, and M. Fromhold, *Calculation of the Casimir - Polder interaction between Bose - Einstein condensates and microengineered surfaces: a pairwise summation approach*, J. Phys.: Conf. Ser. **286**, 012405 (2011).

Popular science

[1] R. Messina, *Sharing Heat in the Near Field*, Physics **8**, 109 (2015).

Books

[1] C. Trapani and R. Messina, *Esercizi di Analisi uno* (Aracne, 2004).

CHAPTER 2

PhD and postdoctoral activity

2.1 Introduction

The aim of this chapter is to provide a brief overview of my research activity before being hired at CNRS in October 2013. The three following sections are dedicated to my PhD, to my first and second postdoc, respectively.

2.2 PhD activity

I did my PhD between 2007 and 2009 and defended my thesis in April 2010. On the basis of a formal agreement between the two institutions, my PhD was shared between Laboratoire Kastler Brossel (Paris, France) and Università di Palermo (Palermo, Italy), with the double supervision of Astrid Lambrecht and Roberto Passante. My activity was focused on the Casimir-Polder force between an atom and a surface, and resulted in the publication of two articles [113, 114].

The first one [113] deals with the study of the modification of the atom-surface force due to the presence of a periodic corrugation. The key point in this work is the introduction of a perturbative treatment of the corrugation, allowing to express the correction to the reflection operator of the corrugated surface as a simple closed-form expression up to the first order in the corrugation amplitude, following the approach presented in Refs. [115–117]. This has allowed to express the correction to the energy (and thus to the force) as a simple expression directly involving a response function $g(k, z)$, along with the Fourier transform of the corrugation profile. We have shown that it is possible to express this response function as a product of three terms

$$g(k, z) = \rho(k, z)\eta_F F_{\mathrm{CP}}^{(0)}, \tag{2.2.1}$$

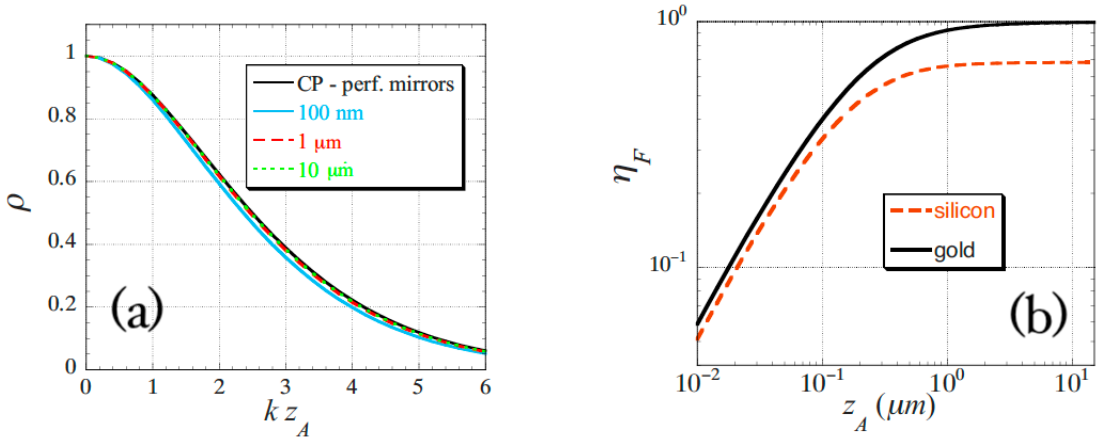

Figure 2.1 : (a) Geometry correction factor ρ as a function of kz_A for a silicon surface and several atom - surface distances. The black line corresponds to the ideal Casimir - Polder result. (b) Correction of the normal dispersive force between a Rb ground-state atom and a plane gold or silicon surface as a function of the separation distance z_A. From Ref. [113].

where $F_{\rm CP}^{(0)}$ is the well-known force between an atom and a perfect conductor, $\rho(k,z)$ describes the deviation due to the presence of the corrugation, while η_F accounts for the correction due to real materials. As shown in Fig. 2.1, these corrections can take values significantly different from 1 even for reasonable values of the geometrical parameters (see Ref. [113] for more details).

Our second work [114] concerned the time evolution of the Casimir - Polder force between an atom and a perfectly conducting wall during the dynamical dressing of the atom. As a matter of fact, the bare ground state of the system (product of the atomic and field ground states) is not an eigenstate of the full system, and the actual ground state of the system (the dressed state) can be obtained by using perturbation theory on the atom - field interaction Hamiltonian term. By solving the Heisenberg equations for all field operators, we were able to calculate the time evolution of the Casimir energy and force when the system starts its evolution from a partially dressed state. This configuration could be experimentally realized by switching on an electric field at a given time t_0, producing a rapid modification of the atomic transition frequency from ω_0 to ω_0', and thus a modification of the fully dressed state. More details can be found in Ref. [114].

2.3 Postdoctoral research at SYRTE laboratory

This section concerns the results I obtained during my first postdoc (2010 and 2011) at SYRTE laboratory, belonging to Observatoire de Paris, under the supervision of Peter Wolf and Marie-

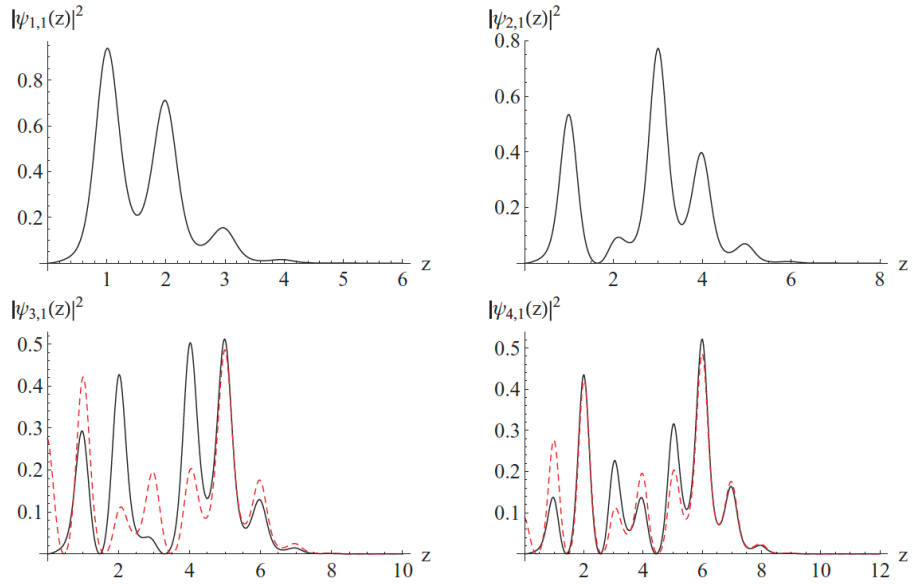

Figure 2.2 : Density probability of modified Wannier - Stark states for $n = 1, 2, 3, 4$. The last two functions (black, solid line) are compared to the corresponding standard Wannier-Stark state (red, dashed line). From Ref. [119].

Christine Angonin. The main purpose of this postdoc was to model theoretically the experiment FORCA-G (*FORce de CAsimir et Gravitation à courte distance*), under design and preparation at that time at SYRTE [118]. The aim of this experiment was to investigate possible deviations from the Newton law of gravitation at small distances ($z < 100\,\mu$m). According to many theories of unification of general relativity and quantum mechanics, this correction is often modelized by means of a Yukawa-type potential

$$V(z) = \frac{GMm}{z}(1 + \alpha_Y e^{-z/\lambda_Y}), \tag{2.3.1}$$

added to the standard Newtonian one, where G is the gravitational constant and m and M the masses of the two particles. In this expression, α_Y and λ_Y are two parameters introduced to characterize the relative strength of the corrective potential and its typical range, respectively. The aim of experiments focusing on this possible deviation is to impose new limits on the allowed values for α_Y and λ_Y.

In the FORCA-G experiment, interferometric techniques are combined with a trapping potential. This is generated by a vertical standing optical wave produced by the reflection of a laser on a mirror. The vertical configuration leads to an external potential on the atom given by the sum of the optical one and a linear gravitational term due to the Earth: this deviation from a purely periodical potential produces a localization of the atomic wave packet, corresponding to

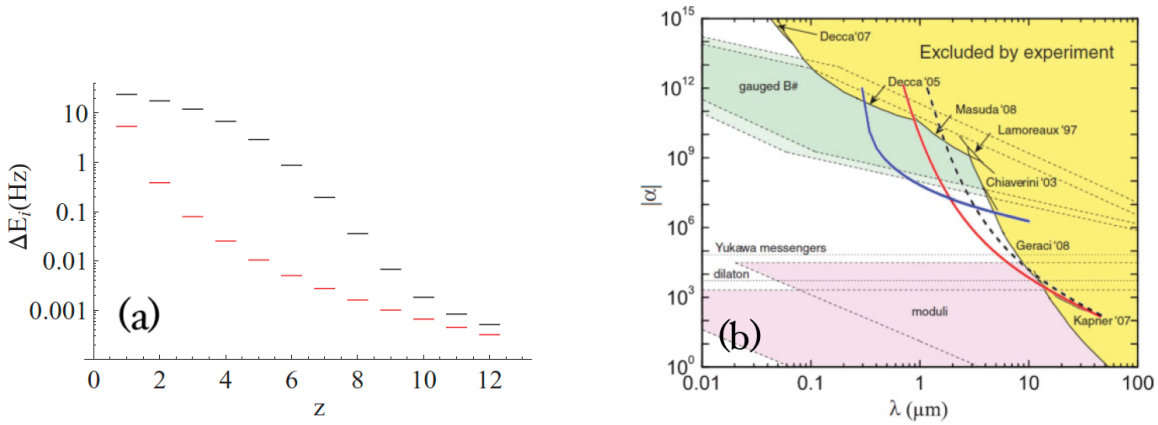

Figure 2.3 : (a) Absolute value expressed in Hertz of the Casimir - Polder energy correction, compared to the Casimir - Polder potential evaluated at the well center (red lower ticks). (b) In yellow are displayed the regions of the (α_Y, λ_Y) plane excluded by experiments. The three superposed curves represent the experimental constraints theoretically calculated for the experiment FORCA-G. They correspond to the near regime, using a superposition between wells $n = 4$ and $n = 6$ (blue solid line, first from the left), the far regime for $n = 40$ (red solid line), and for $n = 70$ (black dashed line). From Ref. [119].

the transition from Bloch to Wannier-Stark states [120]. Moreover the proximity of the trapped atoms to the surface makes an accurate knowledge of the Casimir-Polder force at each atomic site essential.

In our first work on this topic [119], we diagonalized the system Hamiltonian and calculated the atomic wave function in the presence of the surface. Since the perfect periodicity is broken in this configuration, the first atomic wave functions differ from the well-known Wannier - Stark wave functions. This can be seen in Fig. 2.2, where the 4 first wave functions are represented. As a result, we were able to calculate the energy shift due to the Casimir - Polder interaction, calculated by exploiting the knowledge of each wave function. We stressed that the result obtained differs considerably [see Fig. 2.3(a)] from the simple evaluation of the Casimir - Polder energy at the center of each well. Finally, this has allowed us to predict the further regions of the (α_Y, λ_Y) plane that the experiment FORCA-G could exclude [see Fig. 2.3(b)].

Two further works [121, 122] were dedicated to the study of the dynamical aspects of the experiment. In particular in the first article [121] was focused on the optimization of the interferometric path to be chosen in order to maximize the observed contrast. Finally, the second article [122] concerned the lifetime of the atomic states in proximity of the surface, and how these are influenced by a possible deviation from Newton's law of gravitation.

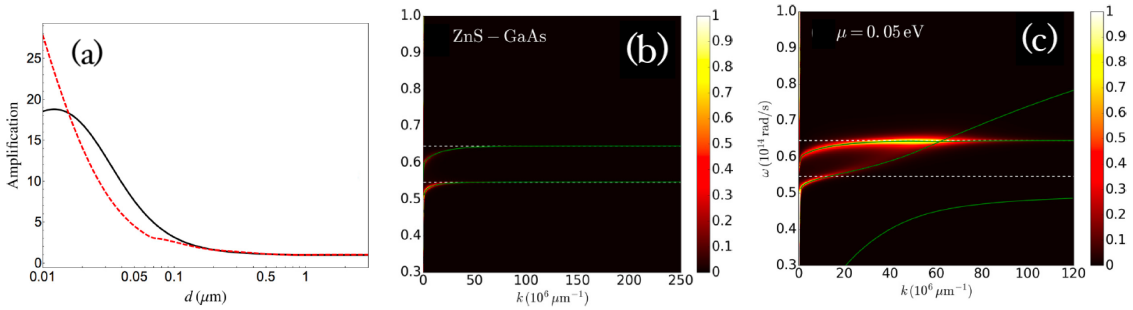

Figure 2.4 : (a) Radiative-heat-flux amplification factor with respect to the graphene chemical potential μ as a function of the distance d. The red dashed curve corresponds to the ratio between the highest and lowest values of the flux in the presence of graphene, while the black curve corresponds to the ratio between the highest value of the flux in the presence of graphene and the flux in the ZnS-GaAs configuration without graphene. (b) Landauer transmission coefficient [measuring the contribution of each mode (ω, k) to the energy exchange] in the ZnS - GaAs configuration. (c) Landauer transmission coefficient in the presence of graphene (chemical potential $\mu = 0.05\,\mathrm{V}$) for $d = 20\,\mathrm{nm}$ in TM polarization. The horizontal lines correspond to the resonance frequencies of GaAs and ZnS. The green lines describe the dispersion relation of the cavity surface modes. From Ref. [123].

2.4 Postdoctoral research at Laboratoire Charles Fabry

This last section concerns my second postdoc (2012 and 2013) at Laboratoire Charles Fabry, under the supervision of Philippe Ben-Abdallah. At this moment I had my first contact with the new topic of near-field radiative heat transfer. Some of the preliminary results on many-body effects were obtained during these two years. Nevertheless, for a better readability, these will be described in the second part of the manuscript.

Among the results obtained during this postdoc, I will briefly focus here on three articles concerning the possibilities offered by graphene in the domain of near-field effects. In a first article [124], we studied the local density of states (LDOS) of the electromagnetic field in proximity of a silicon carbide (SiC) substrate covered by a graphene sheet. We proved that a strong coupling exists between the phonon-polariton supported by the SiC substrate and the plasmon supported by the graphene sheet. This allows to manipulate the spectral properties of the electromagnetic LDOS by acting on the graphene chemical potential and could find application in the field of near-field energy harvesting (spectral matching between the source and the cell).

This idea of manipulation of surface modes was exploited in another work [123] (realized during the postdoc and published some years later) in order to increase the the near-field flux between two semi-infinite planar bodies made of different materials (zinc sulfide, ZnS and gallium arsenide, GaAs). As a matter of fact, it is well known that near-field radiative heat flux is

strongly amplified in the presence of resonant surface modes (in the simple scenario of identical materials), but strongly decreases in the presence of a shift between the resonant modes of the two bodies. By covering the GaAs substrate with a graphene sheet and modulating its chemical potential, we exploited the strong coupling predicted before and obtained a crossing between the dispersion relations of the two bodies (ZnS substrate and graphene-covered GaAs substrate), resulting in a strong amplification of the flux, of more than an order of magnitude (see Fig. 2.4).

Finally, the properties of graphene were also studied in the context of a near-field thermophotovoltaic cell [125]. We showed that, by covering an indium antimonide (InSb) cell by a graphene sheet and considering a boron nitride (hBN) planar body as the source, the presence of graphene is able to enhance the coupling between them and thus produce an increase going up to 10%, if working at close distance $d = 16\,\text{nm}$ between source and cell (see Ref. [125]).

2.5 Publications concerned by this chapter

[113] R. Messina, D. A. R. Dalvit, P. A. M. Neto, A. Lambrecht, and S. Reynaud, *Dispersive interactions between atoms and non-planar surfaces*, Phys. Rev. A **80**, 022119 (2009).

[114] R. Messina, R. Vasile, and R. Passante, *Dynamical Casimir-Polder force on a partially dressed atom near a conducting wall*, Phys. Rev. A **82**, 062501 (2010).

[119] R. Messina, S. Pelisson, M.-C. Angonin, and P. Wolf, *Atomic states in optical traps near a planar surface*, Phys. Rev. A **83**, 052111 (2011).

[121] S. Pelisson, R. Messina, M.-C. Angonin, and P. Wolf, *Dynamical aspects of atom interferometry in an optical lattice in proximity to a surface*, Phys. Rev. A **86**, 013614 (2012).

[122] S. Pelisson, R. Messina, M.-C. Angonin, and P. Wolf, *Lifetimes of atoms trapped in an optical lattice in proximity of a surface*, Phys. Rev. A **88**, 013411 (2013).

[124] R. Messina, J.-P. Hugonin, J.-J. Greffet, F. Marquier, Y. De Wilde, A. Belarouci, L. Frechette, Y. Cordier, and P. Ben-Abdallah, *Tuning the electromagnetic local density of states in graphene-covered systems via strong coupling with graphene plasmons*, Phys. Rev. B **87**, 085421 (2013).

[123] R. Messina, P. Ben-Abdallah, B. Guizal, and M. Antezza, *Graphene-based amplification and tuning of near-field radiative heat transfer between dissimilar polar materials*, Phys. Rev. B **96**, 045402 (2017).

[125] R. Messina and P. Ben-Abdallah, *Graphene-based photovoltaic cells for near-field thermal energy conversion*, Sci Rep **3**, 1383 (2013).

Part II

Presentation of my research activity since 2013

CHAPTER 3

Scattering-matrix approach to Casimir force and radiative heat transfer

Contents

3.1 Introduction

This chapter concerns the development of a general approach to deal with Casimir forces and radiative heat transfer in the presence of bodies having arbitrary geometries and optical properties. The first work in this direction was done in collaboration with Mauro Antezza in 2011. Around that year, also motivated by the increasing number of experimental results, several other theoretical frameworks were introduced, some of them with the aim of treating Casimir forces only [42–46], some others for radiative heat transfer [93–98], while some accounting for both phenomena simultaneously [99–102], as the approach we are going to discuss in this chapter. Some years later, the approach was generalized to the case of three arbitrary bodies, and finally to a configuration involving an arbitrary number N of planar slabs. The results presented below were obtained in collaboration with M. Antezza, P. Ben-Abdallah., S.-A. Biers and I. Patella

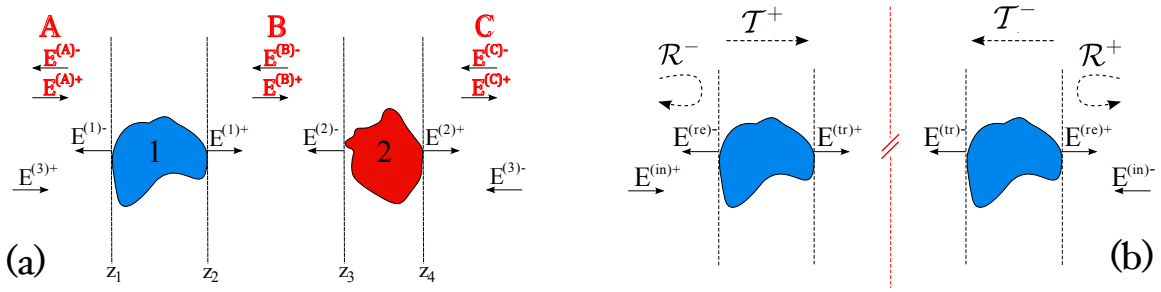

Figure 3.1 : (a) Geometry of the system: two bodies of arbitrary shape and optical properties, dividing the space in three regions. (b) Graphical definition of incident, reflected and transmitted fields, as well as scattering operators. From Ref. [126].

3.2 Two-body theory

The first step in the development of a general approach to treat Casimir forces and radiative heat transfer for arbitrary bodies was realized in the scenario of two interacting bodies, depicted in Fig. 3.1(a). Each body is described, both geometrically and optically, in terms of its reflection and transmission operators, whose definition is graphically given in Fig. 3.1(b). In this context, the two bodies are assumed to be at two different temperatures T_1 and T_2, kept constant by some external thermostat. Moreover, the entire system is supposed to be placed in an external environment, characterized by a third (in general different) temperature T_3. It is then clear that, while we restrict from the beginning our treatment to time-invariant configurations, we consider scenarios out of thermal equilibrium, which thus go beyond the applicability of the fluctuation-dissipation theorem. For this reason we need to introduce an important assumption, typically referred to as *local thermal equilibrium*. We assume that the fact of assigning to each individual body a given temperature T is equivalent to stating that the field it radiates coincides with the one the same body would radiate if it was at thermal equilibrium at the same temperature T. This key ingredient will allow us to explicitly derive the correlation functions of the field emitted by each body in the system, and thus of the total field in each region.

A specific feature of the approach described here is the explicit choice of the basis used to decompose the electromagnetic field. Here we have chosen a plane-wave basis, since it allows to express explicitly the scattering operators in several relevant geometries (plane, sphere, dipole,...) and thus to obtain closed-form expressions of the Casimir force and radiative heat transfer. We stress that this choice of basis imposes to limit our applications to geometries where the bodies are separated by a plane $z = z_0$ [see Fig. 3.1(a)]. Nevertheless, this condition is verified in the majority of experimental configurations (plane - plane, sphere - plane, atom - surface, ...).

From a more technical point of view, our purpose is to express the flux of the Pointing vector (giving the radiative heat transfer) and Maxwell's stress tensor (giving the Casimir force) under the form of a *generalized flux*

$$\varphi_m(\bar{z}) = \int_{z=\bar{z}} d^2\mathbf{r} \begin{cases} \langle S_z \rangle_{\text{sym}} & m = 1 \\ \langle T_{zz} \rangle_{\text{sym}} & m = 2 \end{cases} \tag{3.2.1}$$

where the index m allows to switch between the two expressions. We have shown in Refs. [126, 127] that this can be cast under the form

$$\varphi_m(\bar{z}) = (-1)^{m+1} 2\epsilon_0 c^2 \sum_p \int \frac{d^2\mathbf{k}}{(2\pi)^2} \left(\sum_{\phi=\phi'} \int_{ck}^{+\infty} \frac{d\omega}{2\pi} + \sum_{\phi\neq\phi'} \int_0^{ck} \frac{d\omega}{2\pi} \right) \left(\frac{\phi k_z}{\omega} \right)^m \langle p, \mathbf{k} | C^{\phi\phi'} | p, \mathbf{k} \rangle, \tag{3.2.2}$$

where the quantity $\langle p, \mathbf{k} | C^{\phi\phi'} | p, \mathbf{k} \rangle$ is defined by the relation

$$\begin{aligned} \langle E_p^{\phi}(\mathbf{k}, \omega) E_{p'}^{\phi'\dagger}(\mathbf{k}', \omega') \rangle_{\text{sym}} &= \frac{1}{2} \langle E_p^{\phi}(\mathbf{k}, \omega) E_{p'}^{\phi'\dagger}(\mathbf{k}', \omega') + E_{p'}^{\phi'\dagger}(\mathbf{k}', \omega') E_p^{\phi}(\mathbf{k}, \omega) \rangle \\ &= 2\pi\delta(\omega - \omega') \langle p, \mathbf{k} | C^{\phi\phi'}(\omega) | p', \mathbf{k}' \rangle, \end{aligned} \tag{3.2.3}$$

as the monochromatic correlation function of the electric field. The simple form of this expression highlights the common origin of Casimir forces and radiative heat transfer in terms of field fluctuations, as well as the convenience of treating them under a common framework.

Equation (3.2.2) makes apparent that the quantity we need is the correlation function $\langle p, \mathbf{k} | C^{\phi\phi'} | p, \mathbf{k} \rangle$ of the total field in each region. Referring to Refs. [126, 127] for the details, here we only describe the main steps leading to the knowledge of this quantity. These steps can be summarized as follows:

1. The fields generated by the fluctuating charges inside each body are identified as the source fields, along with the environmental field in which the system is immersed.

2. The correlation functions of the individual source fields are deduced from the assumption of local thermal equilibrium.

3. The total field in each region is explicitly written, in terms of the source fields, as a result of the scattering (reflection and transmission) processes occurring due to the presence of the bodies.

4. The correlation functions of the total field in each region can be deduced.

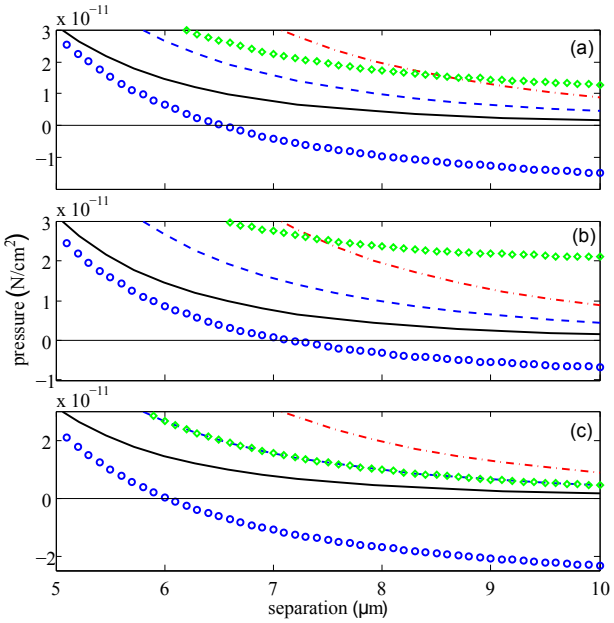

Figure 3.2 : Casimir pressure acting on a $\delta_1 = 2\,\mu$m thick slab (body 1, fused silica) parallel to a $\delta_2 = 1000\,\mu$m thick slab (body 2, silicon). Lines: equilibrium pressures at $T = 0\,$K (black solid), 300 K (blue dashed), 600 K (red dash-dotted). Symbols: non-equilibrium pressures, $T_3 = 0\,$K (blue circles), 300 K (green diamonds), 600 K (magenta plus), with $T_1 = 300\,$K and $T_2 = 0\,$K in (a), $T_1 = 0\,$K and $T_2 = 300\,$K in (b), $T_1 = T_2 = 300\,$K in (c). From Ref. [126].

Without giving here the explicit results for the Casimir force and radiative heat transfer, we present one example of application in the case of Casimir forces. We show in Fig. 3.2 the Casimir pressure between two slabs made of fused silica and having different thickness, placed in an external bath, for different choices of the three temperatures in the system. The solid, dashed and dot-dashed lines correspond to the results at thermal equilibrium ($T_1 = T_2 = T_3$) at different temperatures. As it is well known, the pressure in this scenario is always attractive (positive in our sign convention) for any separation distance and varies with temperature. As the figure clearly shows, the situation changes when a non-equilibrium configuration is considered. In particular, we clearly see that for low environmental temperatures (blue circles), we observe a transition from attraction to repulsion, implying also the existence of an unstable equilibrium position. While a precise design of a configuration for the experimental observation of repulsion in a macroscopic system was out of the scope of our work, these results showed that this is definitely within experimental reach, in particular observing that the transition takes place at a distance between 6 and 7 μm.

3.3 Three-body theory

The development of a general two-body theory served as a first step towards the exploration of many-body effects in Casimir forces and radiative heat transfer. As a matter of fact, some years later the same approach and theory was generalized to the case of three arbitrary bodies [128]. We must stress here that, among the theoretical frameworks developed during the same years and mentioned above, some are indeed in principle able to deal with a many-body scenario. Nevertheless, the final expressions given in these works are often compact and thus show less clearly the role of many-body effects and, more importantly, very few are the actual applications to many-body systems. More specifically, systems of nanoparticles have been addressed, but only within the dipolar approximation or other simplified frameworks [129–136]. Apart from these, results for three slabs [137, 138], or a sphere between two slabs [98] were discussed, but only after the work presented here. This motivated our three-body theory and the applications presented in that work.

We do not discuss here the technical details (which can be found in Ref. [128]), and we

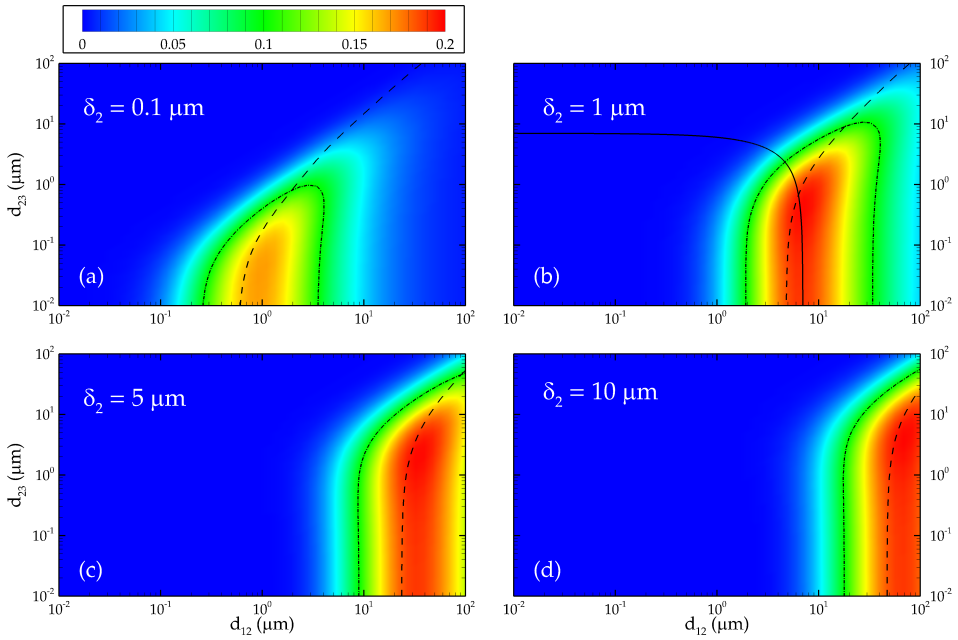

Figure 3.3 : Relative difference of two- and three-body pressures acting on slab 1. The four panels (a), (b), (c) and (d) correspond to four different values of the thickness of slab 2, namely 100 nm, 1 μm, 5 μm and 10 μm respectively. In each panel the dot-dashed curve corresponds to a relative difference of 10%, while the dashed line gives the point where the two-body coming from body 2 equals the one coming from body 3. From Ref. [128].

just present two examples of applications concerning the Casimir force. The first one consists in a quantitative analysis of the deviation of the exact result from an additive approximation. To this aim, we consider a system of three parallel finite-thickness Al_2O_3 slabs and calculate the pressure acting on slab 1 either within our exact approach or by summing the two-body contributions due to slab 2 and 3, respectively. To the best of our knowledge, this is the first quantitative study of this deviation. The relative difference between these two results is plotted in Fig. 3.3 for different thicknesses of the intermediate slab 2. We observe that the error committed in applying an additive approximation can be as high as 20%, clearly within experimental sensitivity. Moreover, it is interesting to observe that the region of large error is concentrated around the points (dashed curve) where the individual contributions due to slabs 2 and 3 are equal. Finally, we observe that the region of error larger than 10% (within the dashed line in figure) corresponds to a relatively large region of distances between bodies 1 and 2 (d_{12}), as well as between bodies 2 and 3 (d_{23}), making an experimental assessment of non-additivity clearly feasible.

The second application concerns the energy and force experienced by a neutral Rubidium atom placed in a cavity of width D formed by two sapphire slabs of equal thicknesses $\delta_1 = \delta_3 = 5\,\mu$m, in a non-equilibrium configuration. The results coming from our three-body theory are shown in Fig. 3.4 with black solid lines, and compared to the results at thermal equilibrium at 0 K and 600 K (red lines). As clear from the figure, the behavior of the energy and of the force

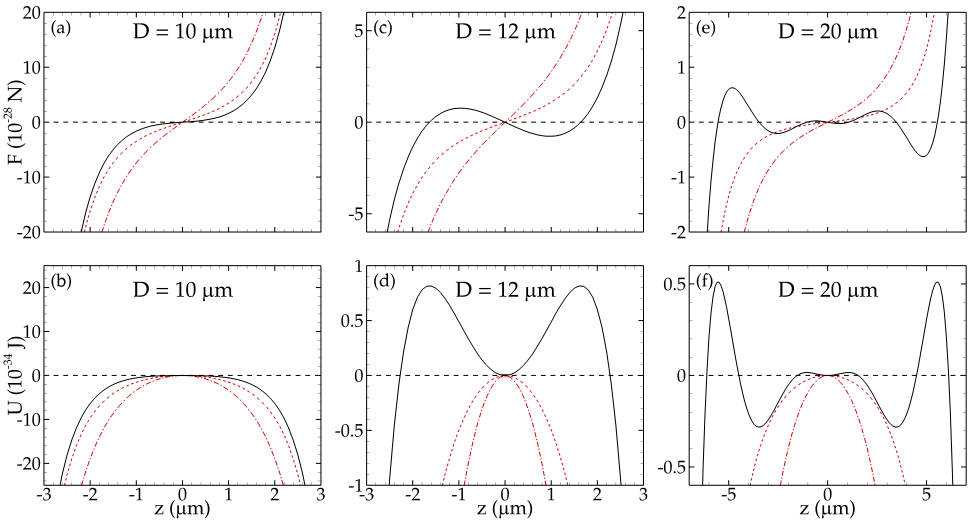

Figure 3.4 : Force [panels (a), (c) and (e)] and potential energy [panels (b), (d) and (f)] associated to a Rubidium atom in a cavity made of two sapphire slabs of equal thicknesses $\delta_1 = \delta_3 = 5\,\mu$m. The temperatures are $T_1 = T_3 = 300$ K and $T_e = 600$ K. The figure shows three different values of the cavity width D. From Ref. [128].

at thermal equilibrium is always qualitatively the same, with only one unstable equilibrium position in the middle of the cavity. On the contrary, the presence of different temperatures dramatically modifies, by modulating the cavity width D, this feature. More specifically, we clearly see that by increasing D, already within a symmetric configuration as the one considered here, we observe the existence of several stable and unstable equilibrium positions, leading to the idea of the design of an atomic trap based on thermal non-equilibrium. As discussed more in detail in Ref. [128], the values of the energy shown in Fig. 3.4 are not sufficient to design an actual atomic trap. Nevertheless, this scheme could work for a Rydberg atom, for example, for which the fact of having a high principal quantum number n leads to a strong increase of the polarizability by a factor close to n^7 with respect to the ground state.

3.4 N-SLAB THEORY

A further step in the study of many-body effects was done in 2017, when we developed a theoretical framework to study the Casimir force and radiative transfer in a system made of arbitrary number N of parallel planar slabs of arbitrary finite thickness and optical properties, immersed in an external environment [139]. In analogy with what described before, the system is charac-

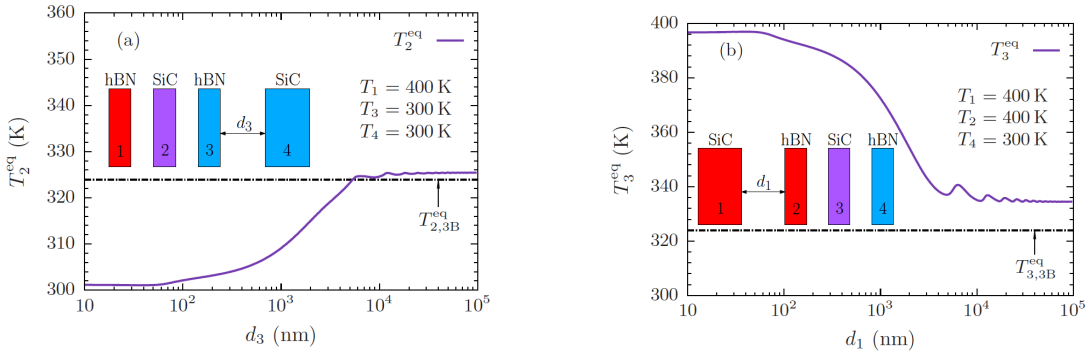

Figure 3.5 : Equilibrium temperatures in four-body systems. (a) Equilibrium temperature of body 2 as a function of the separation distance d_3 with fixed $T_1 = 400\,\mathrm{K}$ and $T_3 = T_4 = 300\,\mathrm{K}$. Bodies 1 and 3 are hBN slabs of width $\delta_1 = \delta_3 = 200\,\mathrm{nm}$, whereas bodies 2 and 4 are made of SiC and have widths $\delta_2 = 200\,\mathrm{nm}$ and $\delta_4 = 5\,\mu\mathrm{m}$, respectively. The rest of the separation distances are fixed to $d_1 = d_2 = 200\,\mathrm{nm}$. (b) Equilibrium temperature of body 3 as a function of the separation distance d_1 with fixed $T_1 = T_2 = 400\,\mathrm{K}$ and $T_4 = 300\,\mathrm{K}$. Bodies 2 and 4 are hBN slabs of width $\delta_2 = \delta_4 = 200\,\mathrm{nm}$, whereas bodies 1 and 3 are made of SiC and have widths $\delta_1 = 5\,\mu\mathrm{m}$ and $\delta_3 = 200\,\mathrm{nm}$, respectively. The rest of the separation distances are fixed to $d_2 = d_3 = 200\,\mathrm{nm}$. In (a) and (b), we also show the equilibrium temperature of the intermediate body in a three-body system: $T_{2,3B}^{eq}$ is obtained by removing body 4 in (a) and $T_{3,3B}^{eq}$ is obtained by removing body 1 in (b). In both cases the environmental temperatures are fixed to $T_0 = T_5 = 300\,\mathrm{K}$. From Ref. [139].

terized by $N+1$ temperatures, and the slabs are supposed to be in local thermal equilibrium. As a consequence, by writing down explicitly the total field (and thus field correlation functions) in each zone determined by the slabs, we were able to calculate explicitly the Poynting vector and Maxwell's stress tensor, obtaining closed-form explicit expressions for the force and heat transfer on each slab. More specifically, these expressions allow to identify clearly the contribution due to each other slab (and the environment), which depends explicitly on all the other bodies present in the system, paving the way for an easier study of purely many-body effects.

We show here a simple example of application of this framework to the case of radiative heat transfer in a four-body system. We consider four parallel slabs, shown in Fig. 3.5, and fix the temperature of three of them, while the temperature T_2 is left free to evolve. We then calculate the equilibrium temperature T_2^{eq} as a function of the position of one of the bodies [see Fig. 3.5 for details]. This value is compared to the three-body scenario, in which the body with varying coordinate is removed. As clear from the figure, the position of the fourth slab acts as a parameter to modulate the equilibrium temperature of the intermediate slab 2. Moreover, even in the limit of large distance of the fourth slab, we do not recover the three-body limit. This is a signature of the participation of the propagative contribution of the flux exchanged with this slab, which does not (in the ideal case of vacuum separating the bodies) tend to zero when increasing the distance.

3.5 Publications concerned by this chapter

[127] R. Messina and M. Antezza, *Casimir - Lifshitz force out of thermal equilibrium and heat transfer between arbitrary bodies*, Europhys. Lett. **95**, 61002 (2011).

[126] R. Messina and M. Antezza, *Scattering-matrix approach to Casimir - Lifshitz force and heat transfer out of thermal equilibrium between arbitrary bodies*, Phys. Rev. A **84**, 042102 (2011).

[128] R. Messina and M. Antezza, *Three-body radiative heat transfer and Casimir-Lifshitz force out of thermal equilibrium for arbitrary bodies*, Phys. Rev. A **89**, 052104 (2014).

[139] I. Latella, P. Ben-Abdallah, S.-A. Biehs, M. Antezza, and R. Messina, *Radiative heat transfer and nonequilibrium Casimir-Lifshitz force in many-body systems with planar geometry*, Phys. Rev. B **95**, 205404 (2017).

CHAPTER 4

Many-body effects in radiative heat transfer

4.1 Introduction

The purpose of this chapter is to give a brief overview on my activity concerning many-body effects in near-field radiative heat transfer. This topic is indeed a very recent and active one. It has been known for a long time that radiative heat transfer is a non-additive phenomenon, meaning that the exact calculation of the flux exchanged in a system made of more that two bodies demands a specific many-body theory taking into account all mutual interactions. This allows to anticipate potential important collective effects on the value and direction of the flux, as well as on its dependence on the distances in the system and its transport regimes.

Nevertheless, such general many-body theories have been developed only during the last decade and, surprisingly, a relatively low number of applications have been theoretically considered. Most of these applications [98, 131–135, 137, 138, 140–148] concern systems of particles treated in the dipolar approximation, whereas only few of them involve macroscopic systems discussed in the framework of an exact theory. On the experimental side, to date only one experiment has been performed on a many-body system [149], and thus many of the theoretically predicted intriguing many-body effects are still waiting for experimental validation.

Apart from describing the main results I obtained in this domain, one of the main purposes of this chapter is to highlight the many facets of many-body effects in the context of radiative heat transfer. On one hand, the fact of having many bodies in a system results in a variety of heat sources exchanging heat with a given body. Moreover, the presence of other bodies modifies, even dramatically, the heat exchange between two of these bodies, which cannot be treated within a two-body theory. Moreover, many-body systems pave the way to the continuum limit, allowing to discuss the properties and regimes of radiative heat transport. Finally, it should be

kept in mind that also a far-field thermal bath can play the role of a third body, and produce relevant effects. The results discussed in this chapter have been obtained in collaboration with M. Antezza, P. Ben-Abdallah, S.-A. Biehs, B. Guizal, C. Henkel, K. Joulain, I. Latella, J. M. Rubi, M. Tschikin and A. W. Rodriguez. I recently participated to a review paper on the many-body radiative heat transfer, accepted on Review of Modern Physics [150], written in collaboration with P. Ben-Abdallah, S.-A. Biehs, J. C. Cuevas, P. S. Venkataram and A. W. Rodriguez.

4.2 Amplification of radiative heat transfer in a three-body system

My first result in the context of many-body effects was obtained in 2012, when I studied in collaboration with Mauro Antezza and Philippe Ben-Abdallah the possibility of amplifying the near-field radiative heat flux between two parallel planar slabs by exploiting the presence of a third one placed between them [151]. This investigation followed a previous work [131], in which this kind of effect was studied in a system involving three dipolar particles. The geometry of the system is shown in Fig. 4.1(a) and (b), in the two- and three-body configurations, respectively. The reference two-body scenario consists of two slabs, identified with indices 1 and 3, separated by a distance d and kept at temperatures $T_1 = 400\,\mathrm{K}$ and $T_3 = 300\,\mathrm{K}$, respectively. If we limit our discussion to the contribution of evanescent waves, largely dominating in the near-field regime considered here, the flux exchanged between the two slabs is given by the well-known expression

$$\varphi_{2\mathrm{s}}(\omega, d) = \hbar\omega\, n_{13}(\omega) \sum_p \int_{ck>\omega} \frac{d^2\mathbf{k}}{(2\pi)^2} \mathcal{T}_{2\mathrm{s},p}(\omega, \mathbf{k}, d) \tag{4.2.1}$$

where the transmission coefficient is given by

$$\mathcal{T}_{2\mathrm{s},p}(\omega, \mathbf{k}, d) = \frac{4\,\mathrm{Im}(\rho_{1p})\mathrm{Im}(\rho_{3p})e^{-2\mathrm{Im}(k_z)d}}{|1 - \rho_{1p}\rho_{3p}e^{-2\mathrm{Im}(k_z)d}|^2}, \tag{4.2.2}$$

involving the Fresnel coefficients ρ, taking also into account the finite thickness of each slab. This configuration is compared to the three-body scenario depicted in Fig. 4.1(b), where d is the distance between adjacent slabs (1-2 and 2-3), while δ is the thickness of the intermediate slab 2. We stress here that this choice of distances in the three-body case makes d the smallest and unique distance in the two configurations, thus making the comparison easier and fair. In other words, if we had kept the distance d between the external bodies, and placed an intermediate slab in the middle, we would have observed a trivial amplification of the flux, simply due to the smaller total thickness of the vacuum gap in the system. On the contrary, the total thickness of the vacuum gap in the three-body case considered here is $2d$, twice as the two-body case.

Another relevant point is the choice of the temperatures in the three-body configuration. For the external bodies we keep the same temperatures $T_1 = 400\,\mathrm{K}$ and $T_3 = 300\,\mathrm{K}$. For the

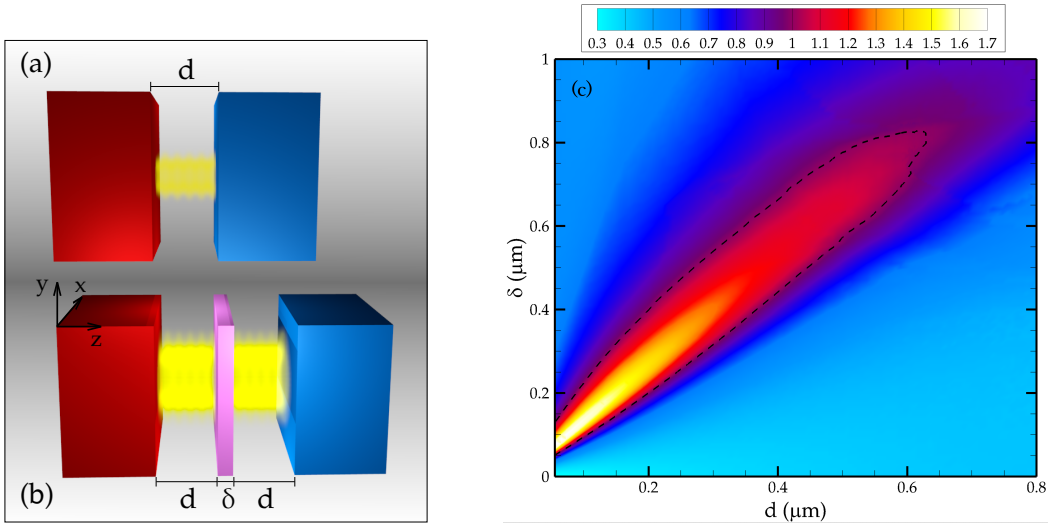

Figure 4.1 : Geometry of the system in the (a) two- and (b) three-slab configurations. The distance d between adjacent slabs (1-2 and 2-3) in the three-body configuration equals the distance between slabs in the two-body case. (c) Total heat-flux amplification $\varphi_{3s}(d,\delta)/\varphi_{2s}(d)$ as a function of distance and slab thickness. The black dashed line corresponds to $\varphi_{3s}(d,\delta)/\varphi_{2s}(d) = 1$. From Ref. [151].

intermediate slab 2, we calculate in every configuration the equilibrium of slab 2, i.e. the temperature at which the flux on slab 2 vanishes. This assumption allows to avoid the introduction of a supplementary thermal source and keep the comparison between the two configurations meaningful.

It is instructive to inspect the explicit analytical expression of the radiative heat flux on slab 3 in a three-body configuration, which reads

$$\varphi_{3s}(\omega,d,\delta) = \hbar\omega \sum_p \int_{ck>\omega} \frac{d^2\mathbf{k}}{(2\pi)^2} \Big[n_{12}(\omega)\mathcal{T}^{(12)}_{3s,p}(\omega,\mathbf{k},d,\delta) + n_{23}(\omega)\mathcal{T}^{(23)}_{3s,p}(\omega,\mathbf{k},d,\delta) \Big], \tag{4.2.3}$$

where the two transmission coefficients are defined as

$$\begin{aligned} \mathcal{T}^{(12)}_{3s,p}(\omega,\mathbf{k},d,\delta) &= \frac{4|\tau_{2p}(\delta)|^2 \mathrm{Im}(\rho_{1p})\mathrm{Im}(\rho_{3p}) e^{-4\mathrm{Im}(k_z)d}}{|1-\rho_{12p}(\delta)\rho_{3p}e^{-2\mathrm{Im}(k_z)d}|^2\,|1-\rho_{1p}\rho_{2p}(\delta)e^{-2\mathrm{Im}(k_z)d}|^2}, \\ \mathcal{T}^{(23)}_{3s,p}(\omega,\mathbf{k},d,\delta) &= \frac{4\,\mathrm{Im}[\rho_{12p}(\delta)]\mathrm{Im}(\rho_{3p}) e^{-2\mathrm{Im}(k_z)d}}{|1-\rho_{12p}(\delta)\rho_{3p}e^{-2\mathrm{Im}(k_z)d}|^2}. \end{aligned} \tag{4.2.4}$$

These expressions depend on the Fresnel reflection coefficient ρ_{12} (see [151] for details), associated with the couple of slabs 1 and 2 considered as a whole body. By inspecting the denominators of these transmission coefficients, we are able to anticipate a richer spectral behavior and, more specifically, a dependence of the frequencies of resonant surface modes on the thickness δ of the intermediate slab.

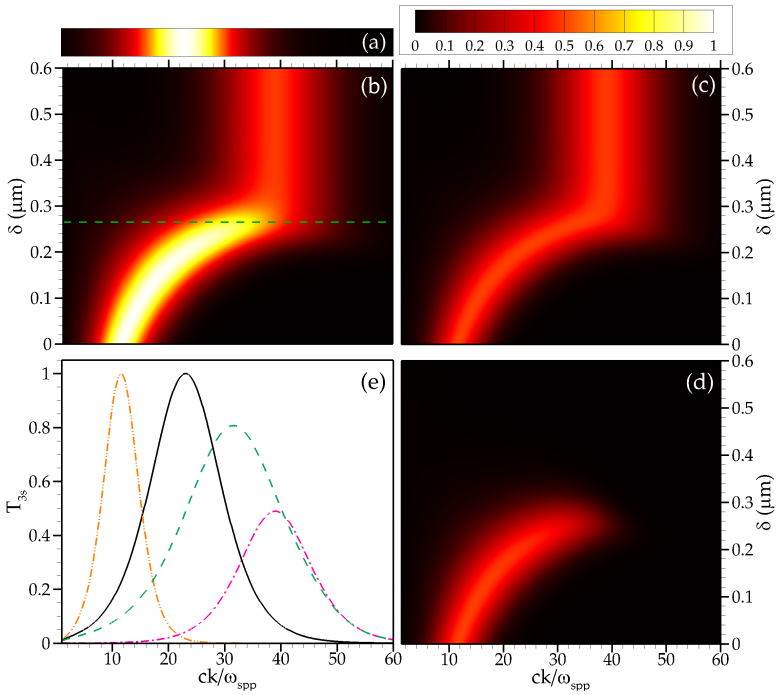

Figure 4.2 : Transmission probabilities of a three-body system for $\omega = \omega_{\rm spp}$ and $d = 200\,\text{nm}$ as a function of dimensionless wavevector $ck/\omega_{\rm spp}$ and thickness δ. (a) $\mathcal{T}_{2\rm s}$; (b) $\mathcal{T}_{3\rm s} = 0.5(\mathcal{T}_{3\rm s}^{(12)} + \mathcal{T}_{3\rm s}^{(23)})$; (c) $0.5\mathcal{T}_{3\rm s}^{(23)}$; (d) $0.5\mathcal{T}_{3\rm s}^{(12)}$; (e) Three-slab transmission probabilities for $\delta = 0\,\text{nm}$ (orange double-dot-dashed line), $\delta = 265\,\text{nm}$ (optimal thickness, green dashed line, same in panel (b)), and $\delta \to +\infty$ (purple dot-dashed line) compared to the two-slab transmission coefficient [black solid line]. From Ref. [151].

The main result of this work is shown in Fig. 4.1(c), where the ratio between the three- and two-body fluxes $\varphi_{3\rm s}(d,\delta)/\varphi_{2\rm s}(d)$ is shown as a function of the distance d and thickness δ. We clearly see that an amplification region exists, with values of the ratio reaching 60% for distances around 150 nm. An insight into the physics behind this effect is given in Fig. 4.2, where the transmission coefficients in the two- and three-body configurations are represented at the frequency of surface resonant mode and $d = 200\,\text{nm}$, along with the spectral flux for different thicknesses in Fig. 4.2(e). We clearly see the behavior in the two two-body limiting scenarios: $\delta = 0$, i.e. absence of slab 2, and $\delta \to \infty$, when slab 3 exchanges heat only with the intermediate slab 2. The transition region is characterized by a clear variation of the position of the peak of the spectral flux, and the optimal thickness [green horizontal line in Fig. 4.2(b)] corresponds to the almost *horizontal* region of participating modes in the three-body transmission coefficient [see Fig. 4.2(b)].

4.3 Heat transfer in multiple dipolar systems

In Chapter 3 we discussed the development of several scattering approaches to both Casimir force and radiative heat transfer in systems made of 2 or 3 arbitrary bodies, or an arbitrary number of parallel planar slabs. While, as shown by means of some applications in Chapter 3, this allowed us to shed light on some purely many-body effects, the treatment of systems involving a large number of bodies can rapidly become challenging both from the analytical and numerical point of view. For this reason, we developed in 2013, along with the approached described before, a framework accounting for the near-field radiative heat transfer in a system made of an arbitrary number of bodies and immersed in a thermal environment, but within the dipolar approximation [152]. While this limits, of course, the range of distances that can be explored, it dramatically reduces the numerical complexity, paving the way to the exploration of interesting many-body effects, such as the ones described below. Compared to the study presented in Ref. [131], the approach described below includes the interaction with an external thermal bath and focuses on the relaxation dynamics as well.

We will first very briefly review the basic ideas behind this approach. Both the total electric field and each dipole $\mathbf{p}_i$ are written as the sum of a fluctuating contribution and an induced part, as follows:

$$\begin{aligned} \mathbf{E}(\mathbf{r}) &= \mathbf{E}^{(\mathrm{b})}(\mathbf{r}) + \mathbf{E}^{(\mathrm{ind})}(\mathbf{r}), \\ \mathbf{p}_i &= \mathbf{p}_i^{(\mathrm{fl})} + \mathbf{p}_i^{(\mathrm{ind})}. \end{aligned} \tag{4.3.1}$$

While the fluctuating parts are statistically described by means of the fluctuation dissipation theorem, the induced part can be expressed by using the free-space Green's function as

$$\begin{aligned} \mathbf{E}(\mathbf{r}) &= \mathbf{E}^{(\mathrm{b})}(\mathbf{r}) + \frac{k^2}{\varepsilon_0}\sum_i \mathbb{G}^{(0)}(\mathbf{r},\mathbf{r}_i)\mathbf{p}_i, \\ \mathbf{p}_i &= \mathbf{p}_i^{(\mathrm{fl})} + \varepsilon_0\alpha_i\Big(\mathbf{E}_i^{(\mathrm{b})} + \frac{k^2}{\varepsilon_0}\sum_{j\neq i}\mathbb{G}_{ij}^{(0)}\mathbf{p}_j\Big). \end{aligned} \tag{4.3.2}$$

These equations constitute a coupled system, from which the field and the dipoles can be obtained. Then, the power absorbed by each body i can be deduced and reads

$$\begin{aligned} \wp_i^{(\mathrm{abs})}(t,T_1,\ldots,T_N,T_\mathrm{b}) = \int_0^{+\infty}\frac{d\omega}{2\pi}\hbar\omega\Big[&\sum_{j\neq i}\frac{4\chi_i\chi_j}{|\alpha_i|^2}n_{ji}(\omega)\mathrm{Tr}\Big(\mathbb{T}_{ij}^{-1}\mathbb{T}_{ji}^{-1\dagger}\Big) \\ &+ \frac{4k^2\chi_i}{|\alpha_i|^2}n_{\mathrm{b}i}(\omega)\sum_{jk}\alpha_j\alpha_k^*\mathrm{Tr}\Big(\mathbb{T}_{ij}^{-1}\mathrm{Im}(\mathbb{G}_{jk}^{(0)})\mathbb{T}_{ki}^{-1\dagger}\Big)\Big], \end{aligned} \tag{4.3.3}$$

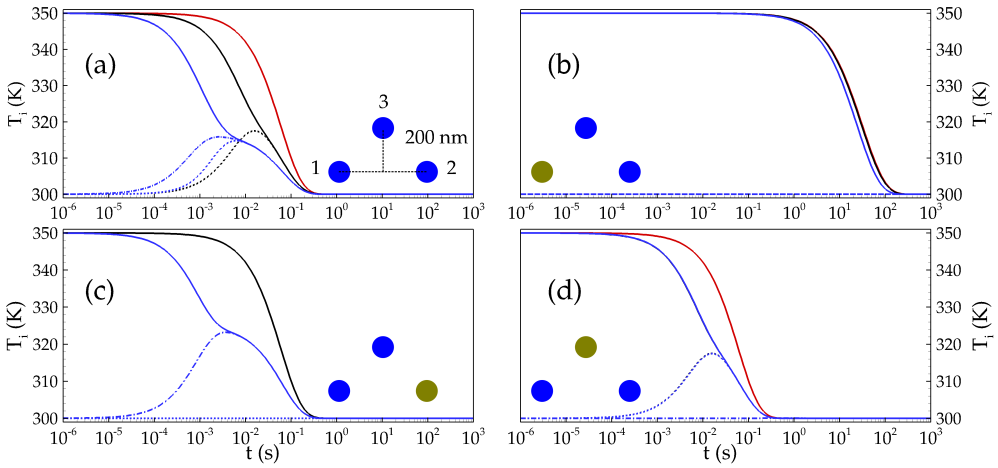

Figure 4.3 : Time evolution of the temperatures in a three-body configuration. The black lines correspond to the two-body case (solid line for dipole 1, dashed line for dipole 2), while the red solid line correspond to dipole 1 alone. Panel (a): three SiC particles. In panels (b), (c) and (d) particles 1, 2 and 3 are respectively replaced by a gold nanosphere. We remark that in (b) the red and black curves relative to particle 1 are almost superposed. The same is true in (c), while in (d) the blue and black curves relative to particles 1 and 2 are superposed. From Ref. [152].

where we have introduced the differences

$$n_{ij}(\omega) = n(\omega, T_i) - n(\omega, T_j) \tag{4.3.4}$$

of Bose-Einstein distributions

$$n(\omega, T) = \left[\exp\left(\frac{\hbar\omega}{k_{\mathrm{B}}T}\right) - 1\right]^{-1}, \tag{4.3.5}$$

along with the quantity

$$\chi_i = \mathrm{Im}(\alpha_i) - \frac{k^3}{6\pi}|\alpha_i|^2, \tag{4.3.6}$$

depending on the polarizability α_i of body i, and the matrix $\mathbb{T}$, which is a $3N \times 3N$ block matrix defined in terms of the (i, j) $N \times N$ sub-matrices $(i, j = 1, \ldots, N)$

$$\mathbb{T}_{ij} = \delta_{ij}\mathbb{1} - (1 - \delta_{ij})k^2\alpha_i\mathbb{G}_{ij}^{(0)}, \quad \mathbb{A}_{ij} = \delta_{ij}\varepsilon_0\alpha_i\mathbb{1}. \tag{4.3.7}$$

The result in Eq. (4.3.3) clearly highlights the decomposition of the power absorbed by body i as the sum of contributions associated with the exchange of energy with each other body j (first line) and with the external bath (second line).

This approach has been used in Ref. [152] to study the dynamics of the temperature distribution in a system of three dipoles immersed in a thermal bath. The results, shown in Fig. 4.3,

compare this dynamics (blue lines) to the one of a two-body system (black lines) and to the relaxation of a single dipole in a thermal bath (red line). The different panels of the figure correspond to configurations in which the three particles are made of the same material (SiC), or one is made of a different one (gold). The most interesting feature to be observed in this figure is the existence of two different time scales associated with the near-field relaxation between particles and the near-field relaxation towards the bath temperature. This is manifest in panel (a), where the blue curves show the thermalization of the three particles toward a common temperature (around 310 K), including the heating of the particles having a lower initial temperature, followed by a global relaxation toward the bath temperature (300 K), on a completely different time scale. These different time scales result from the very different values of the heat fluxes involved. Coherently with this interpretation, we see that when one of the particles is made of a different material, it clearly evolves in a completely different fashion, basically ignoring the other particles, from which it is effectively decoupled. The results shown here go in the direction of a control of the dynamical temperature profile in a system of N particles, mediated by the control of the fluxes exchanged in the system.

4.4 Anomalous heat-transport regimes

The possibility to address radiative heat flux in a N-body system naturally paves the way to the study of radiative heat transport in one-, two- or even three-dimensional chains, networks or arbitrary complex arrangements of individual systems. This allows to discuss the nature of heat transport followed by photons. The problem has been largely discussed in the case of phonons: it is well known that in a bulk material heat transport is diffusive. More technically, this means that if we look at the motion of phonons inside a bulk as a random-walk process, the step length probability between two collision events is Gaussian.

In a first work on this topic [153], we treated the heat transport carried by photons as a generalized random walk (GRW) and discussed its properties in ordered or disordered systems of nanoparticles, within the dipolar approximation. For a system of N nanoparticles having temperatures T_i ($i = 1, \ldots, N$), neglecting the exchange with the external thermal bath, the time evolution of the temperatures satisfies

$$\rho_i C_i V_i \frac{\partial T_i}{\partial t} = \sum_{j \neq i} \mathcal{P}_{i \leftrightarrow j} + S_i, \tag{4.4.1}$$

where ρ_i and C_i represent the nanoparticle mass density and heat capacity respectively while $\mathcal{P}_{i \leftrightarrow j}$ and S_i denote the net power exchanged between two arbitrary particles and the power received by a particle from an external source, respectively. The interparticle term $\mathcal{P}_{i \leftrightarrow j}$, which

can be of course calculated within the formalism discussed in the previous section, can be further simplified in a configuration close to thermal equilibrium as

$$\mathcal{P}_{i\leftrightarrow j} = G(|\mathbf{r}_i - \mathbf{r}_j|; T_i)(T_j - T_i), \tag{4.4.2}$$

by means of the introduction of the thermal conductance G, function of the distance between the two considered particles. This allows in turn to rewrite Eq. (4.4.1) under the form of a Chapman-Kolmogorov equation

$$\frac{\partial T_i}{\partial t} = \int_{R^d} p(\mathbf{r}_i, \mathbf{r}) \frac{T(\mathbf{r}, t)}{\tau(\mathbf{r})} d\mathbf{r} - \frac{T(\mathbf{r}_i, t)}{\tau(\mathbf{r}_i)} + \hat{S}_i, \tag{4.4.3}$$

describing a Markov process in which the probability distribution function (PDF) of step length reads

$$p(\mathbf{r}, \mathbf{r}') = \frac{1}{\rho C V \Delta V} \tau(\mathbf{r}) G(\mathbf{r} - \mathbf{r}'), \tag{4.4.4}$$

and is then directly connected to the conductance G within the particles network. While, for a Gaussian PDF all the statistical moments are finite, properties which identifies a diffusive regime, if the PDF decays algebraically, at least one of the moments diverges and the heat-transport regime becomes diffusive. Within this scenario, and assuming that the conductance scales as ζ/x^γ as a function of the distance x from a reference particle, an analogous way to discuss this transition is to write the time evolution described by Eq. (4.4.1) as a fractional diffusion equation

$$\rho_i C_i V_i \frac{\partial T_i}{\partial t} = -\kappa(-\Delta)^{\alpha/2} T(\mathbf{r}_i) + S_i, \tag{4.4.5}$$

where $\alpha = \gamma - d$, d being the dimensionality of the system, for $\alpha \in [0, 2]$, and the operator $(-\Delta)^{\alpha/2}$ denotes the fractional Laplacian, defined as

$$(-\Delta)^{\alpha/2} T(\mathbf{r}) = c_{d;\alpha}\, \mathrm{PV} \int_{R^d} \frac{T(\mathbf{r}) - T(\mathbf{r}')}{|\mathbf{r} - \mathbf{r}'|^{d+\alpha}} d\mathbf{r}' \tag{4.4.6}$$

with $c_{d;\alpha} = \frac{2^{-\alpha}\pi^{1+d/2}}{\Gamma(1+\alpha/2)\Gamma(\frac{d+\alpha}{2})\sin(\alpha\pi/2)}$ and where PV denotes the principal part. In Eq. (4.4.5) $\kappa = \frac{\zeta}{\Delta V c_{d;\alpha}}$ is the fractional diffusion coefficient inside the plasmonic structure. For $\alpha = 2$ the heat transport process is diffusive, subdiffusive for $\alpha > 2$, and superdiffusive for $\alpha < 2$.

We have numerically studied the heat-transport regime in a 3D system of SiC nanoparticles. The configuration we consider consists of N randomly distributed particles with identical radius R and volume V. The minimum distance between two nanoparticles is $2R$, we consider different filling fractions $f = NV/a^3$, a being the side of the cubic simulation box. In Fig. 4.4 we show the average conductance measured with respect to a reference particle placed in the middle of the

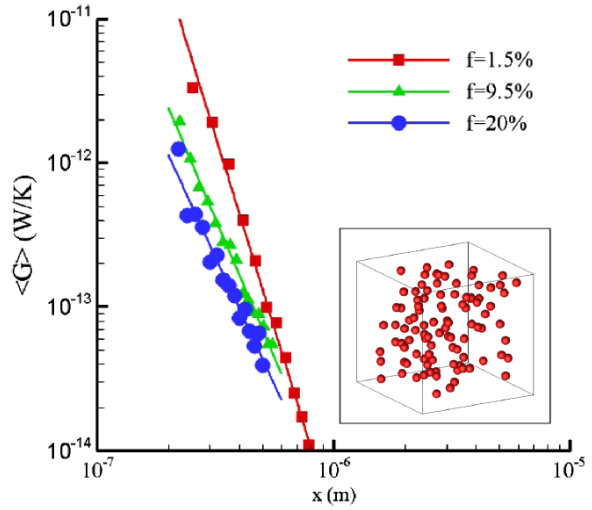

Figure 4.4 : Averaged thermal conductance $\langle G \rangle$ in log-log scale for clusters of SiC spherical particles as a function of the separation distance x, for different volumic fractions f and at temperature $T = 300\,\mathrm{K}$. The statistical averaging is performed with $m = 250$ realizations generated with a uniform random distribution probability. The inset shows an example of network with a volumic fraction $f = 1.5\%$ generated with $N = 100$ nanoparticles. From Ref. [153].

box. We clearly recognize a power-law behavior of $G(x)$. Interestingly, already for the smallest filling fraction considered $f = 1.5\%$ the exponent γ is slightly smaller than 5, meaning that α is close to 2 but smaller, so that we already are in a superdiffusive regime. As shown in figure, γ becomes smaller when increasing the filling fraction, making the transition to the superdiffusive regime unambiguous. In more physical terms, this transition corresponds to the participation of long-range interactions which, in turn, stem from collective (thus many-body) modes existing in the entire structure. This anomalous transport regime can be indeed relevant in the context of fast thermal management, since it allows to design systems going beyond the standard diffusive limits which holds for conduction in solids.

More recently, we have performed a similar study in the case of a macroscopic system, made of N parallel planar slabs [154], by exploiting the formalism discussed in the previous chapter. While we assume that the temperatures of the external slabs are fixed at values T_1 and T_N, we let all the intermediate slabs evolve toward their equilibrium temperature T_i^{eq}. D is the distance between the external slabs and the $N-2$ slabs in the middle, while d is the distance between adjacent slabs of this group. In this scenario, both the temperature profile induced in the system and the dependence of the mutual conductances on the distance are a signature of the heat-transport regime within the system. In analogy with what we have done in the case of

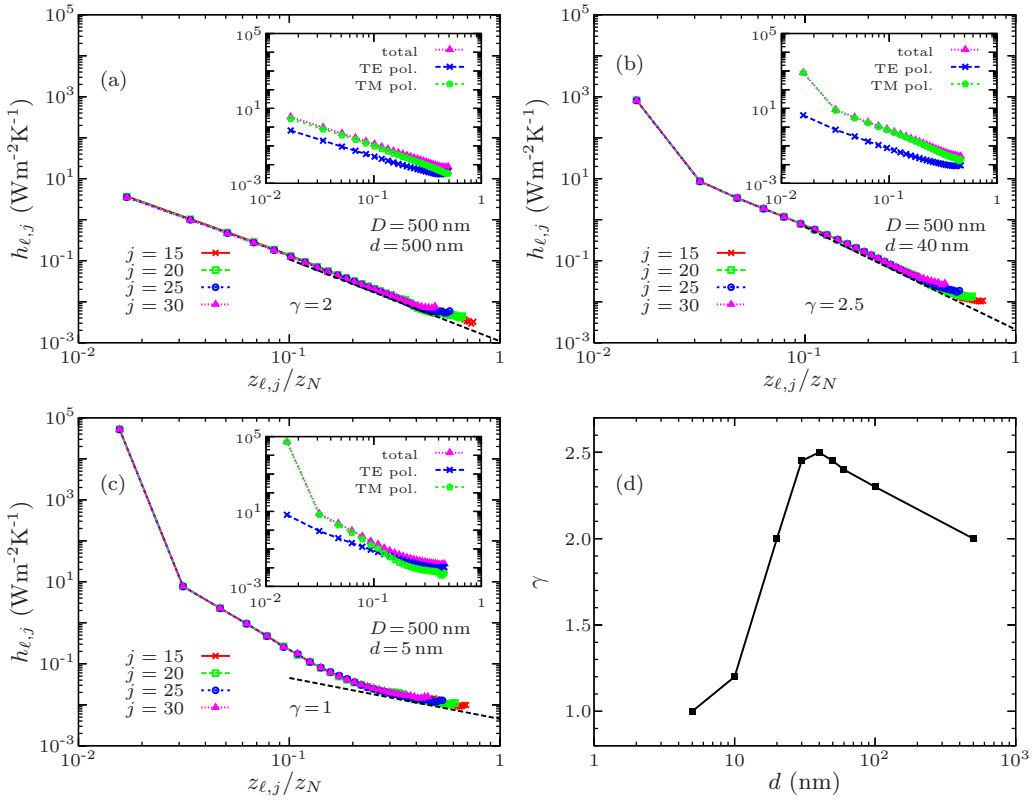

Figure 4.5 : Heat-transfer coefficients $h_{\ell,j}$ with respect to the normalized separation $z_{\ell,j}/z_N$, for fixed values of j and $D = 500\,\text{nm}$, and three values of (a) $d = 500\,\text{nm}$, (b) $d = 40\,\text{nm}$ and (c) $d = 5\,\text{nm}$. Dashed lines indicate the asymptotic behavior of $h_{\ell,j} \sim 1/z_{\ell,j}^{\gamma}$ at large separations. The value of γ indicates the nature of the heat-transport regime, from superdiffusive ($1 < \gamma < 3$) to ballistic ($\gamma \to 1$). The insets decompose $h_{\ell,j}$ for $j = 30$ into TE and TM polarization contributions. (d) Exponent γ as a function of d. From Ref. [154].

nanoparticles, the net flux on slab j is written as a sum of linearized contributions

$$\varphi_j \simeq \sum_{\ell \neq j} h_{\ell,j}(T_\ell - T_j). \tag{4.4.7}$$

By assuming that the heat transfer coefficients scale as $h_{\ell,j} \sim 1/z_{\ell,j}^{\gamma}$, for some exponent $\gamma = 1+\alpha$, where $z_{\ell,j} \equiv |z_\ell - z_j|$ and z_j denotes the position of the j-th slab, one finds (see Ref. [155] for details) that in the continuum limit of $N \to \infty$ (with fixed Nd), T_j is replace by a continuum temperature profile $T(z)$ and

$$\varphi_j \to \varphi(z) \sim (-\Delta)^{\alpha/2} T(z). \tag{4.4.8}$$

In this case, for $1 < \gamma < 3$ we have a superdiffusive regime, degenerating into a diffusive one for $\gamma \to 3$, while for $\gamma \to 1$ we approach the ballistic regime.

We show in Fig. 4.5 the dependence of the heat-transfer coefficient $h_{\ell,j}$ on the distance. For the smallest filling fraction considered here [see Fig. 4.5(a)], corresponding to $d = 500\,\mathrm{nm}$, we find $\gamma = 2$ and we recover the superdiffusive transport regime already observed in the case of dipolar networks. This remains true for $d = 40\,\mathrm{nm}$ [see Fig. 4.5(b)], for which the value of γ increases to 2.5. On the other hand, for the densest system considered here [see Fig. 4.5(c)], we have a clear inversion, since we clearly observe a limit $\gamma \to 1$ and thus a transition to the ballistic regime. This non-trivial dependence on the distance d between adjacent slabs is highlighted in Fig. 4.5(d), where the non-monotonic behavior of γ as a function of d is shown. It is less evident to give an insight concerning this transition to a ballistic regime, since it might seem in contradiction with the existence of collective electromagnetic modes in the structure, mentioned above to discuss the superdiffusive regime. Nevertheless, one key difference between this system and the nanoparticle network which should be highlighted is that when d (distance between adjacent inner slabs) tends to zero with D (distance with respect to the two outer slabs) fixed, a strong imbalance between the inner and outer couplings is produced, absent in the case of random distribution of nanoparticles. This is a further signature of the richness of many-body interactions, which could lead to an active manipulation of relaxation dynamics in complex systems.

4.5 Heat-transfer manipulation in many-body systems

Another relevant topic in which many-body effects can indeed play an important role is the manipulation of radiative heat flux. This aspect has received a remarkable attention during the last years. One first interesting example in this direction is the idea to use a third system as an external source of control (typically amplification) of the heat flux in a two-body scenario. Apart from the examples described above [131,151], this problem has been addressed by several other groups [140,148,156,157] using a variety of properties of the intermediate system (planar or structured slab, two-dimensional atomic system, hyperbolic media) and, in the more specific configuration of nanoparticles, by exploiting their magnetic properties [144], as well as their shape and anisotropy [133,134,158,159]. On a more applicative side, the impact of many-body effects has been recently studied in the context of a heat engine [138], and the combination of near-field many-body effects and insulator-metal transition materials (such as vanadium dioxide) has led to the design of a variety of devices, including radiative thermal memory [160], a radiative thermal transistor [137], as well as thermal-based logic gates [161,162].

We have studied two problems of heat-flux manipulation induced by many-body interactions in configurations involving nanoparticles in the dipolar approximation. More specifically, in two recent works we have studied the role played by a planar substrate placed in proximity of the

two particles [163], while in a more recent one we have analyzed the impact of a third particle, whose temperature and positions can be periodically modulated in time [164].

We first focus on the first work [163], where two particles are supposed to be placed at the same distance from the substrate, and at distance d from each other. Without loss of generality, their positions can be taken as $\mathbf{R}_1 = (0, 0, z)$ and $\mathbf{R}_2 = (d, 0, z)$, the vacuum-substrate interface being placed at $z = 0$. The entire system is assumed to be placed close to thermal equilibrium, where one particle and the substrate have temperature 300 K, while the other particle has a slightly different temperature 300 K+ΔT. Under these assumptions, the first particle experiences a net radiative heat flux, which can be entirely ascribed to the other particle. Nevertheless, this flux is modified by the presence of the substrate. This is formally clear by inspecting the expression of the interparticle flux, which in terms of conductance can be expressed as

$$G = 4 \int_0^{+\infty} \frac{d\omega}{2\pi} \hbar\omega \, \frac{\omega^4}{c^4} \, n'(\omega, T) \chi^2 \mathrm{Tr}\big(\mathcal{G}\mathcal{G}^\dagger\big), \tag{4.5.1}$$

where the dyadic Green tensor of the full system $\mathcal{G}$ can be easily connected to the Green tensor $\mathbb{G}$ of a single interface (see Ref. [163]). Since the latter is written, in the presence of a planar interface, as a sum

$$\mathbb{G} = \mathbb{G}^{(0)} + \mathbb{G}^{(\mathrm{sc})}, \tag{4.5.2}$$

of a vacuum and a scattering term (going to zero in the absence of the substrate), we clearly see the total conductance takes the form of a sum

$$G = G^{(0,0)} + G^{(\mathrm{sc},\mathrm{sc})} + G^{(0,\mathrm{sc})}, \tag{4.5.3}$$

of a vacuum term, a purely scattering and a mixed term. The two last ones two represent the deviation we intend to study from the reference scenario of two particles in vacuum. While in Ref. [163] the role played by the substrate is analyzed in the case of both SiC and gold nanoparticles, as well as in the presence of a graphene sheet on top of the substrate, we limit here the discussion to the scenario of two SiC nanoparticles close to a SiC substrate, referring to Ref. [163] for more details.

The main result is shown in Fig. 4.6(a), where the three contributions to the conductance are represented, along with the total conductance, as a function of the distance d between the nanoparticles, assuming a particle-substrate distance $z = 50\,\mathrm{nm}$. We first observe that, not surprisingly, for very small separation distances the vacuum contributions becomes dominant and the heat exchange is not influenced by the presence of the substrate. On the contrary, this influence becomes manifest at intermediate distances (around 10 μm), where the presence of the substrate results in a dramatic amplification of the heat exchange, of a factor going up to 400 [see inset of Fig. 4.6(a)]. It is finally interesting to highlight a third region, for even larger

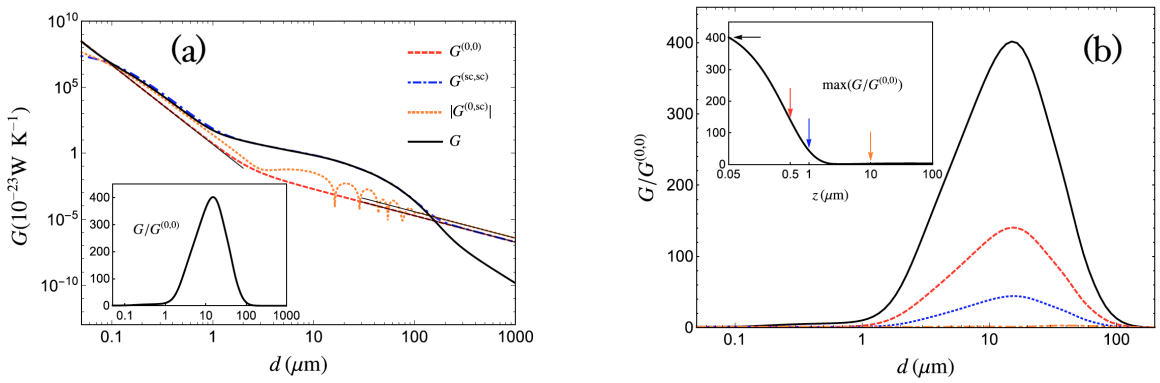

Figure 4.6 : (a) Total conductance G (black solid line) and single contributions $G^{(0,0)}$ (red dashed line), $G^{(\mathrm{sc,sc})}$ (blue dot-dashed line) and $G^{(0,\mathrm{sc})}$ (in absolute value, orange dotted line) as defined in Eq. (4.5.3) between two SiC nanoparticles at distance d, placed at distance $z = 50\,\mathrm{nm}$ from a SiC substrate. The thin black lines correspond to the small- and long-distance power-law behaviors of $G^{(0,0)}$. The inset shows the ratio between conductances in the presence and absence of substrate as a function of d. (b) The inset shows, as a function of the nanoparticles–surface distance z, the maximum of the ratio $G/G^{(0,0)}$ with respect to the interparticle distance d for two SiC nanoparticles on top of a SiC substrate. In the main part of the figure, the same ratio is plotted as a function of d for $z = 50\,\mathrm{nm}$ (black solid line), $500\,\mathrm{nm}$ (red dashed line), $1\,\mu\mathrm{m}$ (blue dotted line) and $10\,\mu\mathrm{m}$ (orange dot-dashed line). From Ref. [163].

distances $d \geq 100\,\mu\mathrm{m}$, for which the presence of the substrate inhibits the heat exchange. More specifically, the modified conductance scales as d^{-4} for large distances, contrarily to the known d^{-2} large-distance behavior in vacuum. Nevertheless, it must be noted that this further effect takes place at distances where the conductance is already dramatically lower than its near-field value. We finally addressed the question concerning the dependence of this amplification on the particle-substrate distance z. The main result is shown in Fig. 4.6(b), where we observe a clear and expected monotonic decreasing behavior with respect to z, along with the dependence on the distance d for several particle heights z. In Ref. [163], we have shown that the effect discussed so far is much weaker in the case of gold nanoparticles, not supporting surface resonant modes in the infrared region of the spectrum. We show that this reduced effect can be strongly compensated by the presence of a graphene sheet on top of the substrate, by means of the coupling between surface modes already in Ref. [124].

We now focus on a more recent work [164], in which many-body effects are induced by the presence of a third nanoparticle, whose position and temperature are periodically modulated in time. This work follows two recent ones, in which the impact on thermal radiation of temporal modulation was addressed [155,165]. The system is depicted in Fig. 4.7(a), where the particles 1 and 2 are placed at distance d along the x axis, while the third particle has coordinates (x_3, y_3), and is supposed to be attached to a tip with the purpose to modulate its position. Moreover,

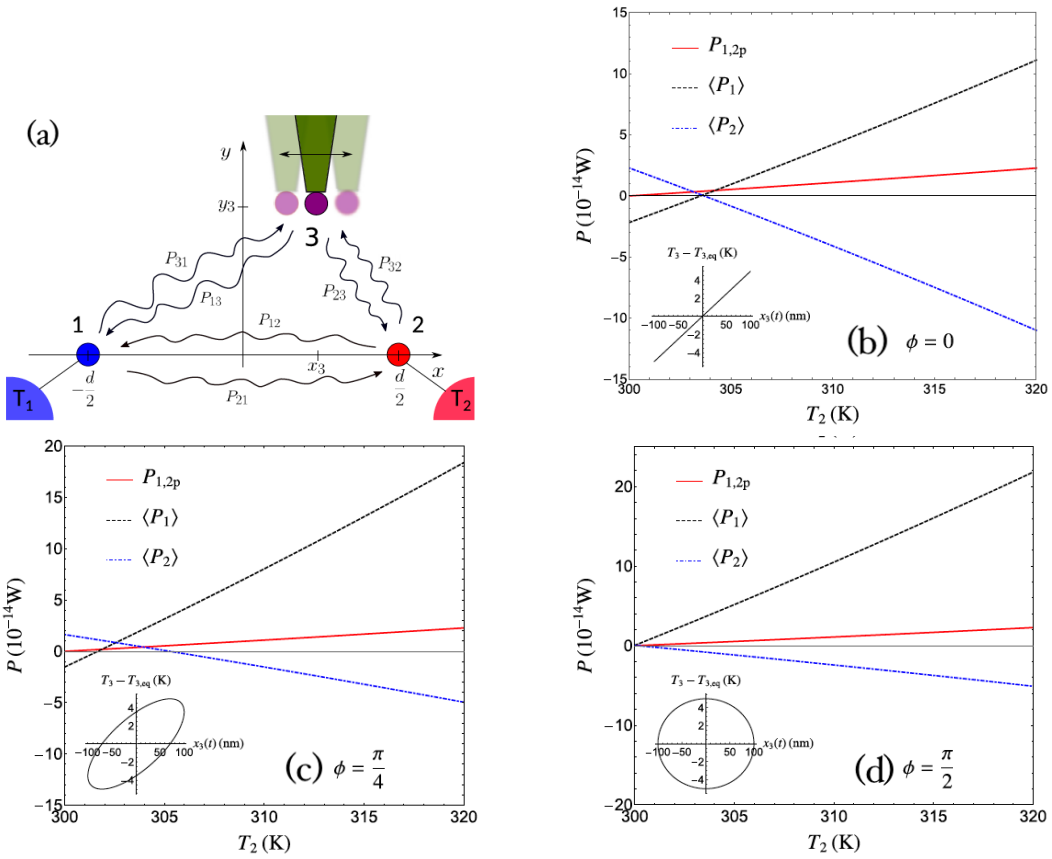

Figure 4.7 : (a) Geometry of the system. Particles 1 and 2 are placed at distance d along the x axis, while particle 3 has coordinates x_3 and y_3. The two individual contributions to the exchanged powers are shown. We also show a schematics of the dynamic oscillation of the x coordinate of particle 3 produced by a tip. (b)-(d) Average power absorbed by particle 1 (black dashed line) and particle 2 (blue dot-dashed line) compared to the two-body power absorbed by particle 1 (red solid line). We have $\Delta x = 2R = 100\,\text{nm}$, $\Delta T = 5\,\text{K}$, $d = 12R = 600\,\text{nm}$ and $y_3 = d/2 = 300\,\text{nm}$. The three panels correspond to different dephasings ϕ between x_3 and T_3: (b) $\phi = 0$, (c) $\phi = \pi/4$, (d) $\phi = \pi/2$. From Ref. [164].

the same tip could be used to modulate its temperature.

The situation we consider is based on a reference scenario in which particles 1 and 2 are at the same temperature $T_1 = T_2 = T_{\text{eq}}$, while the temperature and position of particle 3 are modulated as follows:

$$T_3(t) = T_{3,\text{eq}} + \Delta T \sin(\omega t), \;\; x_3(t) = \Delta x \sin(\omega t + \phi). \tag{4.5.4}$$

We have shown that, under these assumptions, the average power received by particle 1, within

a Taylor expansion up to the second order in ΔT and Δx, reads

$$\langle P_1 \rangle \simeq \frac{\Delta T}{2}\left(\Delta x \frac{\partial^2 P_1}{\partial x_3 \partial T_3}\cos\phi + \frac{\Delta T}{2}\frac{\partial^2 P_1}{\partial T_3^2}\right). \tag{4.5.5}$$

It is instructive to compare the expression obtained here to the one we obtained in a previous work [155] where the temperature was the only varying parameter. In this case, only the second term in Eq. (4.5.5) is left, and thus the average received power is necessarily positive in the absence of a negative thermal differential resistance. This is not the case here, since the magnitude and the sign of the first term, proportional to Δx, can be actively modulated by modifying the dephasing ϕ between temperature and position variations, clearly highlighting the advantage of considering the simultaneous variation of two parameters.

While this discussion is limited to the case $T_1 = T_2$, we have numerically exploited the effect in the more general scenario in which one of the two temperatures (T_2) can be above the other one. Figure 4.7(b)-(d) shows the average power absorbed by particles 1, having temperature $T_1 = 300\,\mathrm{K}$, and 2 as a function of the temperature T_2 and for three different values of the dephasing ϕ. In all scenarios, the power is compared to the one received by particle 1 in a two-body scenario, which of course vanishes for $T_2 = T_1 = 300\,\mathrm{K}$. Figures 4.7(b) and 4.7(c), corresponding to the values of the dephasing $\phi = 0$ and $\phi = \pi/4$, respectively, share an important feature, i.e. the existence of a region where although the temperature T_2 is larger than T_1, particle 1 (2) tends to be cooled down (heated up). This is indeed a pumping effect, whose magnitude can be modulated by means of the dephasing. Another consequence of this feature is the existence of configurations in which one of the particles (or both in the scenario $\phi = 0$) are thermally isolated, i.e. they absorb a net vanishing power, although the system is in a non-equilibrium configuration. The case $\phi = \pi/2$, shown in Fig. 4.7(d), does not present the behavior discussed before, and the powers have the expected sign. Nevertheless, it must be stressed that the power absorbed by particle 1 is still significantly higher than the one the same particle absorbs in a simpler two-body configuration. This analysis gives a further proof of the richness of many-body interactions in near-field radiative heat transfer.

4.6 Heat-transfer saturation in many-body systems

While the conventional fluctuational-electrodynamics approach predicts a divergence of the flux as $1/d^2$ when the distance tends to zero, it has been shown more recently that this divergence is removed and the flux saturates to a constant value when the non-local dielectric reponse of the materials is taken into account [166]. This saturation takes place at distances of the order of some nanometers in the case of a metal.

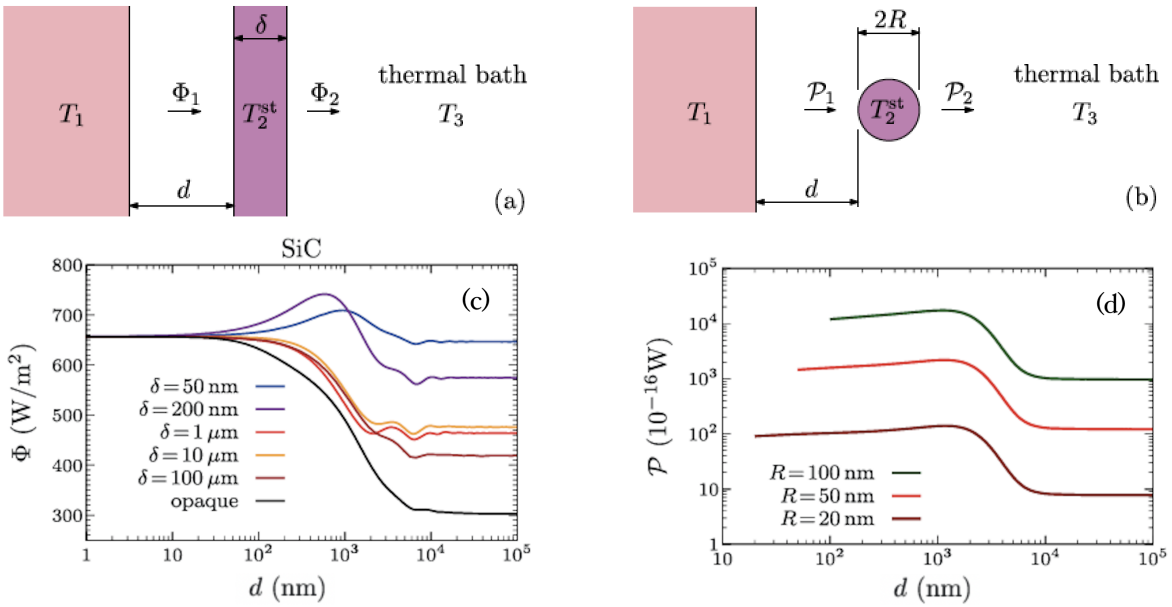

Figure 4.8 : (a,b) Sketch of the system. (a) A membrane is placed close to a substrate at a separation distance d. The substrate is thermalized at a fixed temperature T_1 and the structure is immersed in an thermal bath at temperature T_3. The temperature T_2 of the membrane reaches a steady-state value $T_2^{\rm st}$. (b) A small particle is considered instead of the membrane. (c) Energy flux Φ and membrane temperature $T_2^{\rm st}$ as a function of the separation distance d. The substrate and membrane are made of SiC. (d) Exchanged power and temperatures as a function of the separation distance for the substrate-particle configuration. The substrate and particle are made of SiC. From Ref. [167].

In a recent work [167], we highlighted a saturation phenomenon induced by many-body effects and taking place at much larger distances, of the order of 100 nm. More specifically, we addressed near-field radiative heat transfer in a system made of a thin film or a particle in front of a substrate, in the presence of a thermal bath at a third, possibly different temperature. The main purpose of this work was to highlight that the presence of a bath, often disregarded in previous theoretical works, can indeed fully play the role of a third body, inducing interesting and new physical mechanisms, and possibly leading to a saturation of heat flux.

The two systems we discussed are shown in Fig. 4.8(a)-(b), for the film-substrate and particle-substrate configurations, respectively. In both scenarios, while the substrate and the thermal bath are assumed to be kept at temperatures $T_1 = 400\,\mathrm{K}$ and $T_3 = 300\,\mathrm{K}$, respectively, by means of external thermostats, the temperature of body 2 is supposed to reach its steady-state value $T_2^{\rm st}$ at any distance. This value is determined by imposing that the net flux on body 2 vanishes.

Under these assumptions we have calculated the flux on body 2 as a function of the distance d, for several thickness δ of a SiC film. The results, shown in Fig. 4.8(c), clearly highlight a

saturation of the heat flux for distances of the order of 100 nm. We remark that the asymptotic value at small distances is independent of the thickness, and also coincides with the value of an opaque film (black line). This saturation is associated with the fact that the steady-state temperature $T_2^{\rm st}$ of body 2 tends to T_1 for $d \to 0$, and more specifically we have proved (not shown here, see Ref. [167] for details) that the temperature difference $T_2^{\rm st} - T_1$ scales as d^2 for $d \to 0$, as a result of the $1/d^2$ behavior of near-field radiative heat flux. We have confirmed that the same kind of saturation happens for metallic films as well. Finally, as shown in Fig. 4.8(d), a perfectly analogous phenomenon exists in the case of a particle placed in proximity of a substrate, with a saturation value depending on the radius R of the nanoparticle. Apart from its fundamental interest, this saturation mechanism can be very relevant in the quantitative estimation of the flux in experimental configurations in which the temperature of the second (probe) body is not completely fixed.

4.7 Publications concerned by this chapter

[151] R. Messina, M. Antezza, and P. Ben-Abdallah, *Three-Body Amplification of Photon Heat Tunneling*, Phys. Rev. Lett. **109**, 244302 (2012).

[152] R. Messina, M. Tschikin, S.-A. Biehs, and P. Ben-Abdallah, *Fluctuation-electrodynamic theory and dynamics of heat transfer in systems of multiple dipoles*, Phys. Rev. B **88**, 104307 (2013).

[153] P. Ben-Abdallah, R. Messina, S.-A. Biehs, M. Tschikin, K. Joulain, and C. Henkel, *Heat Superdiffusion in Plasmonic Nanostructure Networks*, Phys. Rev. Lett. **111**, 174301 (2013).

[154] I. Latella, S.-A. Biehs, R. Messina, A. W. Rodriguez, and P. Ben-Abdallah, *Ballistic near-field heat transport in dense many-body systems*, Phys. Rev. B **97**, 035423 (2018).

[163] R. Messina, S.-A. Biehs, and P. Ben-Abdallah, *Surface-mode-assisted amplification of radiative heat transfer between nanoparticles*, Phys. Rev. B **97**, 165437 (2018).

[164] R. Messina and P. Ben-Abdallah, *Many-body near-field radiative heat pumping*, Phys. Rev. B **101**, 165435 (2020).

[167] I. Latella, R. Messina, S.-A. Biehs, J. M. Rubi, and P. Ben-Abdallah, *Saturation of radiative heat transfer due to many-body thermalization*, Sci. Rep. **10**, 8938 (2020).

CHAPTER 5

Casimir forces and radiative heat transfer between gratings

Contents

5.1 Introduction

This chapter concerns my results on Casimir forces and near-field radiative heat transfer in system involving gratings, i.e. periodically nanostructured systems. This work, mainly done in collaboration with M. Antezza, B. Guizal and A. Noto during my activity at Laboratoire Charles Coulomb in Montpellier, is based on the development of numerical codes using the Fourier Modal Method and the Adaptive Spatial Resolution, briefly described in the following. It is also based on the collaboration with H. B. Chan, C. T. Chan, J. A. Crosse, P. A. Maia Neto, V. Marachevsky, C. Y. Ng, L. Tang, and M. Wang.

Systems involving gratings have raised a remarkable interest in the scientific community during the last years, for several reasons. First, the fact of having additional geometrical parameters (even in the simplest one-dimensional configuration, the grating height, period and filling factor), paves the way to the possibility to tailor the value of the force and energy flux, which proves to be relevant for several technological applications. Moreover, introducing a periodic structure along one dimension clearly breaks the translational symmetry with respect to the conventional scenario of two parallel planes, giving rise to new effects in the Casimir domain, such as a lateral force and a torque.

All these reasons have motivated the development of several theoretical works both in the context of Casimir forces [168–175] and near-field radiative heat transfer [176–186]. It should be mentioned that the Casimir force in systems involving gratings has been also the focus of several experiments [21, 26, 27, 31–33, 41], some of which have observed a behavior still not fully understood theoretically.

In the following, we will briefly present the two numerical techniques mentioned above and give an overview of the results obtained.

5.2 Fourier Modal Method

In the work presented in this chapter, the description of the scattering properties of each individual grating has been obtained by means of the Fourier Modal Method (FMM) [187]. We are going to describe the main features of this approach in the case of a one dimensional lamellar grating as the ones shown in Fig. 5.1. This kind of system is characterized by a region [$0 < z < h$ in Fig. 5.1(b)] with a periodic modulation of the dielectric permittivity, while the permittivity is assumed to be independent of x in all the other regions. Each uniform layer is characterized by a thickness δ_i, while for the grating region we define the height h, the period D and, in the simple case shown in figure, the filling ratio $f = l/D$.

The key features of the method are the following. First, a more appropriate choice of the basis is performed, reflecting the periodicity of the system, where the x component of the wavevector is replaced by $k_{x,n} = k_x + 2\pi n/D$, with k_x taking values in the first Brillouin zone $[-\pi/D, \pi/D]$ and n assuming all integer values. Then, while the fields in the uniform layers are directly known, the one in the grating region has to be determined by solving Maxwell's equations, involving the Fourier decomposition of the periodic permittivity. At this stage, a modified factorization rule introduced in Ref. [189] has to be employed in order to accelerate convergence. The next and final step is the imposition of the boundary conditions at the surface separating each couple of layers, from which the $\mathbb{S}$ matrix of the system, and thus its reflection and transmission operators,

can be deduced.

We remark that the solution of this problem requires a truncation of the number of Fourier modes involved in the description of the field. The convergence with respect to this parameter represents then a key issue in the calculations presented here. This point is carefully described in Ref. [188].

5.3 Casimir force out of thermal equilibrium between two gratings

Our first context of application of this framework has been the calculation of the Casimir force between two dielectric gratings in a configuration out of thermal equilibrium [188]. While we have already seen in Chapter 3 the possibility of tailoring the value of the force by acting on several different temperatures, as well as the possibility of achieving a repulsive force, our interest was here to understand to which extent the additional geometric features provide a way to further control the force.

A first example in this direction is provided by the results given in Fig. 5.2(a) showing the force as a function of the distance d between a $10\,\mu$m-thick SiO_2 grating (grating 1) and a semi-infinite silicon one (grating 2), for the set of temperatures $(T_1, T_2, T_e) = (200, 400, 10)\,$K. Both gratings have $f = 0.5$ and $h = 1\,\mu$m. The results (black lines) are compared, both at equilibrium at 200 K and out of equilibrium, to the ones for $f = 0$ (absence of grating and

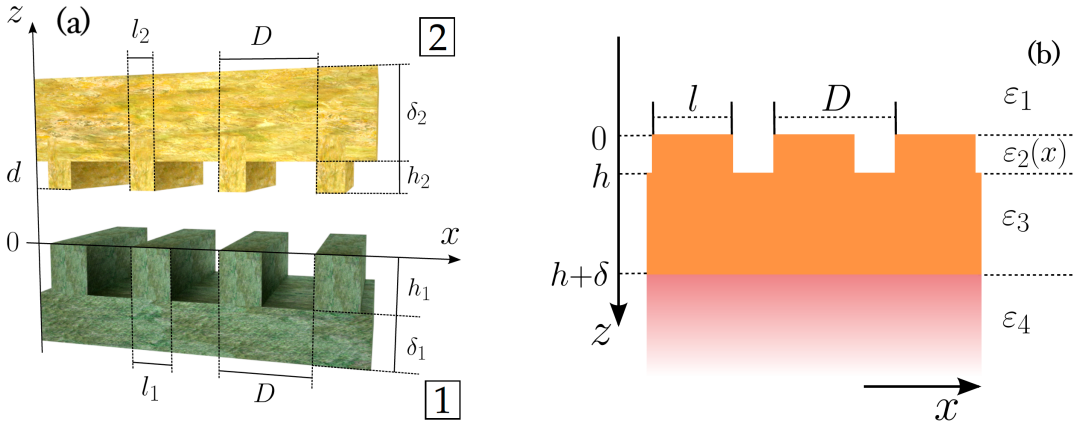

Figure 5.1 : (a) Two gratings, labeled with 1 and 2, at a distance d. The gratings, in general made of different materials, are infinite in the xy plane, and periodic in the x direction with the same period D. They have corrugation depths h_i $(i = 1, 2)$, thicknesses δ_i and lengths of the upper part of the grating l_i. This defines the filling factors $f_i = l_i/D$. (b) Geometry of the FMM calculation. We consider one grating with interface $z = 0$, corrugation depth h, and underlying thickness δ. This defines four zones (see text) with four (in general different) dielectric permittivities. From Ref. [188].

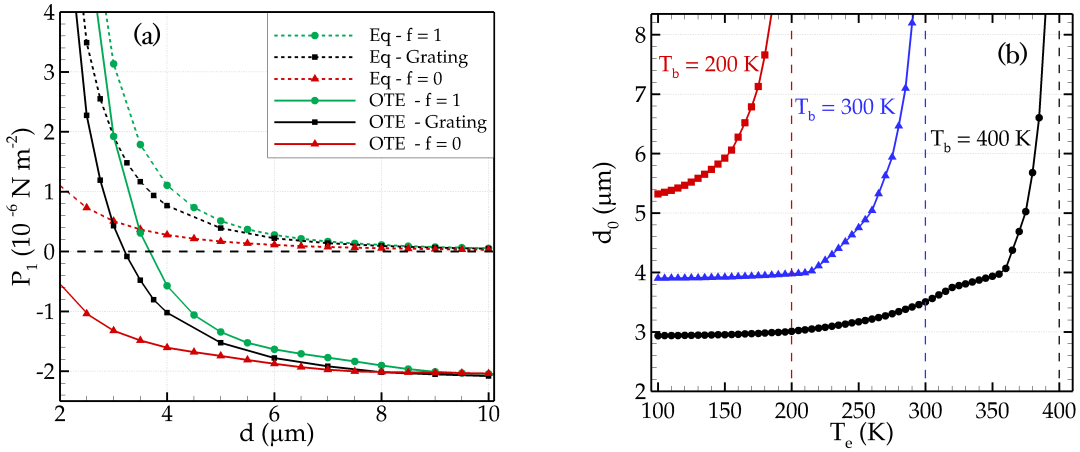

Figure 5.2 : (a) Non-equilibrium pressure $[(T_1, T_2, T_e) = (200, 400, 10)\,\mathrm{K}$, solid lines] compared to equilibrium pressure ($T = 200\,\mathrm{K}$, dashed lines) for two gratings (black squares), and two slab-slab configurations corresponding to filled gratings ($f = 1$, green circles) and an empty ones ($f = 0$, red triangles). (b) Distance d_0 of attractive-repulsive transition of the pressure as a function of T_e for three different values of $T_1 = T_2 = T_b$. From Ref. [188].

larger distance) and $f = 1$ (completely filled grating). It can be seen that the grating results are always intermediate between the two extreme cases. This has an important consequence of allowing to modulate the value of the force at a given distance by choosing the appropriate geometric parameters. Moreover, in the scenario out of thermal equilibrium, it has another relevant implication, which is the possibility to modulate the distance at which the transition between attraction and repulsion is observed.

Figure 5.2(b) gives further insight in this direction. It shows the distance at which the attraction-repulsion transition occurs as a function of the environmental temperature T_e in a configuration of relative thermal equilibrium between the two gratings $T_1 = T_2 = T_b$, for several values of T_b. While we clearly see that, for T_b approaching T_e, we have a vertical asymptote, signature of the impossibility of achieving repulsion at thermal equilibrium, for smaller values of T_e, we confirm the tunability of the transition distance d_0, for distances in the μm range, easily accessible experimentally.

Finally, we have investigated the possibility of tuning the value of the pressure by acting on the three grating parameters, namely the filling fraction f, the period D and the height h. The results are shown in Fig. 5.3, where the pressure P for a given value of the parameter is compared to the one P_0 obtained for the reference configuration $f = 0.5$, $h = 1\,\mu$m and $D = 1\,\mu$m. These results highlight not only an expected different dependence on the three parameters, but also a relatively high degree of control on the pressure (in particular with respect to the filling fraction),

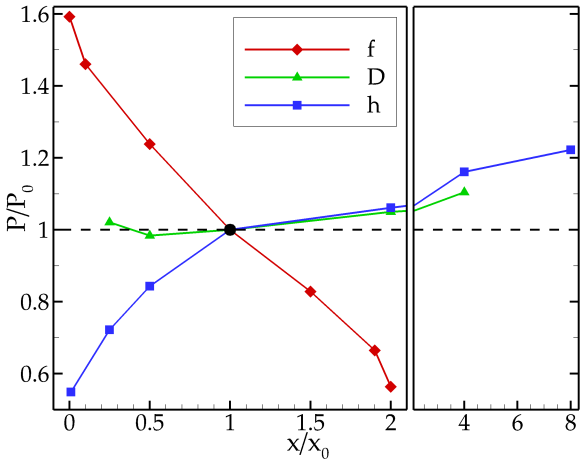

Figure 5.3 : Variation of the pressure between two gratings at $d = 4\,\mu$m [temperatures $(T_1, T_2, T_e) = (200, 400, 10)$ K] as a function of the geometrical parameters. The reference point (black circle) corresponds to the set of parameters $f_1 = f_2 = 0.5$, $h_1 = h_2 = 1\,\mu$m, $\delta_1 = 10\,\mu$m, infinite δ_2, $D = 1\,\mu$m. The three curves show the variation of pressure when changing one parameter at a time. On the y axis, the pressures are normalized with respect to the reference one, while on the x axis each varying parameter is normalized with respect to its reference value ($f_0 = 0.5$, $D_0 = 1\,\mu$m, $h_0 = 1\,\mu$m). From Ref. [188].

up to a factor 1.6 and down to almost 0.5.

5.4 Casimir force between a sphere and a grating

Shortly after the discussion of the Casimir force out of thermal equilibrium between two gratings, we tackled the study of the Casimir force at thermal equilibrium between a sphere and a grating. This configuration is interesting for several reasons. First, the spherical geometry has been used in several experiments measuring both Casimir forces and near-field radiative heat transfer in a sphere - plane configuration, since this allows to get rid of the problem of controlling the parallelism between two planes. Moreover, the mixture of the two (planar and spherical) symmetries, combined with the breaking of the translational symmetry due to the grating structure is at the origin of a lateral (along the grating periodic axis) force, vanishing in the sphere - plane scenario. Finally, it has been recently shown experimentally [32] that a metallic nanostructured grating leads to a strong reduction in the force, not fully understood theoretically.

It should be stressed that typically the theoretical analysis of experiments involving a sphere and a grating [21, 26, 27, 32, 191] is done within the Proximity Force Approximation (PFA) [192]. This approximation consists in tracing back the calculation of the total Casimir force in a specific geometrical configuration to a sum of plane - plane contributions, for which the pressure

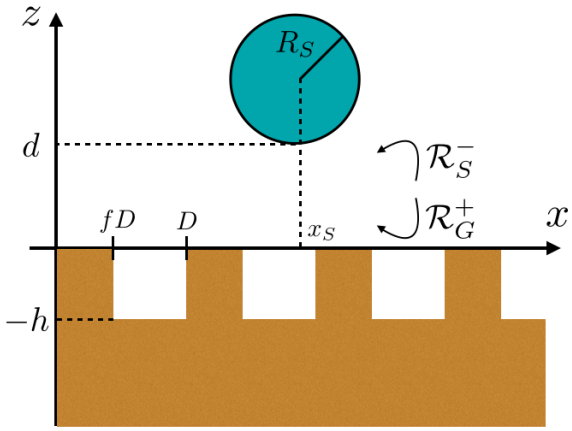

Figure 5.4 : Geometry of the system. A sphere of radius R_S is placed at distance d from the upper plane of a 1D grating, periodic along the x axis with period D. Moreover, f is the filling factor of the grating, h its depth, while x_S is the x coordinate of the sphere center. $\mathcal{R}_S^-$ and $\mathcal{R}_G^+$ are the reflection matrices involved in the calculation of the Casimir interaction. From Ref. [190].

is known analytically. It is thus clear that this approximation ignores the well-known non-additivity of Casimir interactions [193], and for this reason its precision cannot be assessed, except by comparison with exact results taking the sphere curvature fully into account. In the specific sphere - plane or sphere - grating scenario, PFA corresponds to the decomposition of the sphere into concentric hollow cylinders, orthogonal to the plane, and of infinitesimal thickness. Each one contributes to the Casimir energy with the product of its frontal area times the Casimir energy per unit of surface between two half-spaces at the corresponding distance. The final result is the integral of these contributions.

In our work [190], we have calculated the free energy

$$\mathcal{F} = k_B T {\sum_n}' \log\det[\mathbb{I} - \mathcal{M}(\mathrm{i}\xi_n)], \tag{5.4.1}$$

written as the sum over the Matsubara frequencies

$$\xi_n = \frac{2\pi n k_B T}{\hbar}, \qquad n = 0, 1, 2, ... \tag{5.4.2}$$

where the prime stands for an additional factor $1/2$ when accounting for the zero-frequency ($n = 0$) contribution, and involving the round-trip operator $\mathcal{M}$ defined as

$$\mathcal{M} = \mathcal{R}_S^- e^{-\mathcal{K}(d+R_S)} \mathcal{R}_G^+ e^{-\mathcal{K}(d+R_S)} \tag{5.4.3}$$

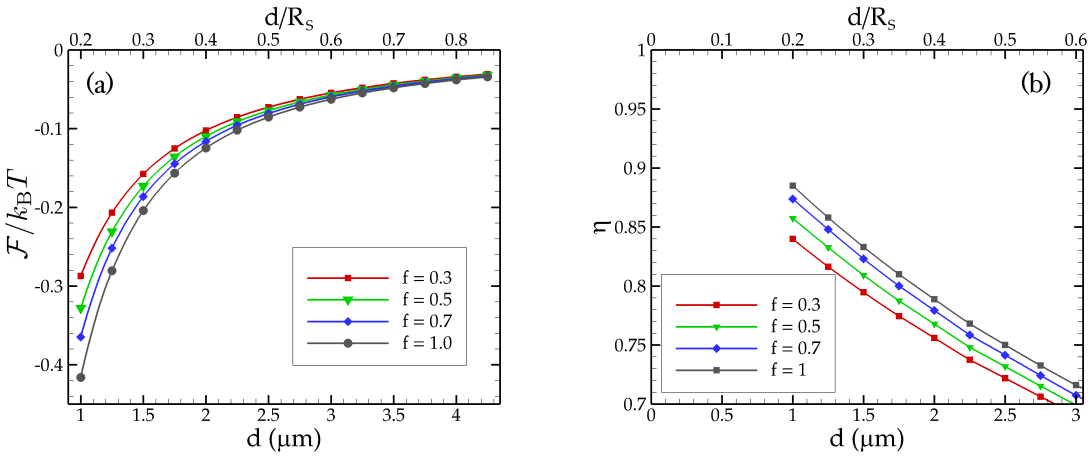

Figure 5.5 : (a) Casimir interaction energy (in units of $k_BT = 25.9\,\text{meV}$) between a gold sphere (radius $R_S = 5\,\mu\text{m}$) and a grating made of fused silica, as a function of the distance d. The grating has period $D = 1\,\mu\text{m}$, depth $h = 500\,\text{nm}$ and four possible filling factors: $f = 0.3, 0.5, 0.7, 1$, the last one corresponding to a sphere-plane configuration. The points are obtained numerically and the solid lines are interpolations. (b) Ratio between the exact Casimir energy and the PFA result as a function of distance for four different values of the filling factor f. From Ref. [190].

where $\mathcal{R}_G^+$ ($\mathcal{R}_S^-$) is the operator accounting for the reflection of waves propagating along the negative (positive) $z-$direction by the grating (sphere) (see Fig. 5.4), and $e^{-\mathcal{K}(d+R_S)}$ is the translation operator (see [190] for more details).

As a result of the geometry of our system, the free energy $\mathcal{F}$ depends both on the vertical distance d and on the lateral coordinate x_S of the sphere, giving rise to the two components of the force. The dependence of $\mathcal{F}$ on d between a metallic (gold) sphere and a dielectric (fused silica) grating is shown in Fig. 5.6(a) for several different filling fractions f. Apart from the clear increase of the normal component of the force when moving to smaller distances, we also observe a monotonic behavior with respect to f, coherently with what already observed in the case of two gratings. Figure 5.6(b) shows the ratio η between the exact and the PFA results as a function of the distance d. We clearly see that in all the configurations shown in figure, PFA overestimates the Casimir energy. Moreover, it becomes more accurate when the distance decreases. A further important consequence of the results shown in Fig. 5.6(b) is that when introducing a periodic structuring ($f < 1$) the value of η becomes even lower, proving that the description of the sphere as a set of parallel planes becomes less accurate in a more complex geometry.

We finally show the dependence of the free energy on the lateral coordinate x_S for a sphere of radius $R_S = 100\,\text{nm}$ at a distance $d = 100\,\text{nm}$ from a grating of period $D = 2\,\mu\text{m}$ and filling factor $f = 0.5$. We clearly see that, while for $h = 0$ (corresponding to a planar case) we have,

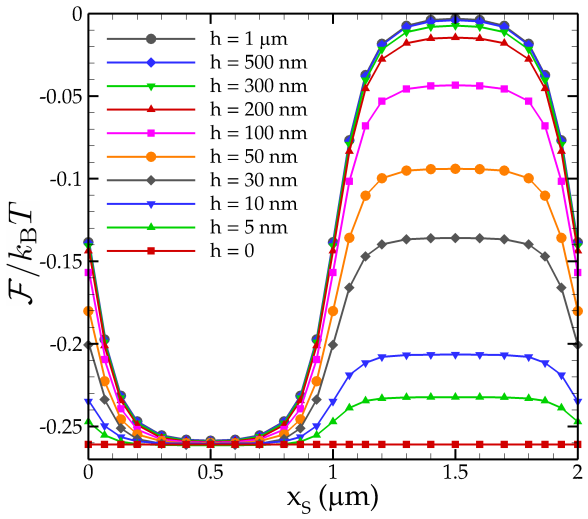

Figure 5.6 : Casimir energy variation with the sphere lateral position. The different curves correspond to different grating heights. From Ref. [190].

as expected, no dependence on x_S and thus no lateral force, the dependence is significantly affected by the height, and reaches an asymptotic behavior around $h = 1\,\mu$m, in the specific case around 10 times the sphere radius and distance from the grating. We clearly highlight two lateral equilibrium positions (one stable, one unstable) at the center of the two grating regions, and the strongest dependence of $\mathcal{F}$ on x_S (i.e. the largest lateral force) is around the discontinuity of the grating. Clearly, this shows that for grating heights larger than $1\,\mu$m, the bottom of the grating is not affecting the sphere - grating interaction anymore. We will provide further analysis of the role played by the grating height in the context of near-field radiative heat transfer in Sec. 5.6.

5.5 Adaptive Spatial Resolution

The two following sections deal with the calculation of the radiative heat transfer and Casimir force in configurations involving metallic gratings. It is well known that the presence of a high dielectric contrast due to the presence of a metallic behavior is at the origin of several instabilities in the numerical evaluation of the scattering operators of a grating [195]. It has been shown that the FMM technique can be modified in order to deal more effectively with this scenario, by introducing the so-called Adaptive Spatial Resolution (ASR) [196]. The details of this approach are discussed in Ref. [194], where this technique is employed to calculated near-field radiative heat transfer between two gold gratings. The main idea behind this technique is the introduction of a coordinate change [197] along the periodic direction, producing an effective smoother behavior of the permittivity as a function of the coordinate.

While these results are described more in detail in Sec. 5.6, we focus here on a single example of calculation in order to show the considerable gain in terms of calculation effort and stability associated with the ASR modification. We consider the calculation of near-field heat flux between two identical gratings of height $h = 2\,\mu$m, period $D = 1\,\mu$m, filling fraction $f = 0.5$, infinite thickness below the grating region, and temperatures $T_1 = 310\,$K and $T_2 = 290\,$K. Figure 5.7 shows the value of the flux as a function of the truncation order, i.e. the number of Fourier modes taken into account in the decomposition. The figure shows that the use of ASR presents two main important advantages: a dramatic increase in the rate of convergence, as well as the disappearance of the oscillatory behavior (around $N = 10$) clearly visible in the result obtained with standard FMM. The use of this technique for a quantitative study of the near-field radiative heat transfer between two gold gratings is the topic of the next section.

5.6 Radiative heat transfer between metallic gratings

As anticipated in the previous section, the use of ASR allows a dramatic increase of the convergence rate in the calculation of the scattering properties of metallic gratings. By means of this technique we have studied in Ref. [194] the radiative heat transfer between two gold gratings in the near-field regime. This work was inspired by a previous one [177], where the effect of the grating height was addressed more in detail. Nevertheless, the dependence on this parameter was studied in a relatively narrow range, that we extend here, providing also a more detailed

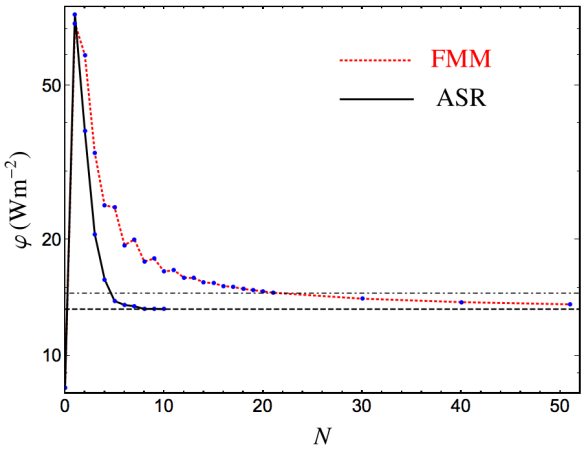

Figure 5.7 : Heat flux between two gratings (see text for details). The flux is calculated using both FMM (red dashed line) and ASR (black solid line), for different truncation orders N. The black dashed line corresponds to the asymptotic value obtained using ASR for $N = 10$, while the gray dot-dashed line is associated to a 10% error with respect to this asymptotic result. From Ref. [194].

spectral study of the effect.

More specifically, we chose the same parameters as in Ref. [177], by considering two identical gold grating have period $D = 1\,\mu$m, filling fraction $f = 0.5$, infinite thickness below the grating region, and temperatures $T_1 = 290\,$K and $T_2 = 310\,$K. The ratio between the radiative flux between the two gratings and the one between two planar slabs is shown in Fig. 5.8. The main part of the plot shows the main result of our work, namely a remarkable amplification of the flux transferred between the two systems as a function of the grating height h. Thanks to our improved numerical technique, we were able to explore large values of this parameter, and highlight a final asymptotic regime, reached for $h \simeq 1\,$mm, where the transferred energy become independent of h. In the same figure we compare our results (black line) to the ones (red points) obtained in Ref. [177]. While the overall trend is similar, this comparison seems to highlight an unstable behavior of the previous calculation, due in our opinion to the use of the unmodified FFM.

In order to get more physical insight on the highlighted flux amplification, we have studied the evolution of the spectral heat flux as a function of the grating height. The results are shown in Fig. 5.9. The case $h = 0$ corresponds to the well-known slab-slab configuration, in which the absence of surface resonances in the frequency window compatible with the temperatures under scrutiny results in the absence of localized peaks. The physical picture becomes more interesting when we increase the value of h. As clear from Fig. 5.9, this results in the appearance of resonances in the flux spectrum, whose position and number strongly depends on h. More specifically, each resonance shifts towards smaller frequencies when increasing h. These new

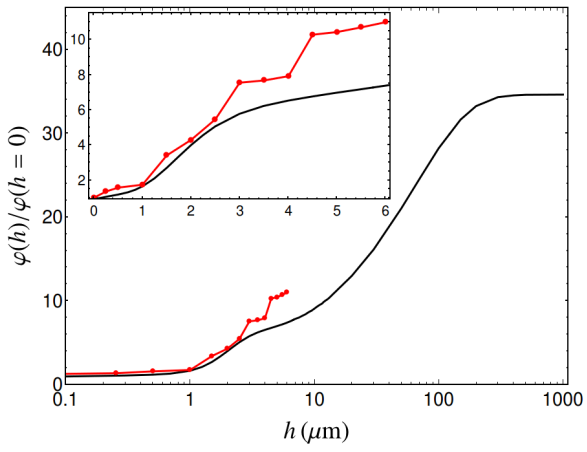

Figure 5.8 : Ratio between the flux for a grating of height h and the one for $h = 0$, i.e. the the one between two planar slabs. Our results (black solid line) are compared to the results of Ref. [177] (red points). From Ref. [194].

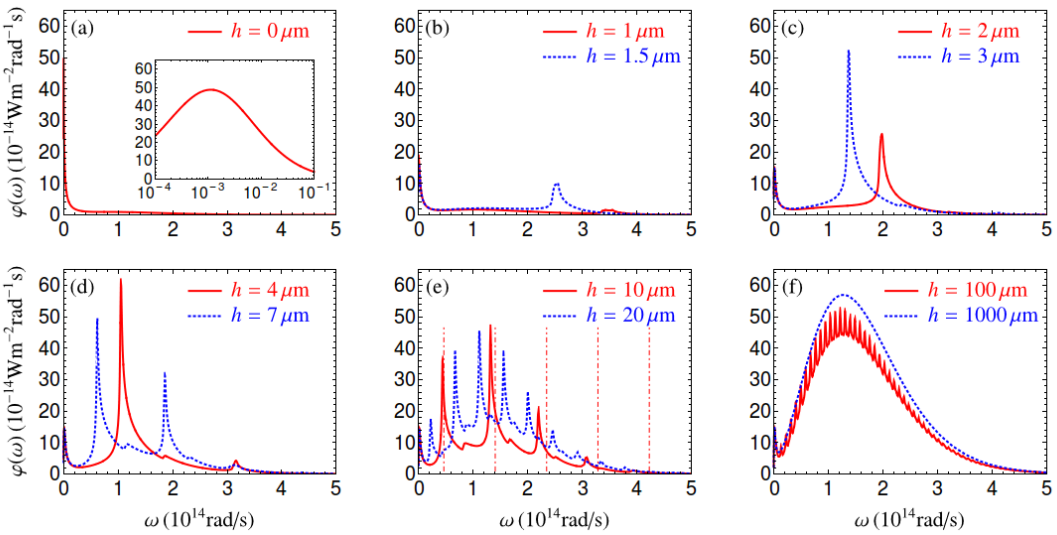

Figure 5.9 : Spectral heat flux for several grating heights h. In panel (a), the inset shows a zoom in logarithmic x scale for small frequencies. From Ref. [194].

peaks are at the origin of the overall increased flux. If we consider values of h the order of $100\,\mu$m, we highlight the appearance of a very dense comb of resonance frequencies, which for even higher values of h tends to a continuous profile, corresponding to the asymptotic scenario discussed above.

It is instructive to compare these resonances to the ones, called spoof plasmons, predicted by the theoretical model developed in Refs. [198, 199]. In these works, the existence of a set of modes in the case of a grating made of a perfect conductor is proven, and these new resonances have frequencies $\omega_n = (2n+1)\pi c/2h$. We clearly see that the distance between two successive frequencies decreases with h, coherently with the results shown above. Moreover, in Fig. 5.9(e), we superpose the first 5 resonances to our spectral flux in the case $h = 10\,\mu$m. We observe that the trend is correct, and the prediction for smaller frequencies works increasingly well. This is not surprising, since in this limit the permittivity of gold diverges, and we get closer to the behavior of a perfect conductor. In conclusion, apart from the direct numerical comparison of the frequency values, this discussion confirms our interpretation concerning the origin of this new resonances, and the associated flux amplification.

5.7 Casimir torque between twisted Gratings

Another relevant consequence of the absence of symmetry can be the existence of a Casimir torque on the two interacting bodies. This topic has been already explored in the past [201–215],

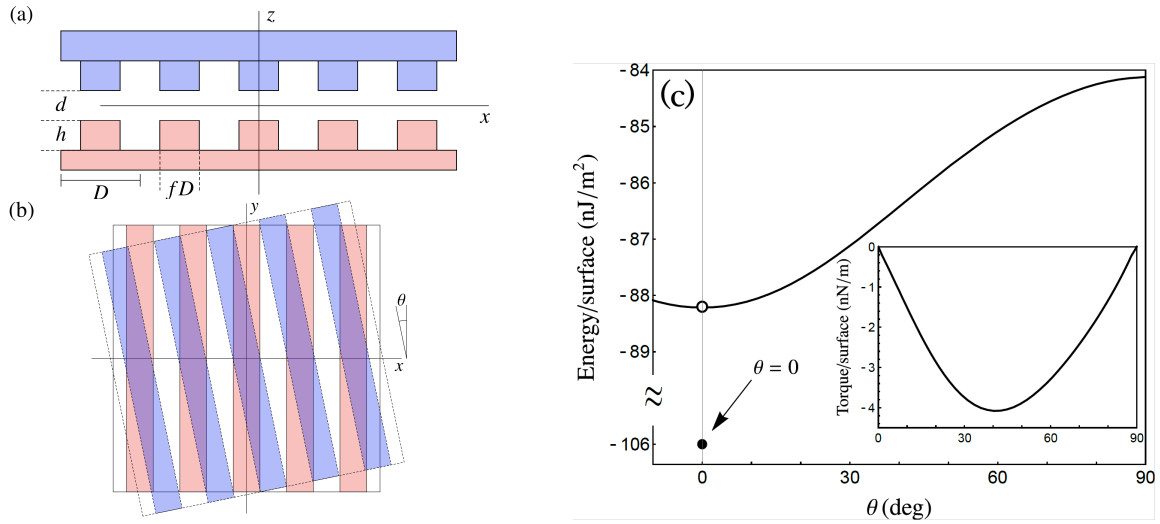

Figure 5.10 : (a) Geometry of the system: two one-dimensional periodic lamellar gratings having period D, filling fraction f and height h, placed at distance d. The figure shows two samples with $n = 5$ periods. (a) side view of two aligned gratings. (b) Top view of two gratings rotated by an angle θ. (c) Angle-dependent Casimir energy per unit surface between two infinite gold gratings (see text for grating parameters) at distance $d = 100\,\text{nm}$. The black dot (not in scale on the vertical axis) shows the energy between two perfectly aligned gratings ($\theta = 0$). The inset shows the torque as a function of θ for $\theta \neq 0$. From Ref. [200].

in a variety of configurations where the anisotropy can be due either to geometrical or intrinsic optical properties. Very recently, this effect has been measured for the first time between two optically anisotropic materials [216].

We have tackled the problem of the Casimir torque existing between two one-dimensional gratings forming an angle θ between them [200] [see Fig. 5.10(a)], and highlighted an anomalous behavior close to $\theta = 0$ (aligned gratings), closely related to the transition between an ideal infinitely extended grating and a finite one.

The torque between the two gratings can be indeed calculated by studying the angle dependence of the Casimir energy. The energy and the torque as a function of θ are given in Fig. 5.10(b) for two infinite gold gratings with parameters $D = 400\,\text{nm}$, $h = 200\,\text{nm}$, $f = 0.5$ placed at a distance $d = 100\,\text{nm}$. We stress that the calculation for an arbitrary angle θ requires a specific theoretical framework (more general than the one for two aligned gratings), discussed in detail in Ref. [213]. From Fig. 5.10(b), we clearly see, as expected from symmetry arguments, that the torque vanishes at $\theta = 0$ and $\theta = 90$ degrees, resulting in a stable and unstable equilibrium position, respectively. Nevertheless, the striking result shown in figure is that, while the Casimir energy tends continuously to a finite value for θ going to 0, this value does not coincide

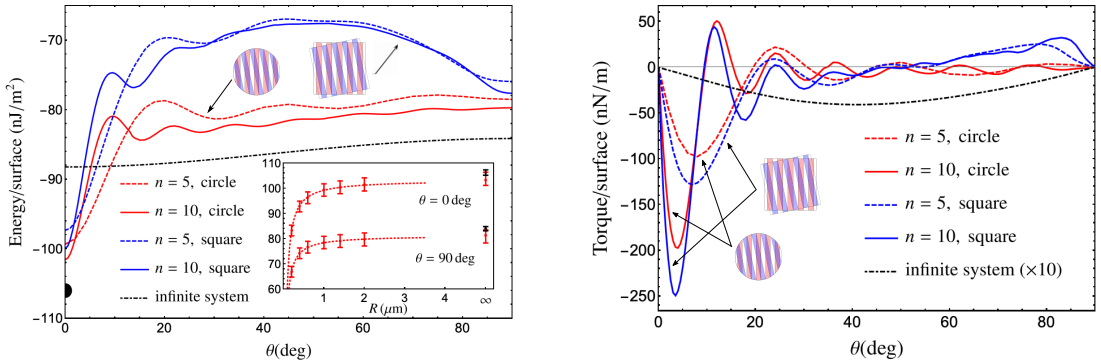

Figure 5.11 : (a) Casimir energy per unit surface between two finite gold gratings having $n = 5$ (red dashed line for two circular gratings having $R = 1\,\mu$m, blue dashed line for two square gratings having $L = 2\,\mu$m) or $n = 10$ (red solid line for two circular gratings having $R = 2\,\mu$m, blue solid line for two square gratings having $L = 4\,\mu$m) unit cells placed at a distance $d = 100\,$nm. The black dot-dashed line corresponds to two infinite gratings. Inset: Casimir energy per unit surface (in absolute value) for $\theta = 0\,$deg (upper curve) and $\theta = 90\,$deg (lower curve) as a function of the radius R of the finite circular grating. The red points obtained numerically are fitted with a function $A + B/R$ (red dotted lines). The asymptotic values for $R \to \infty$ (red dots, not in scale on the horizontal axis) are compared with the ones obtained theoretically for an infinite grating (black dots). All the points are represented with the error bars coming from the respective numerical techniques. (b) Casimir torque per unit surface between two finite gold gratings having $n = 5$ or $n = 10$ unit cells placed at a distance $d = 100\,$nm. The black dot-dashed line corresponds to two infinite gratings, multiplied by a factor of 10 in order to make it more visible. From Ref. [200].

with the one obtained by means of a calculation for aligned gratings.

In order to understand the origin of this anomaly, we have focused our attention of the difference between a finite and an infinite grating. More specifically, we stress that for infinite gratings, if we consider an arbitrary (even very small) angle θ between the two gratings, a given grating line (the axis of a raised part of the grating) of grating 2 will make an infinite number of intersections with the grating lines of grating 1. This means that, for infinite-size gratings, passing from a finite θ to strictly $\theta = 0$ implies passing from an infinite number of crossing points to zero crossing points. This discontinuity is actually never encountered in the case of a real finite grating, since an angle θ below which no intersections occur always exists.

For this reason, we have compared the results for an infinite grating to the ones for finite gratings of circular or square shapes. The associated energy and torque are shown in Fig. 5.11. These results clearly show that considering a finite system we recover the behavior of perfectly aligned gratings in the limit of large grating extension [see inset of Fig. 5.11(a)]. As a result, we highlight a peak of the torque existing for small angles θ, whose value increases with the size of the system. A simple theoretical model allowed us to show that this maximum torque is of

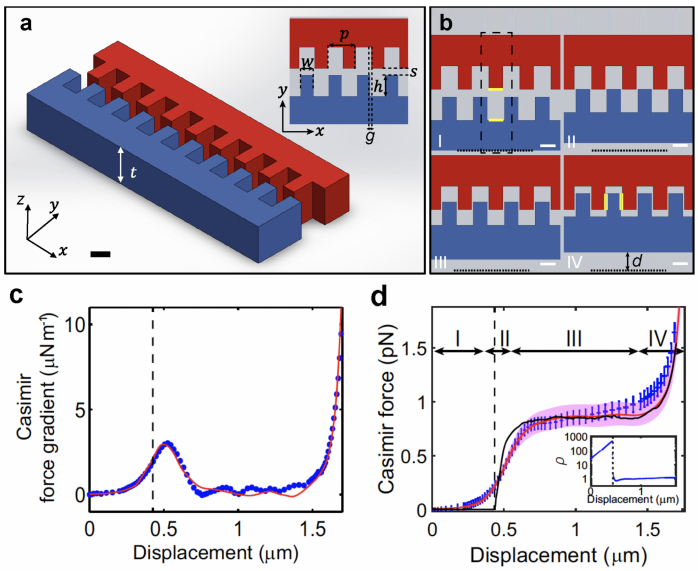

Figure 5.12 : (a) Schematic of a part of the perfectly rectangular silicon grating. Initially, the displacement d of the movable grating (blue) along the y direction is zero. The lateral separation between adjacent grating fingers is $g = p/2 - w \simeq 92\,\text{nm}$ and the initial separation in y is $s = 430\,\text{nm}$. (b) Top view schematic for the interpenetration of the two gratings, describing the four stages of the interpenetration. d is defined as the displacement of the movable grating from this initial position. (c) Measured Casimir force gradient (blue) as a function of displacement. The red line is calculated by SCUFF-EM. (d) The measured force gradient is integrated over displacement to yield the force. The red line is calculated by SCUFF-EM and the black line is generated by the PFA. The inset plots the ratio ρ of the measured force to the force calculated with the PFA. The dashed line labels where the gratings interpenetrate. From Ref. [217].

the order of $\tau_{\text{max}} \simeq -56R$ (R in μm, τ in nN/m), linearly growing with the radius R of the grating, and more and more accurate as the $R \to \infty$. Already for small systems with 10 period repetitions, these values are much higher than the ones measured in Ref. [216], thus within the present experimental sensitivity.

5.8 Experiment on interpenetrated gratings

In this last section we will briefly review an experiment performed within the group of H. B. Chan at Hong Kong University, to which we have contributed with a theoretical simulation of the Casimir force between two gratings [217]. In this experiment, the Casimir force gradient has been measured between two possibly interpenetrated silicon gratings, shown in Fig. 5.12(a) and (b). Each grating has thickness $t = 2.58\,\mu\text{m}$ and period $p = 2\,\mu\text{m}$. For each rectangular protrusion, the width w and length h are 908 nm and $1.5\,\mu$m, respectively. Initially, the separation s in the

y direction between the tip of the protrusions on the two gratings is 430 nm. The two gratings are offset laterally by $p/2$ such that as the bottom grating (blue) moves towards the top one (red) in the positive y direction, they interpenetrate when the displacement d exceeds s.

The scattering approach we developed is not applicable to interpenetrated gratings. For this reason the calculations in the entire range of distances have been performed by means of the SCUFF-EM code [43]. Nevertheless, in order to verify this approach, the results obtained have been confirmed by a scattering calculations in the first region (before interpenetration).

The results shown in Fig. 5.12(c) and (d) clearly highlight a good agreement between theory and measurements, as well as the existence of a non-trivial dependence of force and force gradient on the distance d. It is important to look at the inset of Fig. 5.12(d), showing the ratio between the actual force and the PFA result. While in the regimes III and IV, i.e. after interpenetration, PFA is in good agreement with an exact theory, in the region close to interpenetration, PFA is not able to describe the behavior of the force, resulting in a ratio ρ of more than two orders of magnitude.

5.9 Publications concerned by this chapter

[188] A. Noto, R. Messina, B. Guizal, and M. Antezza, *Casimir-Lifshitz force out of thermal equilibrium between dielectric gratings*, Phys. Rev. A **90**, 022120 (2014).

[190] R. Messina, P. A. Maia Neto, B. Guizal, and M. Antezza, *Casimir interaction between a sphere and a grating*, Phys. Rev. A **92**, 062504 (2015).

[194] R. Messina, A. Noto, B. Guizal, and M. Antezza, *Radiative heat transfer between metallic gratings using Fourier modal method with adaptive spatial resolution*, Phys. Rev. B **95**, 125404 (2017).

[200] M. Antezza, H. B. Chan, B. Guizal, V. N. Marachevsky, R. Messina, and M. Wang, *Giant Casimir Torque between Rotated Gratings and the $\theta = 0$ Anomaly*, Phys. Rev. Lett. **124**, 013903 (2020)

[217] M. Wang, L. Tang, C. Y. Ng, R. Messina, B. Guizal, J. A. Crosse, M. Antezza, C. T. Chan, and H. B. Chan, *Strong geometry dependence of the Casimir force between interpenetrated rectangular gratings*, Nat. Commun. **12**, 600 (2021).

CHAPTER 6

Coupling between conduction and near-field radiative heat transfer

Contents

6.1 Introduction

This chapter is dedicated to the results concerning the coupling between radiative and conductive heat transfer. Surprisingly, albeit its remarkable fundamental interest, this topic has not received the deserved attention during the last decades. As a matter of fact, even in very recent works, the typical assumption has been to consider that the radiative contribution is insufficient to compete with conduction inside each solid [218–220]. We have proved that this is not the case and, depending on the distance and materials taken into account, near-field radiative heat transfer can indeed produce a temperature gradient within each body. Of course, this temperature gradient results, in turn, into a modified value of the radiative flux. As a result, in some scenarios a correct description even of the radiative flux alone demands a quantitative description of the conduction - radiation coupling. As a further remark, this coupling needs to be taken into account also because experiments are exploring increasingly smaller separation gaps, down to the nanometer range [62–68, 71, 72, 77, 80, 82, 221, 222].

The results within Fourier regime were obtained in collaboration with A. W. Rodriguez and W. Jin from Princeton University. This collaboration was funded by a PICS project from CNRS, of which I was principal investigator and which lasted from 2017 to 2019. The results obtained after are mainly the work of M. Reina, PhD student in our group under the supervision of P. Ben-Abdallah and myself from October 2018, and were obtained in collaboration with S.-A. Biehs.

6.2 Coupling in the Fourier regime

While recent works have focused on the open problem of the transition between radiation and conduction in the extreme near-field regime, either within fluctuational electrodynamics [225] or in the context of phonon tunneling [226], we focused on the coupling between these two energy-transport channels. The first two works on this topic [223, 224] were dedicated to the simple geometry of two parallel slabs. Since, as anticipated, the conduction - radiation coupling is supposed to induce a temperature gradient within each slab, we first developed a theoretical framework to calculate the radiative heat transfer between two slabs with an arbitrary temperature profile [see Fig. 6.1(a)]. This was done in Ref. [223], and the main idea behind the calculation is presented in Fig. 6.1(b). A given temperature profile is chosen for a slab, and local thermal equilibrium is assumed inside the body. Each infinitesimal part of the slab is isolated from the rest, and a three-body formalism is applied. This allowed us to express the correlation functions of the field emitted by a slab with an arbitrary temperature profile, and thus the

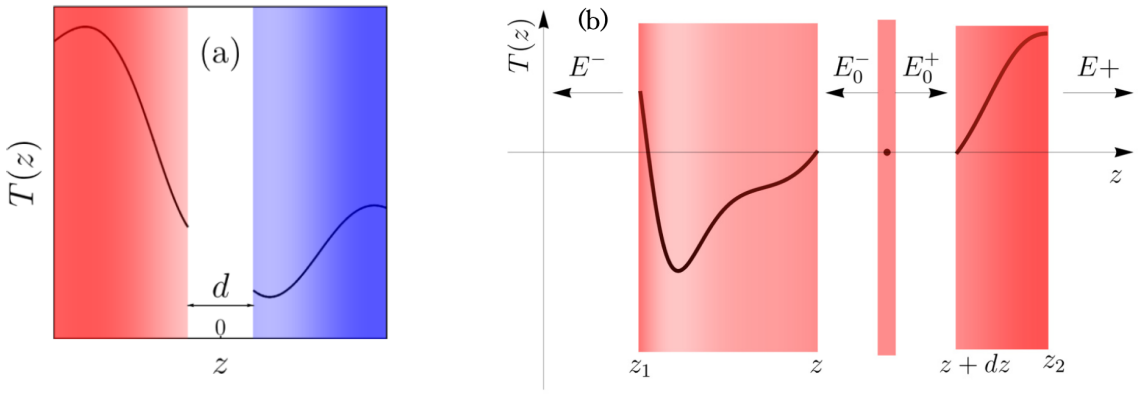

Figure 6.1 : (a) Schematic of two parallel slabs separated by a distance d along the z direction. The two slabs are subject to a temperature profile $T(z)$. (b) Schematic of one slab having a position-dependent temperature $T(z)$. The slab occupies the region $[z_1, z_2]$ and the element from z to $z + dz$ produces the field E_0. The total field emitted by the slab on the left (right) side is E^+ (E^-). From Ref. [223].

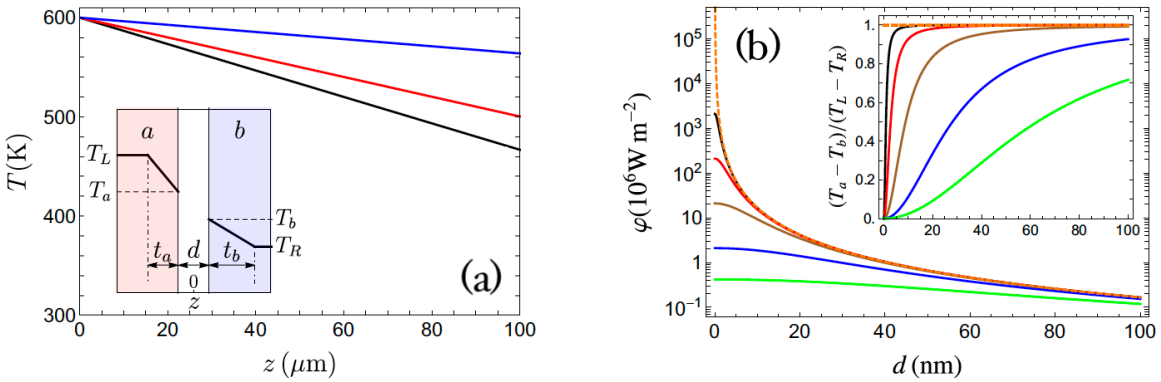

Figure 6.2 : (a) Schematic of two parallel slabs separated by a distance d. The two slabs exhibit a temperature profile $T(z)$. Temperature profile along the temperature-varying region of the hot slab in a configuration involving two silica slabs with $t_a = t_b = 100\,\mu$m held at external temperatures $T_L = 600\,$K and $T_R = 300\,$K at the outer ends, and separated by vacuum gaps d. The three lines correspond to $d = 10\,$nm (black), $20\,$nm (red) and $50\,$nm (blue). (b) Total flux φ and temperature difference $T_a - T_b$ (inset) as a function of distance d between two silica slabs held at $T_L = 600\,$K and $T_R = 300\,$K. The various solid lines correspond to different temperature-varying regions t (from top to bottom): $100\,$nm (black), $1\,\mu$m (red), $10\,\mu$m (brown), $100\,\mu$m (blue) and $500\,\mu$m (green). The orange dashed line shows φ in the absence of temperature gradients. From Ref. [224].

radiative heat transfer between two such slabs.

In Ref. [223], we exploited this result to study asymptotic behavior of the radiative flux when the distance between the slabs tend to zero, in the case of two polar materials, as a function of the properties of the two temperature profiles. We first recovered the known result, according to which for two constant temperatures, the flux diverges as d^{-2} for d going to zero. Nevertheless, we showed that this divergence proves to be mitigated or even removed in some cases. In particular, we showed that if the temperatures at the boundaries with the vacuum gap coincide, the flux diverges as d^{-1}. Moreover, if additionally the first derivatives at the vacuum boundaries have opposite values, the divergence becomes logarithmic, and finally disappears if the second order derivatives of the temperature coincide, giving rise to a constant limiting value of the flux. Besides its fundamental interest, these findings pave the way to the possibility of controlling and tailoring the behavior of the flux, under the condition of being able to manipulate (through several thermostats, for example) the temperature distribution within each body.

We then used this framework to tackle the problem of conduction - radiation coupling, where the temperature profile is not externally controlled but results, as anticipated, from the coupling itself. A first step in this direction was in done in Ref. [224], where the coupling was studied in the Fourier regime, between two planar slabs. In particular, we assumed that the temperature is allowed to vary within a thickness t_a (t_b) in the left (right) slab, as shown in Fig. 6.2(a). In

order to get analytical insight into the induced temperature profile and the resulting modification of the flux, we performed a further approximation, consisting in assuming that the near-field radiative flux is primarily exchanged at the surface between each body and the vacuum gap. This assumption, supposed to be valid for polar materials, allowed us to treat the radiative flux as a boundary condition in Fourier equation and to solve the problem analytically, obtaining the temperatures T_a and T_b [see Fig. 6.2(a)]. The profiles obtained in the case of two silica slabs of thickness $t_a = t_b = 100\,\mu$m are shown in Fig. 6.2(a) for three different distances. It is clear that even at the largest distance considered, i.e. $d = 50\,$nm, the deviation from a uniform temperature profile is manifest and experimentally observable. The impact of slab thickness is shown in Fig. 6.2(b), again for two silica slabs at different distances. Apart from confirming the observable temperature profile (see inset), the flux shows a remarkable deviation from the ideal d^{-2} behavior, with a clear saturation when the distance d approaches zero. These results prove that a coupled theory is indeed relevant for some materials, even at distances of tens (or even hundreds) or nanometers, in order to correctly predict the value of the flux and its possible saturation. These results were shortly after generalized to more complex geometries by means of a fluctuation volume-current approach [227, 228], allowing to show that in the case of two aligned rods the impact of conduction - radiation coupling can be even more dramatic, allowing also to observe non-linear temperature profiles (see Ref. [227] for more details).

6.3 Boltzmann-equation approach

One step further in the study of conduction - radiation coupling was done during the PhD of Marta Reina, student in our group since October 2018. The main purpose of her work was to generalize the study presented before (limited to Fourier regime) to any transport regime. To this aim, we considered again a system made of two finite-thickness parallel slabs, and studied conduction inside each body within the framework of Boltzmann transport equation for phonons [229]. This allowed to go beyond the Fourier regime, and to study the impact of coupling for any slab thickness, and then from the ballistic regime to the diffusive one, fully addressing also all the transition between them. In other words, contrarily to the works described above, in this approach no assumption is made in advance on the specific heat transport regime by conduction.

More specifically, we solved the dynamical energy-conservation equation

$$\frac{\partial u(\mathbf{r},t)}{\partial t} = P_{\text{rad}}(\mathbf{r},t) + P_{\text{cond}}(\mathbf{r},t), \tag{6.3.1}$$

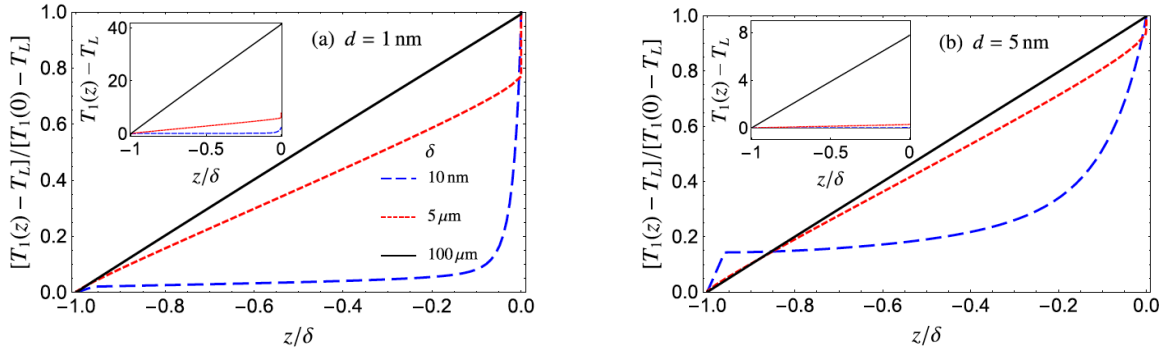

Figure 6.3 : (a) Steady-state temperature (inset) and normalized temperature profile inside the left slab for different thicknesses and a separation distance $d = 1\,\text{nm}$. (b) Same as (a) for $d = 5\,\text{nm}$. From Ref. [229].

where

$$u = \sum_p \int_{\omega_p^{\min}}^{\omega_p^{\max}} d\omega\, \hbar\omega f_0(\omega, T) D_p(\omega) \tag{6.3.2}$$

is the internal energy density inside each slab, $f_0(\omega, T)$ being the equilibrium Bose-Einstein distribution and $D_p(\omega)$ the density of states. The sum in Eq. (6.3.2) is over all polarization branches, between the minimum and maximum allowed frequency for the given branch. Moreover, in Eq. (6.3.1) P_{rad} the radiative power locally dissipated within each body and coming from the other one, and P_{cond} is the conductive contribution. While P_{rad} can be calculated by means of the approach described above, P_{cond} can be directly related to the phonon distribution function f_p, solution of Boltzmann's equation in the relaxation time approximation,

$$\frac{\partial f_p}{\partial t} + \mathbf{v}_{g,p} \cdot \nabla f_p = -\frac{f_p - f_0}{\tau_p[\omega, T(\mathbf{r})]}, \tag{6.3.3}$$

τ_p being the heat-carrier relaxation time and $\mathbf{v}_{g,p}$ the group velocity. The conductive power P_{cond} is the divergence of the conductive flux

$$\varphi_{\text{cond}}(t, \mathbf{r}) = \sum_p \int_{4\pi} d\Omega \int d\omega\, \hbar\omega\, \mathbf{v}_{g,p}(\omega) f_p(t, \omega, \mathbf{r}, \Omega) \frac{D_p(\omega)}{4\pi}. \tag{6.3.4}$$

These equations constitute a coupled system allowing us to follow dynamically the temperature profiles as well as the conductive and radiative fluxes.

The coupled problem was studied in the simple scenario of two SiC parallel slabs, of the same thickness δ and separated by a distance d. The left (right) side of the left (right) slab is assumed to be in contact with a reservoir at temperature T_L (T_R). The stationary temperature profiles inside the left slab are shown in Fig. 6.3 in the configuration $(T_L, T_R) = (300, 400)\,\text{K}$,

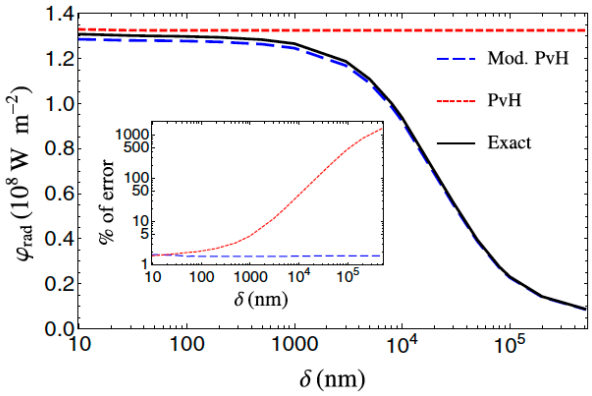

Figure 6.4 : Radiative heat flux exchanged between two SiC slabs with respect to their thickness for a separation distance of $d = 1\,\text{nm}$. We show the exact result (black line), the PvH flux (red dashed line, uniform temperatures $(T_L, T_R) = (300, 400)\,\text{K}$, and the modified PvH flux (blue long dashed line, see text for details). Insets: absolute value of the error with respect to the PvH and modified PvH approaches. From Ref. [229].

for different value of slab thickness and for the two distances $d = 1, 5\,\text{nm}$. These results confirm the result already observed within Fourier's equation and described above, that conduction - radiation coupling is indeed able to produce an observable temperature profile within each slab. Moreover, as expected, this result is stronger for smaller distances, for which the radiative flux is higher and then more likely competes with conduction inside the bodies. The inset of the two figures show the temperature gradient in absolute units, which reaches 40 degrees in the best scenario of thickness $\delta = 100\,\mu\text{m}$. It is interesting to compare the profiles for difference thicknesses in a normalized temperature scale, shown in the main part of Fig. 6.3. As a matter of fact, this comparison allows to focus on the different shape of the profile, signature of the transition between the different heat-transport regimes inside the bodies. We observe that in the case of large thickness ($\delta = 100\,\mu\text{m}$) the profile is linear: this is expected since in this case the Fourier approximation is safely applicable. This is no longer true for the intermediate thickness $\delta = 5\,\mu\text{m}$, of the order of the mean free path. In this scenario, the profile is approximately linear except close to the vacuum gap, where it shows a strong increase. The third configuration corresponds to a thickness $\delta = 10\,\text{nm}$, much smaller than the mean free path, for which the transport regime is ballistic. In this case, we observe a sharp variation of the temperature close to the thermostat as well, in agreement with the fact that we are approaching the so-called Casimir regime, characterized by a uniform temperature inside the body.

We also addressed, as in the work described above, the impact of conduction - radiation coupling on the value of the radiative flux. The exact value calculated within our approach has been compared to two approximate results. The former is the standard Polder and van

Hove (PvH) result, based on the assumption that the temperature is uniform in each slab and coincides with the one imposed by the thermostat. Figure 6.4 shows that this result, which is almost independent of the thickness δ, presents a dramatic deviation from the exact result, in particular for high values of the thickness. This confirms that, at least for materials supporting resonant surface modes and for distances in the nm regime, conduction - radiation coupling has indeed an impact on the value of the radiative flux. The second comparison we did is with the configuration we called *modified PvH theory*, defined as a scenario in which the temperature of each slab is assumed to be uniform and equal to the temperatures at the boundaries with the vacuum gap in the steady states resulting from the coupling with conduction. The purpose of this comparison is to show to which extent the assumption of purely surface exchange holds, at least in the case of polar materials supporting surface resonant modes. Figure 6.4 clearly proves that the modified PvH scheme provides a very good qualitative and quantitative description of the actual flux. Nevertheless, we have to stress that this result is interesting from the fundamental point of view, since it gives an insight concerning the behavior of the flux, but does not provide a simplified calculation path, since the knowledge of the boundary temperatures demands of course the solution of the full conduction - radiation problem discussed here.

6.4 Publications concerned by this chapter

[223] R. Messina, W. Jin, and A. W. Rodriguez, *Exact formulas for radiative heat transfer between planar bodies under arbitrary temperature profiles: Modified asymptotics and sign-flip transitions*, Phys. Rev. B **94**, 205438 (2016).

[224] R. Messina, W. Jin, and A. W. Rodriguez, *Strongly coupled near-field radiative and conductive heat transfer between planar bodies*, Phys. Rev. B **94**, 121410(R) (2016).

[227] W. Jin, R. Messina, and A. W. Rodriguez, *General formulation of coupled radiative and conductive heat transfer between compact bodies*, Phys. Rev. B **95**, 161409 (2017).

[228] W. Jin, R. Messina, and A. W. Rodriguez, *Near-Field Radiative Heat Transfer under Temperature Gradients and Conductive Transfer*, Z. Naturforsch. A **72**, 141 (2017).

[229] M. Reina, R. Messina, and P. Ben-Abdallah, *Conduction-Radiation Coupling between Two Closely Separated Solids*, Phys. Rev. Lett. **125**, 224302 (2020).

Conclusions and Perspectives

In this manuscript I have given an overview of the results I obtained since the beginning of my permanent position at CNRS in 2013. Thanks to several young and motivated PhD students and postdocs, as well all numerous fruitful collaborations, my purpose has been to get a deeper insight in the domains of Casimir forces and near-field radiative heat transfer, sharing the common theoretical framework of fluctuational electrodynamics.

I believe that the results we obtained have shown that many aspects of these effects still deserve attention, both theoretically and experimentally. In general terms, it can be said that the purpose of my activity was twofold. On one had, we wanted to explore new paths to manipulate, in terms of amplitude, spatial and spectral distribution, the force and radiative heat transfer in complex systems. On the other hand, keeping in mind both experimental realizations and potential technological applications, we aimed at unveiling the limits of common theoretical frameworks to describe Casimir forces and radiative heat transfer, moving towards a more realistic quantitative description of these effects, even in geometrically simple configurations.

Both my activity on many-body systems and gratings fit into the first topic, namely the manipulation of force and heat transfer. As a matter of fact, we have shown that many-body systems, studied by means of general theoretical frameworks developed *ad hoc*, pave the way to qualitatively new effects, which in many cases cannot be predicted within a standard two-body additive approach. In this context, I mainly refer to the amplification and pumping-like effects discussed in Secs. 4.2 and 4.5, where three-body systems were addressed, in which the third element can be thought as a *probe system* whose position and physical properties can be tuned (and possibly time-modulated) to tailor the heat transfer between the two initial bodies, taken as a reference. Another interesting example in the domain of Casimir forces is the two-slab atomic trap presented in Sec. 3.3, whose shape and depth strongly depend on the geometrical properties of the cavity. All my activity on gratings goes in the same direction as well. Concerning the force, we have shown that the geometrical properties of rectangular gratings can have a remarkable impact on the Casimir force both at and out of thermal equilibrium (see Sec. 5.3), are at the

origin of a lateral force when brought in proximity of a sphere (see Sec. 5.4), and produce interesting effects in terms of torque in the configuration of twisted gratings (see Sec. 5.7). Also in the context of radiative heat transfer, we have shown in Sec. 5.6 that, in the case of a metallic grating, the modulation of the grating height leads to a rich variation in terms of spectral properties and results in a flux amplification around one order of magnitude.

Some of my results involving many-body systems concern the second topic, i.e. the accurate prediction of Casimir force radiative heat transfer beyond the common theoretical approach used so far. In this sense, we have used our many-body approach to quantitatively analyze the degree of non-additivity already in a simple three-body scenario, as discussed in Sec. 3.3. Moreover, we have been able to highlight the existence of anomalous transport regimes for radiative heat transfer both in systems made of nanoparticles and planar slabs, as shown in Sec. 4.4. We have also shown that in some configurations of possible experimental relevance, the predictions obtained within the common theoretical approaches could be qualitatively and quantitatively wrong. We have first shown, as discussed in Sec. 4.6, that the thermal bath in which a two-body system is immersed can be at the origin of a saturation of the flux when the distance d separating the bodies tend to zero, in strong disagreement with the known $1/d^2$ divergence coming from fluctuational electrodynamics. In the last part of the manuscript, I have described my results concerning the coupling between radiative and conductive heat transfer, showing that at least in the Fourier regime, this coupling can indeed produce a temperature profile within each body, which in turn is at the origin of a modified (significantly reduced) value of the radiative flux.

I believe that the results presented in this manuscript pave the way to numerous possible developments. First, I am convinced that the conduction - radiation coupling, along with the saturation of the flux it entails, deserves at this stage more experimental attention. To this aim, it will be clearly relevant to go beyond the simple geometry of two parallel slabs considered so far. In particular, it would be interesting to understand to which extent this coupling is relevant in configurations such as a sphere or a tip in proximity of a planar substrate, of much easier experimental realizability.

Furthermore, I am convinced that the topic of many-body effects is an emerging branch in which several new features still need to be unveiled. In this context, I believe that the objective of a first unambiguous experimental observation could serve as a path to guide the theoretical investigations. In this sense, having in mind a possible multi-tip experimental configuration, the formalism described here to deal with an N-body dipolar system could be generalized to include multipolar terms. This would allow to address smaller distances with respect to a purely dipolar development, paving the way to an accurate prediction of a higher signal, to the design of an optimal setup and thus an easier experimental observation and comparison

with theory. Moreover, the many-body saturation effect we have highlighted could also play an important role. As a consequence, it would be interesting to extend the formalism developed so far to treat this aspect to geometrical configurations such as a sphere or a tip in proximity of a planar substrate, of much easier experimental realizability. This could be done either by means of a dipolar/multipolar approach, or by exploiting and developing already existing numerical frameworks able to deal with complex geometries.

Parallel to these investigations, I am currently starting to investigate the physics of heat transfer in the extreme near-field regime, namely for distances in the nm scales and below. At these distances, the tunneling of electron and phonon through the vacuum gap separating two bodies is expected to play a role and impact the total flux. Starting from this assumption, several questions are in order. First, the asymptotic scaling as a function of the distance has to be addressed for each heat carrier, including non-local effects when relevant. This could be achieved by means of mesoscopic and/or microscopic approaches. Moreover, the estimate of the total heat flux in a given configuration could be relevant for the analysis of recent experiments which have started to explore this regime of distances. This topic is at the heart of a 3-year project recently financed by ANR (French national funding agency), which started in March and of which I am the principal investigator. This project is in collaboration with the group of S. Mérabia from Institut Lumière Matière (Lyon), whose contribution will be focused on the microscopic modeling of the physical problem by means of ab-initio and molecular-dynamics calculations.

Bibliography

[1] H. B. G. Casimir, *On the attraction between two perfectly conducting plates*, Proc. K. Ned. Akad. Wet. **51**, 793 (1948). 1

[2] H. B. G. Casimir and D. Polder, *The Influence of Retardation on the London-van der Waals Forces*, Phys. Rev. **73**, 360 (1948). 1

[3] I. E. Dzyaloshinskii, E. M. Lifshitz, and L. P. Pitaevskii, *The general theory of van der Waals forces*, Adv. Phys. **10**, 165 (1961). 1

[4] M. Bordag, U. Mohideen, and V. Mostepanenko, *New developments in the Casimir effect*, Phys. Rep. **353**, 1 (2001). 1

[5] S. K. Lamoreaux, *The Casimir force: background, experiments, and applications*, Rep. Prog. Phys. **68**, 201 (2005). 1

[6] G. L. Klimchitskaya, U. Mohideen, and V. M. Mostepanenko, *The Casimir force between real materials: Experiment and theory*, Rev. Mod. Phys. **81**, 1827 (2009). 1

[7] L. M. Woods, D. A. R. Dalvit, A. Tkatchenko, P. Rodriguez-Lopez, A. W. Rodriguez, and R. Podgornik, *Materials perspective on Casimir and van der Waals interactions*, Rev. Mod. Phys. **88**, 045003 (2016). 1

[8] S. K. Lamoreaux, *Demonstration of the Casimir Force in the 0.6 to 6 μm Range*, Phys. Rev. Lett. **78**, 5 (1997). 1

[9] U. Mohideen and A. Roy, *Precision Measurement of the Casimir Force from 0.1 to 0.9 mm*, Phys. Rev. Lett. **81**, 4549 (1998). 1

[10] A. Roy, C.-Y. Lin, and U. Mohideen, *Improved precision measurement of the Casimir force*, Phys. Rev. D **60**, 111101(R) (1999). 1

[11] T. Ederth, *Template-stripped gold surfaces with 0.4-nm rms roughness suitable for force measurements: Application to the Casimir force in the 20–100-nm range*, Phys. Rev. A **62**, 062104 (2000). 1

[12] H. B. Chan, V. A. Aksyuk, R. N. Kleiman, D. J. Bishop, and F. Capasso, *Nonlinear Micromechanical Casimir Oscillator*, Phys. Rev. Lett. **87**, 211801 (2001). 1, 2

[13] H. B. Chan, V. A. Aksyuk, R. N. Kleiman, D. J. Bishop, and F. Capasso, *Quantum Mechanical Actuation of Microelectromechanical Systems by the Casimir Force*, Science **291**, 1941 (2001). 1, 2

[14] G. Bressi, G. Carugno, R. Onofrio, and G. Ruoso, *Measurement of the Casimir Force between Parallel Metallic Surfaces*, Phys. Rev. Lett. **88**, 041804 (2002). 1

[15] R. S. Decca, D. López, E. Fischbach, and D. E. Krause, *Measurement of the Casimir Force between Dissimilar Metals*, Phys. Rev. Lett. **91**, 050402 (2003). 1

[16] R. S. Decca, D. López, E. Fischbach, G. L. Klimchitskaya, D. E. Krause, and V. M. Mostepanenko, *Precise comparison of theory and new experiment for the Casimir force leads to stronger constraints on thermal quantum effects and long-range interactions*, Ann. Phys. **318**, 37 (2005). 1

[17] R. S. Decca, D. López, E. Fischbach, G. L. Klimchitskaya, D. E. Krause, and V. M. Mostepanenko, *Tests of new physics from precise measurements of the Casimir pressure between two gold-coated plates*, Phys. Rev. D **75**, 077101 (2007). 1

[18] D. E. Krause, R. S. Decca, D. López, and E. Fischbach, *Experimental Investigation of the Casimir Force beyond the Proximity-Force Approximation*, Phys. Rev. Lett. **98**, 050403 (2007). 1

[19] F. Capasso, J. N. Munday, D. Iannuzzi, and H. B. Chan, *Casimir Forces and Quantum Electrodynamical Torques: Physics and Nanomechanics*, IEEE J. Sel. Top. Quantum Electron. **13**, 400 (2007). 1

[20] G. Palasantzas, P. J. van Zwol, and J. T. M. De Hosson, *Transition from Casimir to van der Waals force between macroscopic bodies*, Appl. Phys. Lett. **93**, 121912 (2008). 1

[21] H. B. Chan, Y. Bao, J. Zou, R. A. Cirelli, F. Klemens, W. M. Mansfield, and C. S. Pai, *Measurement of the Casimir Force between a Gold Sphere and a Silicon Surface with Nanoscale Trench Arrays*, Phys. Rev. Lett. **101**, 030401 (2008). 1, 58, 61

[22] J. N. Munday, F. Capasso, V. A. Parsegian, and S. M. Bezrukov, *Measurements of the Casimir-Lifshitz force in fluids: The effect of electrostatic forces and Debye screening*, Phys. Rev. A **78**, 032109 (2008). 1

[23] J. N. Munday, F. Capasso, and V. A. Parsegian, *Measured long-range repulsive Casimir–Lifshitz forces*, Nature **457**, 170 (2009). 1

[24] G. Jourdan, A. Lambrecht, F. Comin, and J. Chevrier, *Quantitative non-contact dynamic Casimir force measurements*, Europhys. Lett. **85**, 31001 (2009). 1

[25] S. de Man, K. Heeck, R. J. Wijngaarden, and D. Iannuzzi, *Halving the Casimir force with Conductive Oxides*, Phys. Rev. Lett. **103**, 040402 (2009). 1

[26] Y. Bao, R. Guérout, J. Lussange, A. Lambrecht, R. A. Cirelli, F. Klemens, W. M. Mansfield, C. S. Pai, and H. B. Chan, *Casimir Force on a Surface with Shallow Nanoscale Corrugations: Geometry and Finite Conductivity Effects*, Phys. Rev. Lett. **105**, 250402 (2010). 1, 58, 61

[27] H.-C. Chiu, G. L. Klimchitskaya, V. N. Marachevsky, V. M. Mostepanenko, and U. Mohideen, *Lateral Casimir force between sinusoidally corrugated surfaces: Asymmetric profiles, deviations from the proximity force approximation, and comparison with exact theory*, Phys. Rev. B **81**, 115417 (2010). 1, 58, 61

[28] A. O. Sushkov, W. J. Kim, D. a. R. Dalvit, and S. K. Lamoreaux, *Observation of the thermal Casimir force*, Nat. Phys. **7**, 230 (2011). 1

[29] P. Zuurbier, S. d. Man, G. Gruca, K. Heeck, and D. Iannuzzi, *Measurement of the Casimir force with a ferrule-top sensor*, New J. Phys. **13**, 023027 (2011). 1

[30] G. Bimonte, D. López, and R. S. Decca, *Isoelectronic determination of the thermal Casimir force*, Phys. Rev. B **93**, 184434 (2016). 1

[31] A. A. Banishev, J. Wagner, T. Emig, R. Zandi, and U. Mohideen, *Demonstration of Angle-Dependent Casimir Force between Corrugations*, Phys. Rev. Lett. **110**, 250403 (2013). 1, 58

[32] F. Intravaia, S. Koev, I. W. Jung, A. A. Talin, P. S. Davids, R. S. Decca, V. A. Aksyuk, D. A. R. Dalvit, and D. López, *Strong Casimir force reduction through metallic surface nanostructuring*, Nat. Commun. **4**, 2515 (2013). 1, 58, 61

[33] L. Tang, M. Wang, C. Y. Ng, M. Nikolic, C. T. Chan, A. W. Rodriguez, and H. B. Chan, *Measurement of non-monotonic Casimir forces between silicon nanostructures*, Nat. Photonics **11**, 97 (2017). 1, 58

[34] C. I. Sukenik, M. G. Boshier, D. Cho, V. Sandoghdar, and E. A. Hinds, *Measurement of the Casimir-Polder force*, Phys. Rev. Lett. **70**, 560 (1993). 1

[35] A. Landragin, J.-Y. Courtois, G. Labeyrie, N. Vansteenkiste, C. I. Westbrook, and A. Aspect, *Measurement of the van der Waals Force in an Atomic Mirror*, Phys. Rev. Lett. **77**, 1464 (1996). 1

[36] F. Shimizu, *Specular Reflection of Very Slow Metastable Neon Atoms from a Solid Surface*, Phys. Rev. Lett. **86**, 987 (2001). 1

[37] V. Druzhinina and M. DeKieviet, *Experimental Observation of Quantum Reflection far from Threshold*, Phys. Rev. Lett. **91**, 193202 (2003). 1

[38] T. A. Pasquini, Y. Shin, C. Sanner, M. Saba, A. Schirotzek, D. E. Pritchard, and W. Ketterle, *Quantum Reflection from a Solid Surface at Normal Incidence*, Phys. Rev. Lett. **93**, 223201 (2004). 1

[39] D. M. Harber, J. M. Obrecht, J. M. McGuirk, and E. A. Cornell, *Measurement of the Casimir-Polder force through center-of-mass oscillations of a Bose-Einstein condensate*, Phys. Rev. A **72**, 033610 (2005). 1

[40] B. S. Zhao, H. C. Schewe, G. Meijer, and W. Schöllkopf, *Coherent Reflection of He Atom Beams from Rough Surfaces at Grazing Incidence*, Phys. Rev. Lett. **105**, 133203 (2010). 1

[41] H. Bender, C. Stehle, C. Zimmermann, S. Slama, J. Fiedler, S. Scheel, S. Y. Buhmann, and V. N. Marachevsky, *Probing Atom-Surface Interactions by Diffraction of Bose-Einstein Condensates*, Phys. Rev. X **4**, 011029 (2014). 1, 58

[42] S. J. Rahi, T. Emig, N. Graham, R. L. Jaffe, and M. Kardar, *Scattering theory approach to electrodynamic Casimir forces*, Phys. Rev. D **80**, 085021 (2009). 2, 31

[43] M. T. H. Reid, A. W. Rodriguez, J. White, and S. G. Johnson, *Efficient Computation of Casimir Interactions between Arbitrary 3D Objects*, Phys. Rev. Lett. **103**, 040401 (2009). 2, 31, 71

[44] A. W. Rodriguez, A. P. McCauley, J. D. Joannopoulos, and S. G. Johnson, *Casimir forces in the time domain: Theory*, Phys. Rev. A **80**, 012115 (2009). 2, 31

[45] M. T. H. Reid, J. White, and S. G. Johnson, *Computation of Casimir interactions between arbitrary three-dimensional objects with arbitrary material properties*, Phys. Rev. A **84**, 010503 (2011). 2, 31

[46] M. T. H. Reid, J. White, and S. G. Johnson, *Fluctuating surface currents: An algorithm for efficient prediction of Casimir interactions among arbitrary materials in arbitrary geometries*, Phys. Rev. A **88**, 022514 (2013). 2, 31

[47] M. Antezza, L. P. Pitaevskii, and S. Stringari, *Effect of the Casimir-Polder force on the collective oscillations of a trapped Bose-Einstein condensate*, Phys. Rev. A **70**, 053619 (2004). 2

[48] M. Antezza, L. P. Pitaevskii, and S. Stringari, *New Asymptotic Behavior of the Surface-Atom Force out of Thermal Equilibrium*, Phys. Rev. Lett. **95**, 113202 (2005). 2

[49] M. Antezza, L. P. Pitaevskii, S. Stringari, and V. B. Svetovoy, *Casimir-Lifshitz Force Out of Thermal Equilibrium and Asymptotic Nonadditivity*, Phys. Rev. Lett. **97**, 223203 (2006). 2

[50] M. Antezza, L. P. Pitaevskii, S. Stringari, and V. B. Svetovoy, *Casimir-Lifshitz force out of thermal equilibrium*, Phys. Rev. A **77**, 022901 (2008). 2

[51] J. M. Obrecht, R. J. Wild, M. Antezza, L. P. Pitaevskii, S. Stringari, and E. A. Cornell, *Measurement of the Temperature Dependence of the Casimir-Polder Force*, Phys. Rev. Lett. **98**, 063201 (2007). 2

[52] G. Palasantzas, M. Sedighi, and V. B. Svetovoy, *Applications of Casimir forces: Nanoscale actuation and adhesion*, Appl. Phys. Lett. **117**, 120501 (2020). 2

[53] F. M. Serry, D. Walliser, and G. J. Maclay, *The role of the casimir effect in the static deflection and stiction of membrane strips in microelectromechanical systems (MEMS)*, J. Appl. Physics **84**, 2501 (1998). 2

[54] E. Buks and M. L. Roukes, *Metastability and the Casimir effect in micromechanical systems*, Europhys. Lett. **54**, 220 (2001). 2

[55] S. M. Rytov, *Theory of Electrical Fluctuations and Thermal Radiation* (Academy of Sciences Press of USSR, Moscow, 1953). 2

[56] D. Polder and M. Van Hove, *Theory of Radiative Heat Transfer between Closely Spaced Bodies*, Phys. Rev. B **4**, 3303 (1971). 2

[57] K. Joulain, J.-P. Mulet, F. Marquier, R. Carminati, and J.-J. Greffet, *Surface electromagnetic waves thermally excited: Radiative heat transfer, coherence properties and Casimir forces revisited in the near field*, Surf. Sci. Rep. **57**, 59 (2005). 2

[58] A. I. Volokitin and B. N. J. Persson, *Near-field radiative heat transfer and noncontact friction*, Rev. Mod. Phys. **79**, 1291 (2007). 2

[59] C. R. Otey, L. Zhu, S. Sandhu, and S. Fan, *Fluctuational electrodynamics calculations of near-field heat transfer in non-planar geometries: A brief overview*, J. Quant. Spectrosc. Radiat. Transf. **132**, 3 (2014). 2

[60] B. Song, A. Fiorino, E. Meyhofer, and P. Reddy, *Near-field radiative thermal transport: From theory to experiment*, AIP Advances **5**, 053503 (2015). 2

[61] J. C. Cuevas and F. J. García-Vidal, *Radiative Heat Transfer*, ACS Photonics **5**, 3896 (2018). 2

[62] A. Kittel, W. Müller-Hirsch, J. Parisi, S.-A. Biehs, D. Reddig, and M. Holthaus, *Near-Field Heat Transfer in a Scanning Thermal Microscope*, Phys. Rev. Lett. **95**, 224301 (2005). 3, 73

[63] L. Hu, A. Narayanaswamy, X. Chen, and G. Chen, *Near-field thermal radiation between two closely spaced glass plates exceeding Planck's blackbody radiation law*, Appl. Phys. Lett. **92**, 133106 (2008). 3, 73

[64] A. Narayanaswamy, S. Shen, and G. Chen, *Near-field radiative heat transfer between a sphere and a substrate*, Phys. Rev. B **78**, 115303 (2008). 3, 73

[65] E. Rousseau, A. Siria, G. Jourdan, S. Volz, F. Comin, J. Chevrier, and J.-J. Greffet, *Radiative heat transfer at the nanoscale*, Nat. Photonics **3**, 514 (2009). 3, 73

[66] S. Shen, A. Narayanaswamy, and G. Chen, *Surface Phonon Polaritons Mediated Energy Transfer between Nanoscale Gaps*, Nano Lett. **9**, 2909 (2009). 3, 73

[67] R. S. Ottens, V. Quetschke, S. Wise, A. A. Alemi, R. Lundock, G. Mueller, D. H. Reitze, D. B. Tanner, and B. F. Whiting, *Near-Field Radiative Heat Transfer between Macroscopic Planar Surfaces*, Phys. Rev. Lett. **107**, 014301 (2011). 3, 73

[68] T. Kralik, P. Hanzelka, M. Zobac, V. Musilova, T. Fort, and M. Horak, *Strong Near-Field Enhancement of Radiative Heat Transfer between Metallic Surfaces*, Phys. Rev. Lett. **109**, 224302 (2012). 3, 73

[69] B. Guha, C. Otey, C. B. Poitras, S. Fan, and M. Lipson, *Near-Field Radiative Cooling of Nanostructures*, Nano Lett. **12**, 4546 (2012). 3

[70] S. Shen, A. Mavrokefalos, P. Sambegoro, and G. Chen, *Nanoscale thermal radiation between two gold surfaces*, Appl. Phys. Lett. **100**, 233114 (2012). 3

[71] P. J. van Zwol, L. Ranno, and J. Chevrier, *Tuning Near Field Radiative Heat Flux through Surface Excitations with a Metal Insulator Transition*, Phys. Rev. Lett. **108**, 234301 (2012). 3, 73

[72] P. J. van Zwol, S. Thiele, C. Berger, W. A. de Heer, and J. Chevrier, *Nanoscale Radiative Heat Flow due to Surface Plasmons in Graphene and Doped Silicon*, Phys. Rev. Lett. **109**, 264301 (2012). 3, 73

[73] J. Shi, P. Li, B. Liu, and S. Shen, *Tuning near field radiation by doped silicon*, Appl. Phys. Lett. **102**, 183114 (2013). 3

[74] L. Worbes, D. Hellmann, and A. Kittel, *Enhanced Near-Field Heat Flow of a Monolayer Dielectric Island*, Phys. Rev. Lett. **110**, 134302 (2013). 3

[75] R. St-Gelais, B. Guha, L. Zhu, S. Fan, and M. Lipson, *Demonstration of Strong Near-Field Radiative Heat Transfer between Integrated Nanostructures*, Nano Lett. **14**, 6971 (2014). 3

[76] M. P. Bernardi, O. Dupré, E. Blandre, P.-O. Chapuis, R. Vaillon, and M. Francoeur, *Impacts of propagating, frustrated and surface modes on radiative, electrical and thermal losses in nanoscale-gap thermophotovoltaic power generators*, Sci. Rep. **5**, 11626 (2015). 3

[77] B. Song, Y. Ganjeh, S. Sadat, D. Thompson, A. Fiorino, V. Fernández-Hurtado, J. Feist, F. J. Garcia-Vidal, J. C. Cuevas, P. Reddy, and E. Meyhofer, *Enhancement of near-field radiative heat transfer using polar dielectric thin films*, Nat. Nanotechnol. **10**, 253 (2015). 3, 73

[78] K. Ito, A. Miura, H. Iizuka, and H. Toshiyoshi, *Parallel-plate submicron gap formed by micromachined low-density pillars for near-field radiative heat transfer*, Appl. Phys. Lett. **106**, 083504 (2015). 3

[79] M. Lim, S. S. Lee, and B. J. Lee, *Near-field thermal radiation between doped silicon plates at nanoscale gaps*, Phys. Rev. B **91**, 195136 (2015). 3

[80] K. Kim, B. Song, V. Fernández-Hurtado, W. Lee, W. Jeong, L. Cui, D. Thompson, J. Feist, M. T. H. Reid, F. J. García-Vidal, J. C. Cuevas, E. Meyhofer, and P. Reddy, *Radiative heat transfer in the extreme near field*, Nature **528**, 387 (2015). 3, 73

[81] B. Song, D. Thompson, A. Fiorino, Y. Ganjeh, P. Reddy, and E. Meyhofer, *Radiative heat conductances between dielectric and metallic parallel plates with nanoscale gaps*, Nat. Nanotechnol. **11**, 509 (2016). 3

[82] R. St-Gelais, L. Zhu, S. Fan, and M. Lipson, *Near-field radiative heat transfer between parallel structures in the deep subwavelength regime*, Nat. Nanotechnol. **11**, 515 (2016). 3, 73

[83] S. Lang, G. Sharma, S. Molesky, P. U. Kränzien, T. Jalas, Z. Jacob, A. Y. Petrov, and M. Eich, *Dynamic measurement of near-field radiative heat transfer*, Sci. Rep. **7**, 13916 (2017). 3

[84] T. Králík, V. Musilová, T. Fořt, and A. Srnka, *Effect of superconductivity on near-field radiative heat transfer*, Phys. Rev. B **95**, 060503(R) (2017). 3

[85] K. Ito, K. Nishikawa, A. Miura, H. Toshiyoshi, and H. Iizuka, *Dynamic Modulation of Radiative Heat Transfer beyond the Blackbody Limit*, Nano Lett. **17**, 4347 (2017). 3

[86] A. Fiorino, D. Thompson, L. Zhu, B. Song, P. Reddy, and E. Meyhofer, *Giant Enhancement in Radiative Heat Transfer in Sub-30 nm Gaps of Plane Parallel Surfaces*, Nano Lett. **18**, 3711 (2018). 3

[87] A. Fiorino, L. Zhu, D. Thompson, R. Mittapally, P. Reddy, and E. Meyhofer, *Nanogap near-field thermophotovoltaics*, Nat. Nanotechnol. **13**, 806 (2018). 3

[88] A. Fiorino, D. Thompson, L. Zhu, R. Mittapally, S.-A. Biehs, O. Bezencenet, N. El-Bondry, S. Bansropun, P. Ben-Abdallah, E. Meyhofer, and P. Reddy, *A Thermal Diode Based on Nanoscale Thermal Radiation*, ACS Nano **12**, 5774 (2018). 3

[89] M. Ghashami, H. Geng, T. Kim, N. Iacopino, S. K. Cho, and K. Park, *Precision Measurement of Phonon-Polaritonic Near-Field Energy Transfer between Macroscale Planar Structures Under Large Thermal Gradients*, Phys. Rev. Lett. **120**, 175901 (2018). 3

[90] V. Musilová, T. Králík, T. Fořt, and M. Macek, *Strong suppression of near-field radiative heat transfer by superconductivity in NbN*, Phys. Rev. B **99**, 024511 (2019). 3

[91] J. DeSutter, L. Tang, and M. Francoeur, *A near-field radiative heat transfer device*, Nat. Nanotechnol. **14**, 751 (2019). 3

[92] H. Salihoglu, W. Nam, L. Traverso, M. Segovia, P. K. Venuthurumilli, W. Liu, Y. Wei, W. Li, and X. Xu, *Near-Field Thermal Radiation between Two Plates with Sub-10 nm Vacuum Separation*, Nano Lett. **20**, 6091 (2020). 3

[93] A. W. Rodriguez, O. Ilic, P. Bermel, I. Celanovic, J. D. Joannopoulos, M. Soljačić, and S. G. Johnson, *Frequency-Selective Near-Field Radiative Heat Transfer between Photonic*

Crystal Slabs: A Computational Approach for Arbitrary Geometries and Materials, Phys. Rev. Lett. **107**, 114302 (2011). 3, 31

[94] A. P. McCauley, M. T. H. Reid, M. Krüger, and S. G. Johnson, *Modeling near-field radiative heat transfer from sharp objects using a general three-dimensional numerical scattering technique*, Phys. Rev. B **85**, 165104 (2012). 3, 31

[95] A. W. Rodriguez, M. T. H. Reid, and S. G. Johnson, *Fluctuating-surface-current formulation of radiative heat transfer for arbitrary geometries*, Phys. Rev. B **86**, 220302(R) (2012). 3, 31

[96] A. W. Rodriguez, M. T. H. Reid, and S. G. Johnson, *Fluctuating surface-current formulation of radiative heat transfer: theory and applications*, Phys. Rev. B **88**, 054305 (2013). 3, 31

[97] A. Narayanaswamy and Y. Zheng, *A Green's function formalism of energy and momentum transfer in fluctuational electrodynamics*, J. Quant. Spectrosc. Radiat. Transf. **132**, 12 (2014). 3, 31

[98] B. Müller, R. Incardone, M. Antezza, T. Emig, and M. Krüger, *Many-body heat radiation and heat transfer in the presence of a nonabsorbing background medium*, Phys. Rev. B **95**, 085413 (2017). 3, 31, 35, 39

[99] G. Bimonte, *Scattering approach to Casimir forces and radiative heat transfer for nanostructured surfaces out of thermal equilibrium*, Phys. Rev. A **80**, 042102 (2009). 3, 31

[100] M. Krüger, T. Emig, and M. Kardar, *Nonequilibrium Electromagnetic Fluctuations: Heat Transfer and Interactions*, Phys. Rev. Lett. **106**, 210404 (2011). 3, 31

[101] M. Krüger, G. Bimonte, T. Emig, and M. Kardar, *Trace formulas for nonequilibrium Casimir interactions, heat radiation, and heat transfer for arbitrary objects*, Phys. Rev. B **86**, 115423 (2012). 3, 31

[102] G. Bimonte, T. Emig, M. Kardar, and M. Krüger, *Nonequilibrium Fluctuational Quantum Electrodynamics: Heat Radiation, Heat Transfer, and Force*, Annu. Rev. Condens. Matter Phys. **8**, 119 (2017). 3, 31

[103] C. R. Otey, W. T. Lau, and S. Fan, *Thermal Rectification through Vacuum*, Phys. Rev. Lett. **104**, 154301 (2010). 3

[104] E. Moncada-Villa, V. Fernández-Hurtado, F. J. García-Vidal, A. García-Martín, and J. C. Cuevas, *Magnetic field control of near-field radiative heat transfer and the realization of highly tunable hyperbolic thermal emitters*, Phys. Rev. B **92**, 125418 (2015). 3

[105] K. Chen, P. Santhanam, S. Sandhu, L. Zhu, and S. Fan, *Heat-flux control and solid-state cooling by regulating chemical potential of photons in near-field electromagnetic heat transfer*, Phys. Rev. B **91**, 134301 (2015). 3

[106] K. Chen, P. Santhanam, and S. Fan, *Near-Field Enhanced Negative Luminescent Refrigeration*, Phys. Rev. Applied **6**, 024014 (2016). 3

[107] P. Ben-Abdallah and S.-A. Biehs, *Contactless heat flux control with photonic devices*, AIP Advances **5**, 053502 (2015). 3

[108] R. S. DiMatteo, P. Greiff, S. L. Finberg, K. A. Young-Waithe, H. K. H. Choy, M. M. Masaki, and C. G. Fonstad, *Enhanced photogeneration of carriers in a semiconductor via coupling across a nonisothermal nanoscale vacuum gap*, Appl. Phys. Lett. **79**, 1894 (2001). 3

[109] M. D. Whale and E. G. Cravalho, *Modeling and performance of microscale thermophotovoltaic energy conversion devices*, IEEE Trans. Energy Convers. **17**, 130 (2002). 3

[110] A. Narayanaswamy and G. Chen, *Surface modes for near field thermophotovoltaics*, Appl. Phys. Lett. **82**, 3544 (2003). 3

[111] S. Basu, Z. M. Zhang, and C. J. Fu, *Review of near-field thermal radiation and its application to energy conversion*, Int. J. Energy Res. **33**, 1203 (2009). 3

[112] B. Zhao, K. Chen, S. Buddhiraju, G. Bhatt, M. Lipson, and S. Fan, *High-performance near-field thermophotovoltaics for waste heat recovery*, Nano Energy **41**, 344 (2017). 3

[113] R. Messina, D. A. R. Dalvit, P. A. M. Neto, A. Lambrecht, and S. Reynaud, *Dispersive interactions between atoms and nonplanar surfaces*, Phys. Rev. A **80**, 022119 (2009). 23, 24, 28

[114] R. Messina, R. Vasile, and R. Passante, *Dynamical Casimir-Polder force on a partially dressed atom near a conducting wall*, Phys. Rev. A **82**, 062501 (2010). 23, 24, 28

[115] P. A. M. Neto, A. Lambrecht, and S. Reynaud, *Roughness correction to the Casimir force: Beyond the Proximity Force Approximation*, Europhys. Lett. **69**, 924 (2005). 23

[116] P. A. M. Neto, A. Lambrecht, and S. Reynaud, *Casimir effect with rough metallic mirrors*, Phys. Rev. A **72**, 012115 (2005). 23

[117] D. A. R. Dalvit, P. A. M. Neto, A. Lambrecht, and S. Reynaud, *Lateral Casimir–Polder force with corrugated surfaces*, J. Phys. A: Math. Theor. **41**, 164028 (2008). 23

[118] P. Wolf, P. Lemonde, A. Lambrecht, S. Bize, A. Landragin, and A. Clairon, *From optical lattice clocks to the measurement of forces in the Casimir regime*, Phys. Rev. A **75**, 063608 (2007). 25

[119] R. Messina, S. Pelisson, M.-C. Angonin, and P. Wolf, *Atomic states in optical traps near a planar surface*, Phys. Rev. A **83**, 052111 (2011). 25, 26, 28

[120] M. Glück, *Wannier–Stark resonances in optical and semiconductor superlattices*, Phys. Rep. **366**, 103 (2002). 26

[121] S. Pelisson, R. Messina, M.-C. Angonin, and P. Wolf, *Dynamical aspects of atom interferometry in an optical lattice in proximity to a surface*, Phys. Rev. A **86**, 013614 (2012). 26, 28

[122] S. Pelisson, R. Messina, M.-C. Angonin, and P. Wolf, *Lifetimes of atoms trapped in an optical lattice in proximity of a surface*, Phys. Rev. A **88**, 013411 (2013). 26, 28

[123] R. Messina, P. Ben-Abdallah, B. Guizal, and M. Antezza, *Graphene-based amplification and tuning of near-field radiative heat transfer between dissimilar polar materials*, Phys. Rev. B **96**, 045402 (2017). 27, 28

[124] R. Messina, J.-P. Hugonin, J.-J. Greffet, F. Marquier, Y. De Wilde, A. Belarouci, L. Frechette, Y. Cordier, and P. Ben-Abdallah, *Tuning the electromagnetic local density of states in graphene-covered systems via strong coupling with graphene plasmons*, Phys. Rev. B **87**, 085421 (2013). 27, 28, 51

[125] R. Messina and P. Ben-Abdallah, *Graphene-based photovoltaic cells for near-field thermal energy conversion*, Sci. Rep. **3**, 1383 (2013). 28

[126] R. Messina and M. Antezza, *Scattering-matrix approach to Casimir-Lifshitz force and heat transfer out of thermal equilibrium between arbitrary bodies*, Phys. Rev. A **84**, 042102 (2011). 32, 33, 34, 38

[127] R. Messina and M. Antezza, *Casimir-Lifshitz force out of thermal equilibrium and heat transfer between arbitrary bodies*, Europhys. Lett. **95**, 61002 (2011). 33, 38

[128] R. Messina and M. Antezza, *Three-body radiative heat transfer and Casimir-Lifshitz force out of thermal equilibrium for arbitrary bodies*, Phys. Rev. A **89**, 052104 (2014). 35, 36, 37, 38

[129] P. Ben-Abdallah, *Heat transfer through near-field interactions in nanofluids*, Appl. Phys. Lett. **89**, 113117 (2006). 35

[130] P. Ben-Abdallah, K. Joulain, J. Drevillon, and C. Le Goff, *Heat transport through plasmonic interactions in closely spaced metallic nanoparticle chains*, Phys. Rev. B **77**, 075417 (2008). 35

[131] P. Ben-Abdallah, S.-A. Biehs, and K. Joulain, *Many-Body Radiative Heat Transfer Theory*, Phys. Rev. Lett. **107**, 114301 (2011). 35, 39, 40, 43, 49

[132] M. Langlais, J.-P. Hugonin, M. Besbes, and P. Ben-Abdallah, *Cooperative electromagnetic interactions between nanoparticles for solar energy harvesting*, Opt. Express **22**, A577 (2014). 35, 39

[133] M. Nikbakht, *Radiative heat transfer in anisotropic many-body systems: Tuning and enhancement*, J. Appl. Phys. **116**, 094307 (2014). 35, 39, 49

[134] M. Nikbakht, *Three-body radiation dynamics in systems with anisotropic nanoparticles*, Europhys. Lett. **110**, 14004 (2015). 35, 39, 49

[135] P. Ben-Abdallah, *Photon Thermal Hall Effect*, Phys. Rev. Lett. **116**, 084301 (2016). 35, 39

[136] I. Latella and P. Ben-Abdallah, *Giant Thermal Magnetoresistance in Plasmonic Structures*, Phys. Rev. Lett. **118**, 173902 (2017). 35

[137] P. Ben-Abdallah and S.-A. Biehs, *Near-Field Thermal Transistor*, Phys. Rev. Lett. **112**, 044301 (2014). 35, 39, 49

[138] I. Latella, A. Pérez-Madrid, J. M. Rubi, S.-A. Biehs, and P. Ben-Abdallah, *Heat Engine Driven by Photon Tunneling in Many-Body Systems*, Phys. Rev. Applied **4**, 011001 (2015). 35, 39, 49

[139] I. Latella, P. Ben-Abdallah, S.-A. Biehs, M. Antezza, and R. Messina, *Radiative heat transfer and nonequilibrium Casimir-Lifshitz force in many-body systems with planar geometry*, Phys. Rev. B **95**, 205404 (2017). 37, 38

[140] Z. H. Zheng and Y. M. Xuan, *Enhancement or Suppression of the Near-Field Radiative Heat Transfer Between Two Materials*, Nanoscale Microscale Thermophys. Eng. **15**, 237 (2011). 39, 49

[141] V. Yannopapas and N. V. Vitanov, *Spatiotemporal Control of Temperature in Nanostructures Heated by Coherent Laser Fields*, Phys. Rev. Lett. **110**, 044302 (2013). 39

[142] L. Zhu and S. Fan, *Persistent Directional Current at Equilibrium in Nonreciprocal Many-Body Near Field Electromagnetic Heat Transfer*, Phys. Rev. Lett. **117**, 134303 (2016). 39

[143] R. Messina, P. Ben-Abdallah, B. Guizal, M. Antezza, and S.-A. Biehs, *Hyperbolic waveguide for long-distance transport of near-field heat flux*, Phys. Rev. B **94**, 104301 (2016). 39

[144] J. Dong, J. Zhao, and L. Liu, *Radiative heat transfer in many-body systems: Coupled electric and magnetic dipole approach*, Phys. Rev. B **95**, 125411 (2017). 39, 49

[145] E. Tervo, Z. Zhang, and B. Cola, *Collective near-field thermal emission from polaritonic nanoparticle arrays*, Phys. Rev. Materials **1**, 015201 (2017). 39

[146] M. Nikbakht, *Radiative heat transfer in fractal structures*, Phys. Rev. B **96**, 125436 (2017). 39

[147] B. Czapla and A. Narayanaswamy, *Thermal radiative energy exchange between a closely-spaced linear chain of spheres and its environment*, J. Quant. Spectrosc. Radiat. Transf. **227**, 4 (2019). 39

[148] Y. H. Kan, C. Y. Zhao, and Z. M. Zhang, *Near-field radiative heat transfer in three-body systems with periodic structures*, Phys. Rev. B **99**, 035433 (2019). 39, 49

[149] D. Thompson, L. Zhu, E. Meyhofer, and P. Reddy, *Nanoscale radiative thermal switching via multi-body effects*, Nat. Nanotechnol. **15**, 99 (2020). 39

[150] S.-A. Biehs, R. Messina, P. S. Venkataram, A. W. Rodriguez, J. C. Cuevas, and P. Ben-Abdallah, *Near-field Radiative Heat Transfer in Many-Body Systems*, arXiv:2007.05604 (accepted on Review of Modern Physics) (2020). 40

[151] R. Messina, M. Antezza, and P. Ben-Abdallah, *Three-Body Amplification of Photon Heat Tunneling*, Phys. Rev. Lett. **109**, 244302 (2012). 40, 41, 42, 49, 55

[152] R. Messina, M. Tschikin, S.-A. Biehs, and P. Ben-Abdallah, *Fluctuation-electrodynamic theory and dynamics of heat transfer in systems of multiple dipoles*, Phys. Rev. B **88**, 104307 (2013). 43, 44, 55

[153] P. Ben-Abdallah, R. Messina, S.-A. Biehs, M. Tschikin, K. Joulain, and C. Henkel, *Heat Superdiffusion in Plasmonic Nanostructure Networks*, Phys. Rev. Lett. **111**, 174301 (2013). 45, 47, 55

[154] I. Latella, S.-A. Biehs, R. Messina, A. W. Rodriguez, and P. Ben-Abdallah, *Ballistic near-field heat transport in dense many-body systems*, Phys. Rev. B **97**, 035423 (2018). 47, 48, 55

[155] I. Latella, R. Messina, J. M. Rubi, and P. Ben-Abdallah, *Radiative Heat Shuttling*, Phys. Rev. Lett. **121**, 023903 (2018). 48, 51, 53

[156] H. Simchi, *Graphene-based three-body amplification of photon heat tunneling*, J. Appl. Phys. **121**, 094301 (2017). 49

[157] J. Song, L. Lu, Q. Cheng, and Z. Luo, *Three-Body Heat Transfer Between Anisotropic Magneto-Dielectric Hyperbolic Metamaterials*, J. Heat Transfer **140**, 082005 (2018). 49

[158] R. Incardone, T. Emig, and M. Krüger, *Heat transfer between anisotropic nanoparticles: Enhancement and switching*, Europhys. Lett. **106**, 41001 (2014). 49

[159] O. R. Choubdar and M. Nikbakht, *Radiative heat transfer between nanoparticles: Shape dependence and three-body effect*, J. Appl. Phys. **120**, 144303 (2016). 49

[160] V. Kubytskyi, S.-A. Biehs, and P. Ben-Abdallah, *Radiative Bistability and Thermal Memory*, Phys. Rev. Lett. **113**, 074301 (2014). 49

[161] P. Ben-Abdallah and S.-A. Biehs, *Towards Boolean operations with thermal photons*, Phys. Rev. B **94**, 241401 (2016). 49

[162] C. Kathmann, M. Reina, R. Messina, P. Ben-Abdallah, and S.-A. Biehs, *Scalable radiative thermal logic gates based on nanoparticle networks*, Sci. Rep. **10**, 3596 (2020). 49

[163] R. Messina, S.-A. Biehs, and P. Ben-Abdallah, *Surface-mode-assisted amplification of radiative heat transfer between nanoparticles*, Phys. Rev. B **97**, 165437 (2018). 50, 51, 55

[164] R. Messina and P. Ben-Abdallah, *Many-body near-field radiative heat pumping*, Phys. Rev. B **101**, 165435 (2020). 50, 51, 52, 55

[165] S. Buddhiraju, W. Li, and S. Fan, *Photonic Refrigeration from Time-Modulated Thermal Emission*, Phys. Rev. Lett. **124**, 077402 (2020). 51

[166] P.-O. Chapuis, S. Volz, C. Henkel, K. Joulain, and J.-J. Greffet, *Effects of spatial dispersion in near-field radiative heat transfer between two parallel metallic surfaces*, Phys. Rev. B **77** (3), 035431 (2008). 53

[167] I. Latella, R. Messina, S.-A. Biehs, J. M. Rubi, and P. Ben-Abdallah, *Saturation of radiative heat transfer due to many-body thermalization*, Sci. Rep. **10**, 8938 (2020). 54, 55

[168] A. Lambrecht and V. N. Marachevsky, *Casimir Interaction of Dielectric Gratings*, Phys. Rev. Lett. **101**, 160403 (2008). 58

[169] P. S. Davids, F. Intravaia, F. S. S. Rosa, and D. A. R. Dalvit, *Modal approach to Casimir forces in periodic structures*, Phys. Rev. A **82**, 062111 (2010). 58

[170] F. Intravaia, P. S. Davids, R. S. Decca, V. A. Aksyuk, D. López, and D. A. R. Dalvit, *Quasianalytical modal approach for computing Casimir interactions in periodic nanostructures*, Phys. Rev. A **86**, 042101 (2012). 58

[171] J. Lussange, R. Guérout, and A. Lambrecht, *Casimir energy between nanostructured gratings of arbitrary periodic profile*, Phys. Rev. A **86**, 062502 (2012). 58

[172] R. Guérout, J. Lussange, H. B. Chan, A. Lambrecht, and S. Reynaud, *Thermal Casimir force between nanostructured surfaces*, Phys. Rev. A **87**, 052514 (2013). 58

[173] N. Graham, *Casimir energies of periodic dielectric gratings*, Phys. Rev. A **90**, 032507 (2014). 58

[174] J. Wagner and R. Zandi, *Calculating Casimir interactions for periodic surface-relief gratings using the C method*, Phys. Rev. A **90**, 012516 (2014). 58

[175] S. Y. Buhmann, V. N. Marachevsky, and S. Scheel, *Impact of anisotropy on the interaction of an atom with a one-dimensional nano-grating*, Int. J. Mod. Phys. A **31**, 1641029 (2016). 58

[176] S.-A. Biehs, F. S. S. Rosa, and P. Ben-Abdallah, *Modulation of near-field heat transfer between two gratings*, Appl. Phys. Lett. **98**, 243102 (2011). 58

[177] R. Guérout, J. Lussange, F. S. S. Rosa, J.-P. Hugonin, D. A. R. Dalvit, J.-J. Greffet, A. Lambrecht, and S. Reynaud, *Enhanced radiative heat transfer between nanostructured gold plates*, Phys. Rev. B **85**, 180301(R) (2012). 58, 65, 66

[178] J. Lussange, R. Guérout, F. S. S. Rosa, J.-J. Greffet, A. Lambrecht, and S. Reynaud, *Radiative heat transfer between two dielectric nanogratings in the scattering approach*, Phys. Rev. B **86**, 085432 (2012). 58

[179] X. L. Liu and Z. M. Zhang, *Graphene-assisted near-field radiative heat transfer between corrugated polar materials*, Appl. Phys. Lett. **104**, 251911 (2014). 58

[180] J. Dai, S. A. Dyakov, and M. Yan, *Enhanced near-field radiative heat transfer between corrugated metal plates: Role of spoof surface plasmon polaritons*, Phys. Rev. B **92**, 035419 (2015). 58

[181] H. Chalabi, E. Hasman, and M. L. Brongersma, *Near-field radiative thermal transfer between a nanostructured periodic material and a planar substrate*, Phys. Rev. B **91**, 014302 (2015). 58

[182] H. Chalabi, E. Hasman, and M. L. Brongersma, *Effect of shape in near-field thermal transfer for periodic structures*, Phys. Rev. B **91**, 174304 (2015). 58

[183] H. Chalabi, A. Alù, and M. L. Brongersma, *Focused thermal emission from a nanostructured SiC surface*, Phys. Rev. B **94**, 094307 (2016). 58

[184] J. Dai, S. A. Dyakov, and M. Yan, *Radiative heat transfer between two dielectric-filled metal gratings*, Phys. Rev. B **93**, 155403 (2016). 58

[185] J. Dai, S. A. Dyakov, S. I. Bozhevolnyi, and M. Yan, *Near-field radiative heat transfer between metasurfaces: A full-wave study based on two-dimensional grooved metal plates*, Phys. Rev. B **94**, 125431 (2016). 58

[186] Y. Yang and L. Wang, *Spectrally Enhancing Near-Field Radiative Transfer between Metallic Gratings by Exciting Magnetic Polaritons in Nanometric Vacuum Gaps*, Phys. Rev. Lett. **117**, 044301 (2016). 58

[187] H. Kim, J. Park, and B. Lee, *Fourier Modal Method and its Applications in Computational Nanophotonics* (CRC Press, Boca Raton, 2012). 58

[188] A. Noto, R. Messina, B. Guizal, and M. Antezza, *Casimir-Lifshitz force out of thermal equilibrium between dielectric gratings*, Phys. Rev. A **90**, 022120 (2014). 59, 60, 61, 71

[189] G. Granet and B. Guizal, *Efficient implementation of the coupled-wave method for metallic lamellar gratings in TM polarization*, J. Opt. Soc. Am. A **13**, 1019 (1996). 58

[190] R. Messina, P. A. Maia Neto, B. Guizal, and M. Antezza, *Casimir interaction between a sphere and a grating*, Phys. Rev. A **92**, 062504 (2015). 62, 63, 64, 71

[191] F. Chen, U. Mohideen, G. L. Klimchitskaya, and V. M. Mostepanenko, *Demonstration of the Lateral Casimir Force*, Phys. Rev. Lett. **88**, 101801 (2002). 61

[192] B. V. Derjaguin, I. I. Abrikosova, and E. M. Lifshitz, *Direct measurement of molecular attraction between solids separated by a narrow gap*, Q. Rev. Chem. Soc. **10**, 295 (1956). 61

[193] P. W. Milonni, *The Quantum Vacuum* (Academic, San Diego, 1994). 62

[194] R. Messina, A. Noto, B. Guizal, and M. Antezza, *Radiative heat transfer between metallic gratings using Fourier modal method with adaptive spatial resolution*, Phys. Rev. B **95**, 125404 (2017). 64, 65, 66, 67, 71

[195] B. Guizal, H. Yala, and D. Felbacq, *Reformulation of the eigenvalue problem in the Fourier modal method with spatial adaptive resolution*, Opt. Lett. **34**, 2790 (2009). 64

[196] G. Granet, *Reformulation of the lamellar grating problem through the concept of adaptive spatial resolution*, J. Opt. Soc. Am. A **16**, 2510 (1999). 64

[197] T. Vallius and M. Honkanen, *Reformulation of the Fourier modal method with adaptive spatial resolution: application to multilevel profiles*, Opt. Express **10**, 24 (2002). 64

[198] J. B. Pendry, L. Martín-Moreno, and F. J. García-Vidal, *Mimicking Surface Plasmons with Structured Surfaces*, Science **305**, 5684 (2004). 67

[199] F. J. Garcia-Vidal, L. Martín-Moreno, and J. B. Pendry, *Surfaces with holes in them: new plasmonic metamaterials*, J. Opt. A: Pure Appl. Opt. **7**, S97 (2005). 67

[200] M. Antezza, H. B. Chan, B. Guizal, V. N. Marachevsky, R. Messina, and M. Wang, *Giant Casimir Torque between Rotated Gratings and the $\theta = 0$ Anomaly*, Phys. Rev. Lett. **124**, 013903 (2020). 68, 69, 71

[201] E. I. Kats, *Van der Waals forces in non-isotropic systems*, Sov. Phys. JETP **33**, 634 (1971). 67

[202] V. A. Parsegian and G. H. Weiss, *Nonretarded van der Waals Interaction between Anisotropic Long Thin Rods at All Angles*, J. Chem. Phys. **56**, 4393 (1972). 67

[203] Y. S. Barash, *Moment of van der Waals forces between anisotropic bodies*, Radiophys. Quantum Electron. **21**, 1138 (1978). 67

[204] S. J. van Enk, *Casimir torque between dielectrics*, Phys. Rev. A **52**, 2569 (1995). 67

[205] J. N. Munday, D. Iannuzzi, Y. Barash, and F. Capasso, *Torque on birefringent plates induced by quantum fluctuations*, Phys. Rev. A **71**, 042102 (2005). 67

[206] R. B. Rodrigues, P. A. M. Neto, A. Lambrecht, and S. Reynaud, *Vacuum-induced torque between corrugated metallic plates*, Europhys. Lett. **76**, 822 (2006). 67

[207] J. C. Torres-Guzmán and W. L. Mochán, *Casimir torque*, J. Phys. A: Math. Gen. **39**, 6791 (2006). 67

[208] T. G. Philbin and U. Leonhardt, *Alternative calculation of the Casimir forces between birefringent plates*, Phys. Rev. A **78**, 042107 (2008). 67

[209] A. Šiber, R. F. Rajter, R. H. French, W. Y. Ching, V. A. Parsegian, and R. Podgornik, *Dispersion interactions between optically anisotropic cylinders at all separations: Retardation effects for insulating and semiconducting single-wall carbon nanotubes*, Phys. Rev. B **80**, 165414 (2009). 67

[210] X. Chen and J. C. H. Spence, *On the measurement of the Casimir torque*, Phys. Status Solidi B **248**, 2064 (2011). 67

[211] Z. Xu and T. Li, *Detecting Casimir torque with an optically levitated nanorod*, Phys. Rev. A **96**, 033843 (2017). 67

[212] D. A. T. Somers and J. N. Munday, *Casimir-Lifshitz Torque Enhancement by Retardation and Intervening Dielectrics*, Phys. Rev. Lett. **119**, 183001 (2017). 67

[213] R. Guérout, C. Genet, A. Lambrecht, and S. Reynaud, *Casimir torque between nanostructured plates*, Europhys. Lett. **111**, 44001 (2015). 67, 68

[214] K. Yasui and K. Kato, *Oriented Attachment of Cubic or Spherical $BaTiO_3$ Nanocrystals by van der Waals Torque*, J. Phys. Chem. C **119**, 24597 (2015). 67

[215] P. Thiyam, P. Parashar, K. V. Shajesh, O. I. Malyi, M. Boström, K. A. Milton, I. Brevik, and C. Persson, *Distance-Dependent Sign Reversal in the Casimir-Lifshitz Torque*, Phys. Rev. Lett. **120**, 131601 (2018). 67

[216] D. A. T. Somers, J. L. Garrett, K. J. Palm, and J. N. Munday, *Measurement of the Casimir torque*, Nature **564**, 386 (2018). 68, 70

[217] M. Wang, L. Tang, C. Y. Ng, R. Messina, B. Guizal, J. A. Crosse, M. Antezza, C. T. Chan, and H. B. Chan, *Strong geometry dependence of the Casimir force between interpenetrated rectangular gratings*, Nat. Commun. **12**, 600 (2021). 70, 71

[218] B. T. Wong, M. Francoeur, and M. Pinar Mengüç, *A Monte Carlo simulation for phonon transport within silicon structures at nanoscales with heat generation*, Int. J. Heat Mass Transf. **54**, 1825 (2011). 73

[219] B. T. Wong, M. Francoeur, V. N. S. Bong, and M. P. Mengüç, *Coupling of near-field thermal radiative heating and phonon Monte Carlo simulation: Assessment of temperature gradient in n-doped silicon thin film*, J. Quant. Spectrosc. Radiat. Transf. **143**, 46 (2014). 73

[220] J. Z. J. Lau, V. N. S. Bong, and B. T. Wong, *Parametric investigation of nano-gap thermophotovoltaic energy conversion*, J. Quant. Spectrosc. Radiat. Transf. **171**, 39 (2016). 73

[221] T. Kralik, P. Hanzelka, V. Musilova, A. Srnka, and M. Zobac, *Cryogenic apparatus for study of near-field heat transfer*, Rev. Sci. Instrum. **82**, 055106 (2011). 73

[222] K. Kloppstech, N. Könne, S.-A. Biehs, A. W. Rodriguez, L. Worbes, D. Hellmann, and A. Kittel, *Correction: Publisher Correction: Giant heat transfer in the crossover regime between conduction and radiation*, Nat. Commun. **9**, 16224 (2018). 73

[223] R. Messina, W. Jin, and A. W. Rodriguez, *Exact formulas for radiative heat transfer between planar bodies under arbitrary temperature profiles: Modified asymptotics and sign-flip transitions*, Phys. Rev. B **94**, 205438 (2016). 74, 75, 79

[224] R. Messina, W. Jin, and A. W. Rodriguez, *Strongly coupled near-field radiative and conductive heat transfer between planar bodies*, Phys. Rev. B **94**, 121410(R) (2016). 74, 75, 79

[225] K. Joulain, *Near-field heat transfer: A radiative interpretation of thermal conduction*, J. Quant. Spectrosc. Radiat. Transf. **109**, 294 (2008). 74

[226] V. Chiloyan, J. Garg, K. Esfarjani, and G. Chen, *Transition from near-field thermal radiation to phonon heat conduction at sub-nanometre gaps*, Nat. Commun. **6**, 6755 (2015). 74

[227] W. Jin, R. Messina, and A. W. Rodriguez, *General formulation of coupled radiative and conductive heat transfer between compact bodies*, Phys. Rev. B **95**, 161409 (2017). 76, 79

[228] W. Jin, R. Messina, and A. W. Rodriguez, *Near-Field Radiative Heat Transfer under Temperature Gradients and Conductive Transfer*, Z. Naturforsch. A **72**, 141 (2017). 76, 79

[229] M. Reina, R. Messina, and P. Ben-Abdallah, *Conduction-Radiation Coupling between Two Closely Separated Solids*, Phys. Rev. Lett. **125**, 224302 (2020). 76, 77, 78, 79